

ABSTRACT

Effects of Surface Heterogeneity on the Colloidal Stability, Protein Adsorption and Bacterial Interaction of Nanoparticles

Rixiang Huang, Ph.D.

Advisor: Boris L.T. Lau, Ph.D.

Interfacial processes like aggregation and deposition control the transport and fate of natural and engineering nanoparticles (NPs) in the environment, which are relevant to important environmental processes, applications, and effects of NPs. These processes are controlled by a wide range of NP properties. Depending on the time frame and nature of the interfacial processes, a combination of different techniques (including dynamic light scattering, isothermal titration calorimetry, batch adsorption and spectroscopic techniques) were used to systematically investigate the effects of surface heterogeneity on the colloidal stability, protein adsorption and bacterial interaction of self-assembled monolayer coated gold nanoparticles (AuNPs). These AuNPs have similar size and shape but quantitative difference in the ligand composition and distribution on their surface, therefore serve as ideal models for heterogeneous surfaces that are ubiquitous in the environment and engineering system.

Key findings of this work include: 1) In addition to surface chemical composition, the organization of different functional groups on NP surface was also found to influence the electrical double layer structure and the relative contribution of different interfacial

forces. Therefore, direct comparison of zeta potential of different particles and the prediction using the classical Derjaguin-Landau-Verwey-Overbeek (DLVO) theory should be made with cautions; 2) The effects of surface heterogeneity were found to be scale-dependent in NP-protein interactions. The size of proteins and surface features of NPs together determined the interaction mechanism (e.g., binding stoichiometry and forces involved). The interaction mechanism subsequently affects the protein corona structure; 3) When these AuNPs adsorb onto bacterial cells, the adsorption kinetics is in agreement with the DLVO prediction, where the magnitude of electrostatic repulsion determines the diffusion of NPs onto bacterial cell. The adsorption capacity reflects the influence of surface heterogeneity on the association of bacterial surface components with these AuNPs. Overall, these findings improve our understanding on the effects of surface heterogeneity on representative interfacial processes that control the transport and fate of NPs. This work also provided new insights into better design of surfaces for various applications.

Effects of Surface Heterogeneity on the Colloidal Stability, Protein Adsorption and
Bacterial Interaction of Nanoparticles

by

Rixiang Huang, B.Eng., M.S.

A Dissertation

Approved by the Department of Geology

Stacy C. Atchley, Ph.D., Chairperson

Submitted to the Graduate Faculty of
Baylor University in Partial Fulfillment of the
Requirements for the Degree
of
Doctor of Philosophy

Approved by the Dissertation Committee

Boris L.T. Lau, Ph.D., Chairperson

Stephen I. Dworkin, Ph.D.

William C. Hockaday, Ph.D.

Andrew S. Madden, Ph.D.

Sascha Usenko, Ph.D.

Joe C. Yelderman, Ph.D.

Accepted by the Graduate School
December 2013

J. Larry Lyon, Ph.D., Dean

Copyright © 2013 by Rixiang Huang

All rights reserved

TABLE OF CONTENTS

LIST OF FIGURES	viii
LIST OF TABLES	xii
ACKNOWLEDGMENTS	xiii
DEDICATION	xiii
CHAPTER ONE Introduction	1
Motivations	1
Objectives	4
Organization of this Dissertation Research.....	5
Experimental Techniques.....	10
CHAPTER TWO Colloidal Stability of Self-Assembled Monolayer-Coated Gold Nanoparticles: The Effects of Surface Compositional and Structural Heterogeneity	11
Abstract	11
Introduction.....	12
Materials and Methods.....	15
Results and Discussion	17
Conclusions.....	29
CHAPTER THREE Protein–nanoparticle interactions: the effects of surface compositional and structural heterogeneity are scale dependent.....	30
Abstract	30
Introduction.....	31
Materials and Methods.....	34
Results and Discussion	37
Implications and Conclusions	47
CHAPTER FOUR Effects of Surface Compositional and Structural Heterogeneity on Albumin-Nanoparticle Interactions: Protein Coronas or Protein Clouds?	49
Abstract	49
Introduction.....	50
Materials and Methods.....	52
Results and Discussion	55

Implications and Conclusion.....	69
CHAPTER FIVE Nanoparticle Adsorption onto Bacterial Cells: Effects of Surface Heterogeneity	71
Abstract	71
Introduction.....	71
Materials and Methods.....	73
Results and Discussion	76
Conclusions and Future Work	82
CHAPTER SIX Conclusions, Implications and Future Research	84
Conclusions.....	84
Implications.....	86
Future Research	86
APPENDIX.....	88
APPENDIX A Derjaguin - Landa - Verwey - Overbeek (DLVO) Theory	89
APPENDIX B Dynamic Light Scattering.....	93
APPENDIX C Isothermal Titration Calorimetry.....	94
APPENDIX D Size Characterization of MUS, brOT and OT Particles	96
APPENDIX E Representative Aggregation Profiles of AuNPs in a Range of NaCl Concentration	98
APPENDIX F ITC Experiment Results for Interaction between AuNPs and Ubiquitin or Fibrinogen.	99
APPENDIX G Synthesis and Size Characterization of MPA/brOT and MPA/OT Particles.....	102
APPENDIX H Size Change of MUS, brOT and OT Particles in the Presence of Different Concentrations of BSA.....	104
APPENDIX I The Secondary Structure of BSA in the Presence of MPA-type AuNPs	105
APPENDIX J Fluorescence Quenching of BSA by AuNPs.	106
APPENDIX K ITC Results for BSA-MUS AuNP interaction.	107

APPENDIX L Measurement of the Esterase Activity of BSA.....	108
APPENDIX M AuNPs Adsorption Kinetics onto <i>E.coli</i> and <i>B.cereus</i> cell.	110
REFERENCES	111

LIST OF FIGURES

Figure 1-1 Schematic illustration of particle-particle interactions examined in Chapter 2.	6
Figure 1-2 Schematic illustration of particle-protein interactions examined in Chapter 3.	7
Figure 1-3 Schematic illustration of the particle-albumin interactions examined in Chapter 4.....	8
Figure 1-4 Schematic illustration of the particle-bacteria interactions examined in Chapter 5.....	9
Figure 2-1 EPMs of the three types of AuNPs as functions of NaCl concentrations at pH 7.0. Error bars represent standard deviations (A); The CCCs of the three types of AuNPs measured in NaCl, error bars represent the uncertainty range of CCC (B).	22
Figure 2-2 EPMs of the three types of AuNPs as functions of CaCl ₂ and MgCl ₂ concentrations at pH 7.0. Error bars represent standard deviations (A); The CCCs of the three types of AuNPs measured in CaCl ₂ and MgCl ₂ , error bars represent the uncertainty range of CCC (B).	23
Figure 2-3 Adsorption kinetics of the AuNPs onto <i>E. coli</i> in 10 mM phosphate buffer (pH 7.4).	24
Figure 2-4 Schematic of possible water distribution around the three types of AuNPs. ..	25
Figure 2-5 Schematic of electrical double layer structure surrounding the MUS particle.....	26
Figure 3-1 (A) Hydrodynamic diameter of unbound fibrinogen and AuNPs at pH 4.0 and pH 7.4. (B) ζ -potentials of proteins at pH 4.0 and pH 7.4.	38
Figure 3-2 Hydrodynamic diameter change of AuNPs following the addition of proteins at pH 4.0 (A) and pH 7.4 (B), error bars represent the variations between duplicate experiments.	39
Figure 3-3 CD spectra of ubiquitin at pH 4.0 (left) and 7.4 (right) in the presence of varying AuNP concentrations.	41
Figure 3-4 CD spectra of fibrinogen at pH 4.0 (left) and 7.4 (right) in the presence of varying AuNP concentrations.	43

Figure 3-5 ITC data from the titration of 1 mmol/L ubiquitin (left) and 80 μ mol/L fibrinogen (right) into 7.03 μ mol/L MUS AuNP. Heat flow versus time during injection of proteins at 25 °C and heat evolved per mole of added proteins (corrected for the heat of protein dilution) against the molar ratio (protein/AuNP) for each injection are shown at the top and bottom, respectively. The line is the model fitting (The data corresponding to the heat of dilution of protein were shown in Appendix F).....	44
Figure 4-1 Size change of AuNPs due to the adsorption of BSA (A) and the secondary structure of BSA following the addition of MUS-type AuNPs at pH 7.4.....	59
Figure 4-2 Stern-Volmer plot (left) and the shift of Trp emission (right) for BSA in the presence of increasing concentrations of MUS-type AuNPs.....	61
Figure 4-3 Stern-Volmer plot (left) and the shift of Trp emission (right) for BSA in the presence of increasing concentrations of MPA-type AuNPs.....	61
Figure 4-4 The proposed binding geometries for BSA and (A) MUS/brOT or MPA/brOT and (B) MUS/OT or MPA/OT AuNPs based on DLS and fluorescent quenching measurements. NP and protein size were not drawn to scale (cartoons of AuNP and BSA were adopted and modified from Verma et al.(Verma et al. 2008) and Dubeau et al. (Dubeau et al. 2010), respectively)	62
Figure 4-5 ITC data from the titration of 500 μ M BSA into 8.4 μ M MUS/brOT (left) and 7.7 μ M MUS/OT AuNP (right). Heat flow versus time during injection of proteins at 25 °C and heat evolved per mole of added proteins (corrected for the heat of protein dilution) against the molar ratio (protein/AuNP) for each injection are shown at the top and bottom, respectively. (The data corresponding to the heat of dilution of protein were shown in Appendix K).	65
Figure 4-6 ITC data from the titration of 500 μ M BSA into 9.0 μ M MPA/brOT (left) and 9.3 μ M MPA/OT (right). Heat flow versus time during injection of BSA at 25 °C and heat evolved per mole of added BSA (corrected for the heat of BSA dilution) against the molar ratio (BSA/AuNP) for each injection are shown at the top and bottom, respectively. (The data corresponding to the heat of dilution of BSA are shown in Appendix K).	66
Figure 5-1 Adsorption kinetics of three types of AuNPs expressed as number of NPs per cell, onto <i>E. coli</i> (A) and <i>B. cereus</i> (B), error bar represent the variation of duplicate samples. Concentration of <i>E. coli</i> and <i>B. cereus</i> cell was 4.2×10^8 and 1.6×10^8 cell/mL, respectively. <i>E. coli</i> adsorption data was based on Huang et al.(Huang et al. 2013a).	77

Figure 5-2 Adsorption isotherm (A) and with linear Langmuir isotherm fitting (B) of the three types of AuNP onto <i>E. coli</i> cells, error bar represent the variation of duplicate samples.	78
Figure 5-3 AuNPs adsorption on <i>E. coli</i> with and without trypsin treatment, initial AuNPs concentration was 1.46 ± 0.03 and 3.01 ± 0.04 mg/L Au ⁺ for concentration 1 and 2, respectively.....	80
Figure 5-4 EPM of the bacteria with and without trypsin treatment, error bar represent standard deviation (n = 3).	81
Figure 5-5 Schematic diagram of NP adsorption onto bacterial cell, the color symbols of different shapes represent different proteins and the long chains represent lipopolysaccharides.	82
Figure A Gouy-Chapman model (left) and Stern model (right) for electrical double layer structure developed at a negatively-charged surface.	90
Figure C Schematic diagram of an ITC setup (left) and representative result and analysis (right).	95
Figure D1 Representative TEM images of the MUS, brOT and OT AuNPs (from left to right).	96
Figure D2 Size distribution of the three types AuNPs expressed in percentage.	96
Figure D3 Volume-based size distribution of the three types of AuNPs from DLS measurement.	97
Figure E Representative aggregation profiles of MUS (left) and OT (right) in NaCl obtained from time-resolved DLS measurements over a range of electrolyte concentrations. The CCC uncertainty was found to range from 250 mM to 350 mM and 800 mM to 1200mM.	98
Figure F1 ITC data from the titration of 100 μ M ubiquitin (left) and 80 μ M fibrinogen (right) into 10 mM 7.4 phosphate buffer. Heat flow versus time during injection of proteins at 25 °C and heat evolved per injection of proteins was present above and below respectively.	99
Figure F2 ITC data from the titration of 1 mM ubiquitin into 8.4 μ M 66-34 brOT (left) and 7.7 μ M 66-34 OT (right) AuNP. Heat flow versus time during injection of proteins at 25 °C and heat evolved per mole of added proteins (corrected for the heat of protein dilution) against the molar ratio (protein/AuNP) for each injection are shown at the top and bottom, respectively.	100
Figure F3 ITC data from the titration of 0.08 mM fibrinogen into 8.4 μ M 66-34 brOT (left) and 7.7 μ M 66-34 OT (right) AuNP. Heat flow versus time	

during injection of proteins at 25 °C and heat evolved per mole of added proteins (corrected for the heat of protein dilution) against the molar ratio (protein/AuNP) for each injection are shown at the top and bottom, respectively.	101
Figure G1 Size distribution of the MPA-type AuNPs based on TEM characterization (number frequency was based on random counting of more than 1000 particles).....	103
Figure G2 Hydrodynamic size distribution of the two types of AuNPs measured by DLS.	103
Figure H Hydrodynamic size change of three types of AuNPs in the presence of a series concentration of BSA.....	104
Figure I The secondary structure of BSA following the addition of MPA-type AuNP at pH 7.4.....	105
Figure J Tryptophan fluorescence emission of BSA in the presence of varying AuNP concentration (0~0.004 μ M).	106
Figure K ITC data from the titration of 500 μ M of BSA into 10 mM 7.4 phosphate buffer (left) and into 7.03 μ M MUS AuNP. Heat flow versus time during injection of proteins at 25 °C and heat evolved per injection of proteins was present above and below respectively.	107
Figure L Effect of MPA/brOT and MPA/OT on the esterase activity of BSA, the activity was expressed as the activity relative to that of free BSA without the presence of AuNPs (error bar represent standard deviation, n = 3).	109
Figure M Free AuNP concentration in suspension during the adsorption kinetics experiment of <i>E. coli</i> (A) and <i>B. cereus</i> (B). Concentration of <i>E. coli</i> and <i>B. cereus</i> cell was 4.2×10^8 and 1.6×10^8 cell/mL, respectively. <i>E. coli</i> adsorption data was based on Huang et al.(Huang et al. 2013a).	110

LIST OF TABLES

Table 3-1 Thermodynamic quantities of ubiquitin-AuNPs interaction derived from ITC (Error bar represents the variation between duplicate experiments).	45
Table 3-2 Thermodynamic quantities of fibrinogen-AuNPs interaction derived from ITC (Error bar represents the variation between duplicate experiments).	46
Table 4-1 Physical and chemical properties of the two types of AuNPs used in this study.	57
Table 4-2 Fitting parameters of the Stern-Volmer model for BSA with different particles.	61
Table 4-3 Thermodynamic quantities of BSA and MPA-type NPs interaction derived from ITC.	66
Table 5-1 k_{obs} and θ_{∞} Values determined from three AuNPs adsorbed on <i>E.coli</i> and <i>B.cereus</i>	77
Table 5-2 Fitting parameters for Langmuir adsorption isotherm for <i>E.coli</i>	79

ACKNOWLEDGMENTS

I would like to express my greatest gratitude to my advisor Dr. Boris Lau, who has been a great advisor and mentor, for not just providing me the opportunities to study in Baylor and grow as a researcher, but also being positive role models in many aspects. He allows and helps me to think and work independently, while being considerate and supportive whenever I made mistakes.

I would like also to thank my committee members, Dr. William Hockaday, Dr. Steve Dworkin, Dr. Joe Yelderman, Dr. Andrew S. Madden and Dr. Sascha Usenko, for the time and efforts they have spent on serving on my committee. Dr. Hockaday is an expert in organic geochemistry, with whom I have many thoughtful and inspiring discussions. I am glad to be able to work under him on several projects in organic geochemistry. Dr. Dworkin and Dr. Yelderman are scientists in geochemistry and hydrogeology respectively, and they gave great lectures. Dr. Yelderman can always describe things in an interesting way and likes to share his experience. Dr. Dworkin has the gift of describing things incisively and vividly. From them I learn how to be a good teacher. I also like to thank other professors that have given me great lectures here at Baylor, Dr. Peter Allen, Dr. Stacy Atchley, Dr. Steve Driese, just list a few.

I also like to thank my collaborators (Dr. Randy Carney and Dr. Francesco Stellacci) in École Polytechnique Fédérale de Lausanne, for their generous help in this dissertation research.

Throughout these years, I am glad to be able to work with and learn from colleagues in Lau's lab: Dr. Olga Furman, Dr. Kaoru Ikuma, Mike Nguyen and Fan Zhang, with whom my life in the lab was not monotonous, but with colorful memory.

I also would like to thank Dr. Moehnke Craig, Dr. Alejandro Ramirez, Dr. Michelle Nemec, and Miss Natalia Anderson, who were always ready to help with analytical instruments and other research needs.

Baylor Geology has been another home to me. I enjoy the communications and friendships with many nice people. Thanks to the wonderful administrative staff, who helps create and maintain a warm environment and a positive attitude in this department. Mrs. Paulette Penney has been helping with many things with patience and a careful mind, so everything was kept organized and went smoothly. Thanks also to Mrs. Sharon Browning, Jamie Ruth, Erin Stinchcomb and Janelle Atchley, without whom my life will not be easy.

I want to sincerely thank my former roommate Joshua McCoy who has been a true brother, my neighbors - the Heckenlivelys, the Edwards and the Selbys, who treat me like their family member. My thanks also go to the brothers and sisters in the WCC, who have been keeping me in their thoughts and praying for me along the years.

Last but not least, I am grateful to my parents, my sister and my brother, for their persistent love and great sacrifice. I especially owe my beloved wife Xiaowei a great debt of gratitude, for her unwavering love, understanding and support. They all share my hopes and dreams.

To Xiaowei

CHAPTER ONE

Introduction

Motivations

Natural nanoparticles (NPs) including silica, metal oxides and organic matters, are widely present and of great importance to the biogeochemistry of the environment (Hochella et al. 2008; Madden and Hochella 2005; Nowack and Bucheli 2007; Wigginton et al. 2007). With different reactivity than their bulk counterparts, the transport and fate of these NPs are also closely related to the cycling and mobilization of trace elements and contaminants (Madden et al. 2006).

The emergence of nanotechnology leads to mass production and widespread application of nanomaterials. For examples, zero-valent iron NPs are being used for environmental remediation (Li et al. 2006), carbon-based nanomaterials are made for water treatment (Savage and Diallo 2005; Shannon et al. 2008), and silver NPs are widely utilized in consumer and antibacterial products (Lee et al. 2005; Quadros et al. 2013). The production and use of these nanomaterials will inevitably lead to their release into the environment (Benn and Westerhoff 2008) and some of them may ultimately end up in the bodies of organisms. In the past decade, extensive research on the toxicity of these nanomaterials has shown varying degrees of undesirable effects (Magrez et al. 2006; Nel et al. 2006). This causes great concerns on the safe application and environmental effects of these nanomaterials (Klaine et al. 2008; Nowack and Bucheli 2007).

Whether the purpose is to understand the role of natural NPs in biogeochemical processes or to evaluate the effects of engineered nanomaterials, it is important to understand the transport, transformation and fate of these NPs in the environment (Levard et al. 2012; Mylon et al. 2004).

They are all greatly controlled by various interfacial processes, for example, their homo- and hetero-aggregation, and deposition. Homo-aggregation involves the transport of a particle to the vicinity of another particle of the same type (similar size and surface) and subsequently attached to it, while hetero-aggregation involves particles of a different type (Lin 2012). When the size of the interacting objects is much larger than the NPs and is relatively immobile, NP's attachment is referred to as deposition. Representative interfacial processes controlling the transport, transformation and fate of NPs include their aggregation in different water environments, deposition onto mineral or biofilm surfaces, and protein adsorption following their entry into organisms.

In addition to solution chemistry, these interfacial processes are controlled by a wide range of properties of NPs and the interacting surfaces, like their size, shape and surface properties. Among them, surface properties may be the most important factor.

Advancement in material science enables the synthesis of a vast variety of NPs with different compositions and surfaces. For example, carbon nanomaterial can be functionalized with different chemical groups and metal NPs can be coated with different organics for specific applications (Han et al. 2007; Sun et al. 2002). On the other hand, the types of particle or surface that NP may encounter in the environment can also be countless, including suspended natural colloids (e.g., bacterial cells and inorganic particulates), various mineral surfaces, biofilm, and organism tissues. They possess diverse and complex surfaces that are usually heterogeneous in chemical compositions and physical structures (as reviewed below). Although the effects of surface properties (e.g., charge and polarity) on various interfacial processes have been extensively studied (Dunphy Guzman et al. 2006; Song et al. 2011), surface heterogeneity as an important surface property has been disproportionately neglected. Therefore, the primary goal of

this dissertation was to investigate the effects of surface heterogeneity on nanoscale interfacial process in representative scenarios.

Surface heterogeneity is a broad and scale-dependent concept. It can be used to describe inhomogeneity of any physical or chemical properties within a two dimensional surface. Its scale ranges from the variability of the earth's surface (e.g., difference in geological setting and vegetation) to chemical diversity on a protein surface (Koster and Suarez 1992; Park et al. 1992). Characterization of the heterogeneity and understanding its impact on related processes are important in various scientific disciplines, including climate modeling and colloid science (Avissar 1990; Walz 1998).

In natural or engineered NPs and the interacting surfaces, surface heterogeneity is usually referred to as the coexistence of different chemical functionalities and physical structures. For examples, charge heterogeneity as the coexistence of positively- and negatively-charged groups, polarity heterogeneity as the coexistence of polar and nonpolar groups. The different ways of coexistence introduce the physical (or structural) heterogeneity. Surface heterogeneity exerts its effects on interfacial processes of NPs by influencing the electrical double layer (EDL) structure (see Appendix A for further description of the EDL) and interfacial forces (Drelich and Wang 2011; Duval et al. 2004; Walz 1998; Zembala 2004).

Since the behavior of ions (e.g., ion hydration and distribution) is dependent on the nature of surface (e.g., charge and polarity) (Calero et al. 2011), surface heterogeneity will increase the complexity of EDL structure and make it challenging to model and to derive electrostatic interaction. Surface heterogeneity may also introduce anisotropic force distribution and forces in addition to van der Waals and electrostatic interaction. For example, hydrophobic patches and extracellular structures on bacterial surface lead to anisotropic force distribution as demonstrated

by atomic forces microscopy (Dorobantu et al. 2008; Dorobantu et al. 2009). Therefore, the failure of the classical Derjaguin-Landau-Verwey-Overbeek (DLVO) theory (see Appendix A for more details on DLVO theory) was commonly ascribed to surface heterogeneity (Tufenkji and Elimelech 2004; Tufenkji and Elimelech 2005).

Aggregation and deposition of colloidal particles have been extensively studied for colloid stability in estuary, drinking water and wastewater treatments, and groundwater movement (Mayer 1982; Sigleo and Means 1990). Conventional theories in colloidal science developed for micron-sized particles are the basis for the current studies on the interfacial phenomena of NPs (Petosa et al. 2010). However, since the assumptions often applied to micron-sized particles may be invalid in the case of NPs, experimental results sometimes deviate from these theories. For example, in the calculation of electrostatic interaction, the condition that $\kappa\alpha \gg 1$ (κ^{-1} is Debye length, α is the particle radius) required in some derivations may not be fulfilled in the case of nanoparticles (Ohshima et al. 1982). Due to the large surface to volume ratio of NPs, interactions involving NPs are more sensitive to small changes in surface compared to that for microscale particles. To better describe and predict the environmental behavior of NPs, it is important to investigate how surface heterogeneity affects the applicability of the DLVO theory and to identify the causes of deviation.

Objectives

The overarching objective of this dissertation was to systematically investigate the influence of surface heterogeneity on the interfacial processes involving NPs in the context of their environmental behavior and effects. Specific objectives of individual studies were: 1) To study how chemical composition and spatial organization of functionalities on surface affect the electrokinetic properties and self-aggregation behavior of self-assembled monolayer coated NPs

in the presence of monovalent and divalent electrolytes; 2) To mechanistically investigate the interaction between NPs and proteins of different sizes and shapes, and to understand how surface heterogeneity of NPs affects the interaction and subsequent functionality of NPs and proteins; 3) To quantitatively measure the interaction between NPs and bacteria, and to identify the effects of surface heterogeneity from both NPs and bacteria.

Organization of this Dissertation

To study the effects of surface heterogeneity, self-assembled monolayers (SAMs) coated AuNPs were used as model NPs. SAMs are organic assemblies formed by adsorption of organic ligands (thiols in this case) on surface and spontaneously organize into various structures, and the terminal chemical functional group of the organic ligand determines their functionality (Love et al. 2005). Particle-particle interactions (Chapter two), particle-protein interactions (Chapters three & four), and particle-bacteria interactions (Chapter five) were systematically studied in this dissertation work. A summary of the results and major contributions was presented in Chapter six.

Particle-Particle Interactions

In Chapter two, the electrokinetic properties and aggregation behavior of three types of AuNPs were studied in the presence of various monovalent and divalent electrolytes. These AuNPs were capped with three different SAM configurations and they were: (1) AuNPs with charged and nonpolar terminals organized into nano-scale structure (OT), (2) AuNPs with randomly distributed terminals (brOT), and (3) AuNPs with homogeneously charged terminals (MUS). Specifically, the electrophoretic mobility in a wide range of concentration of NaCl, MgCl₂ and CaCl₂ were measured, the aggregation kinetics in the respective conditions were monitored by time-resolved dynamic light scattering (DLS) experiments (See Appendix B for

further description of DLS). Adsorption kinetics of these AuNPs on *Escherichia coli* was also measured to identify the difference between homo-aggregation and particle-surface interaction. This study served to investigate the stability of these AuNPs (Figure 1-1).

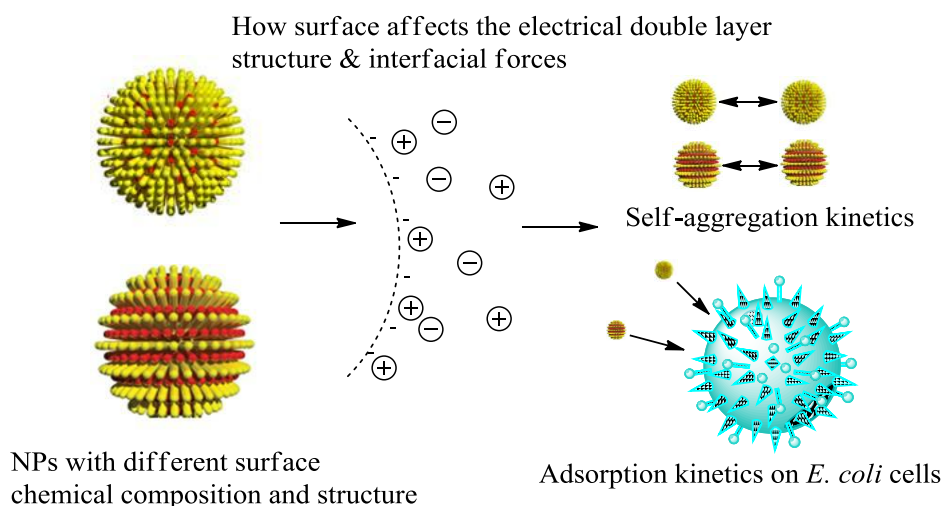


Figure 1-1 Schematic illustration of particle-particle interactions examined in Chapter 2.

Particle-Protein Interactions

Protein-NP interaction is of great relevance in the toxicity and the biomedical application of nanomaterials. How NP's properties affect protein-NP interaction is important for understanding the mechanism of toxicity and a better design of NPs for specific applications (Gagner et al. 2012).

A wide range of NP properties (e.g., particle size, surface charge and surface hydrophobicity) have been found to control the interaction mechanism and the final protein composition of the protein corona - the proteins coating on the surface of NPs (Meder et al. 2012; Tenzer et al. 2011). Particle size (or curvature) determines the contact area between protein and NPs. Protein can interact with NP surface through non-specific interaction or covalent binding, depending on the chemical functionality of the NP surface (Rana et al. 2010).

When NP is present in actual serum environment, it will be exposed to a vast amount and variety of proteins with different affinities to the NPs (Zhang et al. 2011a). There will be a series of adsorption and exchange reactions before thermodynamic equilibrium is reached (Lundqvist et al. 2011; Monopoli et al. 2012). The protein corona is thus rather dynamic, with changing protein composition and structure in different physiochemical environments.

In Chapter three, the interactions between these AuNPs and two proteins with different sizes and shapes - ubiquitin and fibrinogen were examined (Figure 1-2). DLS and circular dichroism spectroscopy were used to reveal different interactions at pH above and below the isoelectric points of the proteins. The interaction thermodynamics were measured by isothermal titration calorimetry (ITC, a description on the basics of this technique can be found in Appendix C). The variation in protein types and particle surfaces enabled the analysis of effects of surface heterogeneity at different scales on protein-NP interaction.

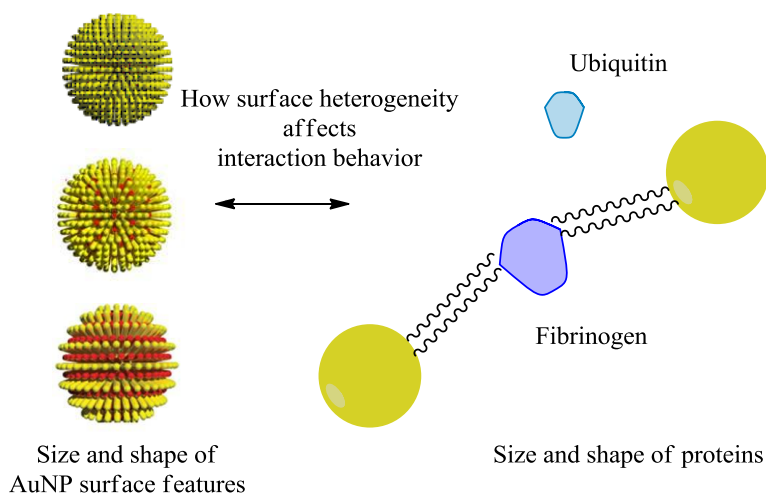


Figure 1-2 Schematic illustration of particle-protein interactions examined in Chapter 3.

Chapter four is an extension of the study of NP-protein interaction. The interaction between serum albumin and AuNPs were further studied to reveal the effects of surface

heterogeneity on interaction mechanism and resulting protein corona structure (Figure 1-3). The interaction mechanism and protein corona structure were characterized by a combination of DLS, circular dichroism (CD) spectroscopy, fluorescence quenching and ITC. An additional two types of AuNPs, MPA/brOT and MPA/OT (resembling brOT and OT in their surface organizations of the coating ligands, with the negatively-charged MUS substituted for mercaptopropionic acid (MPA)), were used to examine whether the protein adsorption behavior is dependent on structural heterogeneity and independent of specific polar groups.

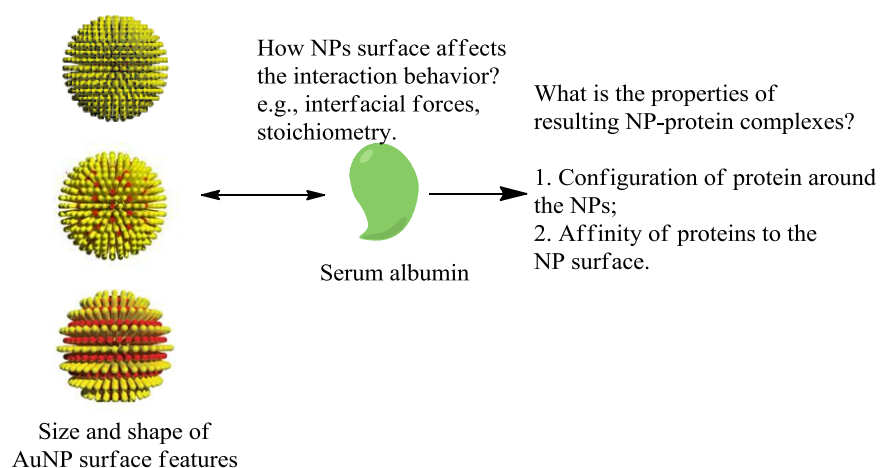


Figure 1-3 Schematic illustration of the particle-albumin interactions examined in Chapter 4.

Particle-Bacteria Interactions

NP-bacteria interaction is relevant in many applications of NPs and environmental issues, including natural NP formation, the application and toxicity of nanomaterials (Bhattacharya and Gupta 2005; Theron et al. 2008). For examples, the interaction of silver NPs with environmental biofilms, and the synthesis of NP-embedded materials for antibacterial and antifouling applications (Fabrega et al. 2009; Hetrick et al. 2009; Weir et al. 2008).

On bacterial surface, there are flagellum, pili and other extracellular components that constitute a three dimensional structure (McEwen et al. 2010; Namba and Vonderviszt 1997).

Although the size of bacterium is about one micrometer, the size of their surface components and characteristic patches are at the nanoscale, which is comparable to the size of NPs. Atomic force microscopy (AFM) studies demonstrated the chemical and physical heterogeneity and the distribution of anisotropic forces on the bacterial surface (Camesano and Abu-Lail 2002; Dorobantu et al. 2009; Gaboriaud and Dufrene 2007; Sokolov et al. 2000). Therefore, NPs are anticipated to interact with bacterial surface through different mechanisms, depending on the properties of both NP and the interacting surface components. Electrostatic interaction seems to be the predominant mechanism especially when the NPs and bacterial cell carry opposite surface charges (Schwegmann et al. 2010; Zhang et al. 2011b). Hydrophobic interaction also contribute to the adsorption when there is a significant degree of hydrophobicity on the NP surface (Xiao and Wiesner 2013).

In Chapter five, the adsorption dynamics of the three types of AuNPs - MUS, brOT and OT onto *E. coli* and *Bacillus cereus* was investigated to understand the effects of surface heterogeneity in both AuNPs and bacteria Figure 1-4. The contribution of surface proteins on AuNP adsorption was also quantified.

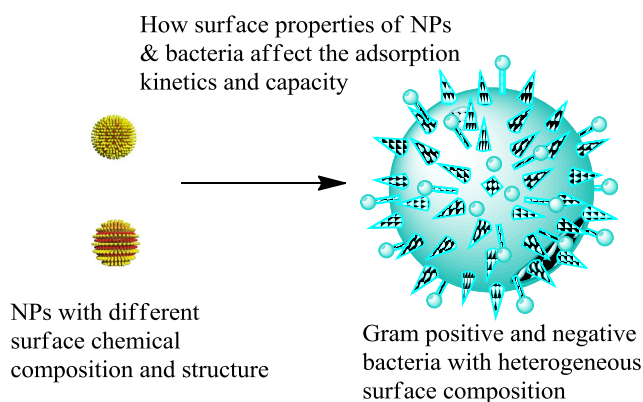


Figure 1-4 Schematic illustration of the particle-bacteria interactions examined in Chapter 5.

Experimental Techniques

Depending on the size of the interacting objects and the time frame of various interactions, a combination of experimental techniques were used to quantify the interaction kinetics and to characterize the role of surface properties on reaction mechanism when NPs interact with themselves, proteins and bacteria. For the self-aggregation of NPs and protein-NP interaction, particle size is a good indicator of the reaction process, and the interaction time ranges from seconds to minutes and the sizes of interest are at the nanometers. In this case, DLS is suitable for monitoring these reactions and was used in this study. Protein-NP interaction involves non-covalent forces and desolvation/solvation process that results in heat exchange with the environment. By capturing the heat profiles during protein-NP interaction, ITC directly measures the binding affinity constant, enthalpy changes, and binding stoichiometry between NPs and proteins, and other thermodynamic parameters can be derived. Since these parameters can reveal the interaction mechanism in a quantitative manner, ITC was employed to characterize the NP-protein interactions in this dissertation. For NP-bacteria interaction, since the size of bacteria is hundreds times larger than that of the AuNPs, size change may not be sensitive enough to characterize the interaction process. Besides, it may take longer time to reach equilibrium compared to NP-protein interaction. Therefore, batch adsorption experiment was used to quantify the adsorption kinetics and capacity. Other techniques (such as zeta-potential measurement, CD and fluorescence spectroscopy) were also used to characterize the studied interactions.

CHAPTER TWO

Colloidal Stability of Self-Assembled Monolayer-Coated Gold Nanoparticles: The Effects of Surface Compositional and Structural Heterogeneity

This chapter has been published as:

Huang, R.; Carney, R. P.; Stellacci, F.; Lau, B. L. T., *Colloidal Stability of Self-Assembled Monolayer-Coated Gold Nanoparticles: The Effects of Surface Compositional and Structural Heterogeneity*. Langmuir, 2013, 29 (37) 11560–11566.

<http://pubs.acs.org/doi/abs/10.1021/la4020674>

Copyright © 2013, American Chemical Society

Abstract

Surface heterogeneity plays an important role in controlling colloidal phenomena. This study investigated the self-aggregation and bacterial adsorption of self-assembled monolayer coated gold nanoparticles (AuNPs) with different surface compositional and structural heterogeneity. Evaluation was performed on AuNPs coated with (1) one ligand with charged terminals (MUS), (2) two homogeneously distributed ligands with respectively charged and nonpolar terminals (brOT) and (3) two ligands with respectively charged and nonpolar terminals with stripe-like distribution (OT). The brOT particles have less negative electrophoretic mobility (EPM) values, smaller critical coagulation concentration (CCC) and larger adsorption rate on *Escherichia coli* than that of AuNPs with homogeneously charged groups, in good agreement with DLVO predictions. Although the ligand composition on the surface of AuNPs is the same, OT particles have less negative EPM values and faster rate of bacterial adsorption, but much larger CCC compared to brOT. The deviation of OT particles from brOT and MUS in their self aggregation behavior reflects the effects of surface heterogeneity on electrical double layer structures at the interface. Results from the present study demonstrated that, besides chemical

composition, organization of ligands on particle surface is important in determining their colloidal stability.

Introduction

Surface heterogeneity is a ubiquitous phenomenon in both natural and engineering systems. For example, surface of microbes and cells usually has a diversity of biomolecules, including phospholipids, proteins and polysaccharides, which have completely different functional groups and properties (Pereira et al. 2009). Even proteins alone have rather complex surface composition and structure, which is determined by the constituting amino acids, specifically their diverse side-chains. Inorganic materials like activated carbon (Franz et al. 2000), siliceous materials (Bolis et al. 1997) and clay minerals (Tombacz and Szekeres 2006) also have heterogeneous surfaces in terms of the nature, amount, and geometrical arrangement of different functional groups at the surface. Materials' surface chemical composition and structure influence many surface properties and interfacial processes (Nel et al. 2009; Walz 1998; Zembala 2004).

In spite of its importance, surface heterogeneity is difficult to be studied because, (1) it is a broadly defined concept (surface heterogeneity is defined in this study as the coexistence of chemically different substances in different patterns on the surface), (2) natural surfaces are sometimes too complex for exact characterization and quantitative correlation with observed properties, and (3) many experimental parameters measuring surface properties like contact angle and surface potentials are scale-dependent, therefore may not be universally applicable. Although there were numerous studies devoted to characterize surface heterogeneity, few of them were able to establish a quantitative relationship between measured surface properties and surface heterogeneity (Dorobantu et al. 2008; Drelich and Miller 1994; Drelich et al. 1996;

Duval et al. 2004; Gaboriaud and Dufrene 2007; Taboada-Serrano et al. 2005). It has been widely accepted that materials at the nano-scale behave differently when compared to their counterpart at larger scales, relatively little is known about the effects of surface heterogeneity at the nano-scale on surface properties like electrokinetics and interfacial forces. Understanding these effects and the underlying mechanism are critical since it is of great relevance to various interfacial processes occurred in biological and environmental systems (e.g., (Nel et al. 2009) (Duffadar et al. 2009)).

The combination of gold nanoparticles (AuNPs) and thiol-based self-assembled monolayers (SAMs) has widespread applications and provides attractive opportunities for basic research in interfacial chemistry (Love et al. 2005). AuNPs with different surface chemical compositions and nano-scale surface structures, as modulated by SAMs, were synthesized (Jackson et al. 2006), and interesting properties regarding wettability (Centrone et al. 2008), interfacial energy (Kuna et al. 2009), cell penetration (Verma et al. 2008) and protein adsorption (Jackson et al. 2004) were found to be due to surface composition as well as surface structure. When correctly chosen (Verma et al. 2008), it is possible to select nanoparticles that are nearly identical in size distribution, shape, surface charge, and ligand density with quantitative differences only in composition and arrangement of ligands on the surface. For example particles coated with a 2:1 mixture of 11-mercapto undecanesulfonate, MUS and 1-octanethiol (OT) show stripe-like domains on their ligand shell, while particles coated with a 2:1 of MUS and 3,7 dimethyl octane 1-thiol (brOT) have a random distribution of ligand molecules; yet all of the other structural parameters for these particles are statistically identical (Verma et al. 2008). Hence these particles can be considered as nanoscale “isomers” (i.e., two particles differing only

in surface functional group distribution but not - to a first approximation- in their composition), making them ideal for testing surface feature-activity relationships.

Colloidal stability, mostly involves particle-particle and particle-surface interactions, has been extensively evaluated by the classic Derjaguin-Landau-Verwey-Overbeek (DLVO) theory. Despite its great success, deviations from this theory have been frequently reported, and most of which have been generally ascribed to surface heterogeneity and its influence on interfacial forces without strict correlation to specific type of heterogeneity (roughness, chemical or structural heterogeneity) (Duval et al. 2004; Elimelech et al. 2003; Taboada-Serrano et al. 2005; Tufenkji and Elimelech 2005). For nanomaterials with diverse structures and large surface-to-volume ratio, surface plays a more significant role than for the larger colloids. The classical DLVO theory does not account for all these effects (e.g., irregular shapes and coatings of nanoparticle (NP)), making the evaluation of NP stability challenging (Petosa et al. 2010). Therefore, a better understanding and quantification of how surface heterogeneity influences interfacial processes is necessary to improve the ability of DLVO theory in predicting NP stability.

The objective of this research was to identify the effects of surface heterogeneity (compositional and structural) on the colloidal stability of SAM-coated AuNPs. Evaluation was performed on AuNPs that are coated with (1) one ligand with charged terminals, (2) two homogeneously distributed ligands with respectively charged and nonpolar terminals and (3) two ligands with respectively charged and nonpolar terminals but distributed in a stripe-like pattern. The electrokinetics and aggregation kinetics of these AuNPs in various electrolytes were measured, their adsorption kinetics onto *E. coli* cells was also measured to study the particle-

surface interaction. The colloidal stability was analyzed within the context of the DLVO theory to validate its applicability.

Materials and Methods

Preparation of AuNP suspensions

Three types of AuNP used in this study are coated with 1) one ligand with charged headgroups (11-mercapto undecanesulfonate, MUS), 2) a *random* distribution of both charged and nonpolar headgroups (MUS and branched-octanethiol, brOT) and 3) an *ordered* pattern of charged and nonpolar headgroups (MUS and octanethiol, OT). Detailed information regarding the synthesis and characterization of these three types of AuNPs can be found in previous studies (Uzun et al. 2008; Verma et al. 2008).

All chemicals used in this study were ACS reagent grade and were purchased from Sigma Aldrich, unless otherwise noted. Filtered ($< 0.2 \mu\text{m}$) ultrapure water (Millipore Simplicity, $> 18 \text{ M}\Omega\cdot\text{cm}$) was used to prepare all stocks. To prepare the AuNPs stock solutions, 6 mg of each type of AuNPs was added into 20 ml ultrapure water, the solutions were sonicated in an ultrasonic bath (VWR, B2500A-MT) for 30 min. After ultrasonication, the AuNPs suspensions were centrifuged at 9 000 g (Avanti A-J., Beckman-Coulter, Brea, CA) for 30 min in order to remove nondispersive aggregates ($> 20 \text{ nm}$) in the suspensions. The supernatant was carefully withdrawn using pipette and stored in clean glass vials in 4°C . The stock solution was further characterized by transmission electron microscopy (TEM) and dynamic light scattering (DLS, Malvern Zetasizer Nano ZS) to determine the size distribution and morphology of the particles (Appendix D). All measurements were performed at $\text{pH } 7.0 \pm 0.2$ (buffered with 0.2 mM NaHCO_3 and adjusted with HCl) and at the temperature of 25°C .

EPM Measurements

The EPM of three types of AuNPs were measured using a Zetasizer Nano ZS (Malvern Instruments, Malvern, UK) over a range of electrolytes concentrations. The nanoparticle concentrations for EPM measurements were around 0.1~0.2 times of the concentrations of the corresponding AuNP stock suspensions. For most electrolyte concentrations, 6 measurements were conducted for duplicate samples at each electrolyte concentration.

Dynamic Light Scattering (DLS)

The early stage aggregation kinetics of the three types of AuNPs was determined by time-resolved DLS measurements using an ALV/CGS-3 compact goniometer (ALV GmbH, Germany). For each aggregation experiment, 980 μL of electrolyte stock solution was introduced into the glass vial containing 20 μL AuNPs stock suspension to achieve a final volume of 1 ml. Therefore, the AuNP concentration for the DLS measurements was 0.02 times of the concentration of the stock suspension. The vial was shaken for about 1 s with a vortex mixer and quickly inserted into the sample holder. The DLS measurements were started immediately and the intensity-weighted hydrodynamic diameters of the aggregating AuNPs were monitored over time periods of 20 min. It took about 15 s to get the first data point. All DLS measurements were performed at a scattering angle of 120° , each autocorrelation function was accumulated for 5 s with a 5 s wait time between measurements. The intensity-weighted hydrodynamic diameter was then derived using a second-order cumulant analysis.

Adsorption onto E. coli cells

E. coli K12 cells were grown in Luria-Bertani (LB) medium at 30°C with shaking and were harvested in the late exponential growth phase. The harvested cells were washed three times with phosphate buffer (10 mM, pH 7.4) and resuspended in the buffer solution to reach a

concentration of approximately 4×10^8 CFU/mL. For adsorption kinetics experiments, AuNPs and *E. coli* cells were mixed in 15 mL polypropylene centrifuge tubes. Five mL of the cell suspension were transferred into the tubes and adsorption experiments were started by adding 100 μ L AuNPs stock solution to each tube. The final dissolved concentration of AuNPs was around 2.5 mg/L. Phosphate buffers without *E. coli* cells were used as control. The tubes were placed in an incubator and shook at 200 rpm under 30 ± 2 °C.

Adsorption kinetics was studied by monitoring the decrease in the concentration of the suspended AuNPs in the bulk solution. The suspensions (350 μ L) were sampled at 5, 15, 30, 60, 90, 120, 180 min and centrifuged at 6000 rpm \times 5 min (Eppendorf 5417c centrifuge) to separate the suspended AuNPs from *E. coli* cells (with or without adsorbed NPs). Based on the measurements by DLS, the size of AuNPs in cell-free buffer was stable throughout the experiment. Besides, there was no significant difference in Au concentration for the control samples with and without centrifugation. These observations suggested that there was no interference from aggregation or sedimentation and that the change in Au concentration was mainly due to adsorption onto the bacterial cells. After centrifugation, 200 μ L of the suspension were pipetted into new clean 15 mL polypropylene centrifuge tubes and the suspension was digested by Aqua regia before ICP-MS analysis.

Results and Discussion

Characterization of AuNPs

The synthesis and characterization of the three types of AuNPs used in this study have been extensively described in previous work (Huang In review; Uzun et al. 2008; Verma et al. 2008). The AuNPs were also further characterized by TEM and dynamic light scattering to confirm the similarities in size and shape, and to the ones previously synthesized (Appendix D).

They are mostly spherical and slightly angular, and have a core diameter around 4.5 nm (4.5 ± 1.1 , 4.7 ± 0.9 and 3.9 ± 0.8 nm for MUS, brOT and OT particles, respectively). The ligand shell has a thickness around 1.5 nm. The hydrodynamic sizes are around 10.9 ± 1.6 nm (10.8 ± 0.2 , 12.5 ± 2.4 and 9.4 ± 1.0 nm for MUS, brOT and OT particles, respectively). MUS was coated with all MUS ligands, brOT was coated with 67% MUS and 33% branched-octanethiol, and OT was coated with 67% MUS and 33% octanethiol. Since the nonpolar and polar ligands were randomly distributed on brOT's surface, the heterogeneity was considered to be at molecular scale. The nonpolar and polar ligands were found to separate into alternative stripe-like domains on OT's surface with a spacing around 1 nm (Uzun et al. 2008), its heterogeneity were at the nanoscale.

Influence of Surface Charge Density on Electrokinetics and Self-Aggregation of AuNPs

The MUS and brOT AuNPs have different densities of sulphonate group, which determines the surface charge of the AuNPs, thus they were chosen to identify the effects of surface charge density on the electrokinetics and stability of NPs. The EPMS of MUS and brOT measured in the presence of NaCl, CaCl₂ and MgCl₂ electrolytes at pH 7.0 are shown in Figure 2-1A and Figure 2-2A. Both AuNPs exhibited negative EPMS over the range of electrolyte concentrations employed for the measurements. With increasing electrolyte concentrations, the EPMS of both AuNPs became less negative, due to an increase in charge screening (for NaCl) or charge neutralization (for CaCl₂ and MgCl₂). These two effects, which originated from the different behaviors between monovalent and divalent cations in the NP-liquid interface (Ca²⁺ and Mg²⁺ can form complex with the sulphonate - served as the charge-determining ion, while Na⁺ only accumulate in the vicinity of the AuNPs - served as the indifferent ion), are also responsible for the less negative EPM values of both AuNPs in the presence of CaCl₂ and MgCl₂ than in

NaCl. Specific adsorption of divalent cations has also been found with carbon-based nanomaterials (Chen and Elimelech 2006; Saleh et al. 2008). The less negative EPM values in the presence of CaCl_2 than in MgCl_2 could possibly be due to a stronger affinity of Ca^{2+} than Mg^{2+} to the sulphonate.

Significant difference in EPM in the presence of NaCl can be observed between MUS and brOT. Since MUS has a higher charge density, a higher NaCl concentration was required to screen the charge compared to that for brOT. In contrast, there was no significant difference in EPM in the presence of both CaCl_2 and MgCl_2 for the two types of AuNPs, which may be due to the dissimilar propensities of the sulphonates of the two AuNPs to undergo complex formation with the divalent cations. Since MUS and brOT were covered by 100% MUS and 66% MUS (randomly distributed) respectively, there were more opportunities for a Ca^{2+} or Mg^{2+} ion to bind to two adjacent sulphonate groups to form a bidentate sulphonate complex for MUS than brOT. As a result, even though MUS has a more negative EPM due to higher density of sulphonate on the surface, there will be more Ca^{2+} or Mg^{2+} binding to it than to brOT. The same argument has been proposed for multi-walled carbon nanotubes involving the complexation between Ca^{2+} and surface carboxyl group (Yi and Chen 2011).

The critical coagulation concentration (CCC) of the salt for a colloid is commonly defined as the bulk salt concentration where the repulsive barrier vanishes and the aggregation rate reaches the maximum and will not increase even when higher concentrations of electrolyte are used (the colloidal system undergoes diffusion-limited aggregation) (Kissa 1999).

Representative aggregation profiles obtained from time-resolved DLS measurements over a range of electrolyte concentrations are presented in Appendix E. Since the size of these AuNPs is relatively small and their diffusion coefficient is relatively large, it is difficult to capture the

initial aggregation dynamics (first measurable diameter \gg initial diameter). As a result, it is not possible to obtain an exact CCC value using the traditional method, which calculated the early-stage aggregation kinetics from the slope of initial size change. Instead, an uncertainty range for the CCC was obtained, which was determined to be between the threshold concentration (concentration equal to or higher than this tested concentration will not increase the aggregation kinetics) and the next lower concentration (where aggregation kinetics is noticeably smaller than the maximum). This method was used throughout this study.

The CCC ranges for MUS and brOT in NaCl, and in CaCl₂ and MgCl₂ are presented in Figure 2-1B and 2-2B, respectively. The CCC ranges for MUS and brOT in NaCl were determined to be 250 mM to 350 mM and 125 mM to 225mM, while in CaCl₂ are 1.5 to 3 and 1.5 to 3 mM, and in MgCl₂ 5 to 15 and 5 to 15 mM respectively. The CCC values for both CaCl₂ and MgCl₂ are much lower than their respective CCCs determined in NaCl. Since Ca²⁺ and Mg²⁺ can specifically bind to the surface sulphonate, they are much more effective in reducing the energy barrier experienced between the AuNPs compared to Na⁺ ions, which do not adsorb onto the particle surface but only accumulated in the vicinity of the AuNPs surface and only screen the charge. Secondly, the CCC ranges for the two types AuNPs in MgCl₂ were all larger than that in CaCl₂, which is possibly due to the different affinities of Ca²⁺ and Mg²⁺ to the surface sulphonate groups, and subsequently their different capabilities in neutralizing surface charge and reducing the energy barrier. All three types of AuNPs were coated with SAMs and it is the terminal functional group of the SAMs that determine the surface properties of these AuNPs. Therefore, it is the interaction between the divalent cations and the sulphonate groups that matters (rather than the Au surface). Unfortunately, there is no available information on the binding affinity between alkyl sulfonic acid and Ca²⁺ or Mg²⁺. However, similar phenomena

(with evidence of binding constants) were observed in a previous study with carboxyl group (Yi and Chen 2011). Finally, the range of CCC for brOT in NaCl was lower than that for MUS, but was not significantly different from each other in both CaCl₂ and MgCl₂, which again can be ascribed to the different functionalities of monovalent and divalent cations. Since more Ca²⁺ and Mg²⁺ would be adsorbed onto MUS than onto brOT due to the different surface densities of sulphonate, the divalent cations balanced the surplus of sulphonate on MUS. All these observations are consistent with the EPM measurements, which showed that the EPMs in divalent electrolytes were much lower than that in monovalent electrolytes, and there was no significant difference in EPMs between the two AuNPs over the range of CaCl₂ and MgCl₂ concentrations tested (Figure 2-1A and 2-2A) in spite of the difference in the surface densities of sulphonate. Different EPMs and CCCs in NaCl but similar EPMs and CCCs in CaCl₂ for particles with different charge densities, due to the different binding modes as suggested by Yi et al. (Yi and Chen 2011), is now substantiated with the knowledge of exact surface composition and distribution at the molecular level.

Influence of Nano-scale Surface Structure on Electrokinetics and Self-Aggregation of AuNPs

Since brOT and OT had nearly identical hydrophilic to hydrophobic ligand ratios and differed only in the arrangement of hydrophilic and hydrophobic moieties of the ligand shell, they were compared to identify the effect of nano-scale surface structure.

The EPMs of brOT and OT measured in the presence of NaCl, CaCl₂ and MgCl₂ electrolytes at pH 7.0 are shown in Figure 2-1A and Figure 2-2A. The CCC ranges for brOT and OT in NaCl are presented in Figure 2-1B, in Ca²⁺ and Mg²⁺ are in Figure 2-2B. The EPM values of OT in the presence of divalent cations are much less negative than that in NaCl, and the CCC ranges (4 to 8 mM CaCl₂ and 20 to 50 mM MgCl₂) are also much smaller than in NaCl (1000

mM to 1200 mM). The EPMs and CCC range in Ca^{2+} are also smaller than that in Mg^{2+} . These are consistent with what was observed for the MUS and brOT. Less negative EPMs value and decreasing stability at higher electrolytes concentration due to the compression of electrical double layer seems to suggest that the stability of OT can also be qualitatively predicted by the DLVO theory.

When it comes to the comparison between OT and brOT, interesting phenomena arise. First of all, even though OT and brOT are similar in size, ligand composition and surface charge density, and different only in the surface organization of the functional groups, the EPM values of OT are significantly smaller than that of brOT in both monovalent and divalent electrolytes. Secondly, regardless of electrolytes (NaCl , CaCl_2 or MgCl_2), despite its less negative EPMs compared to brOT or MUS, OT has significantly larger CCC ranges. This is obviously not captured by the DLVO theory. Possible causes for the deviation of OT particles were discussed in below sections.

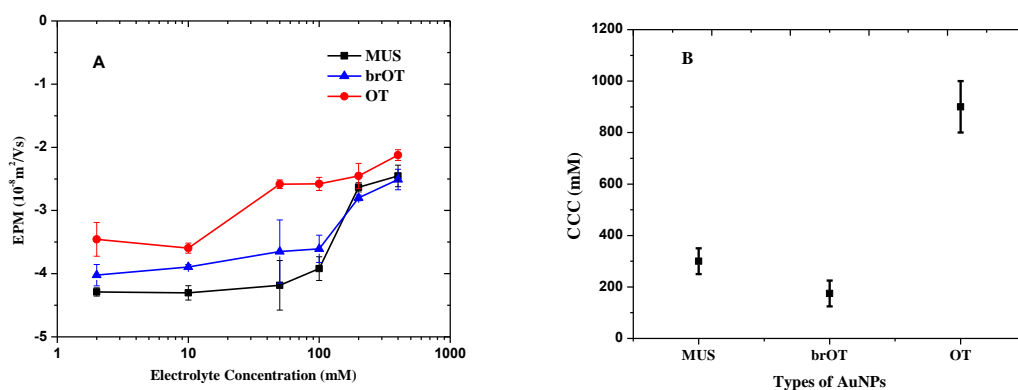


Figure 2-1 EPMs of the three types of AuNPs as functions of NaCl concentrations at pH 7.0. Error bars represent standard deviations (A); The CCCs of the three types of AuNPs measured in NaCl , error bars represent the uncertainty range of CCC (B).

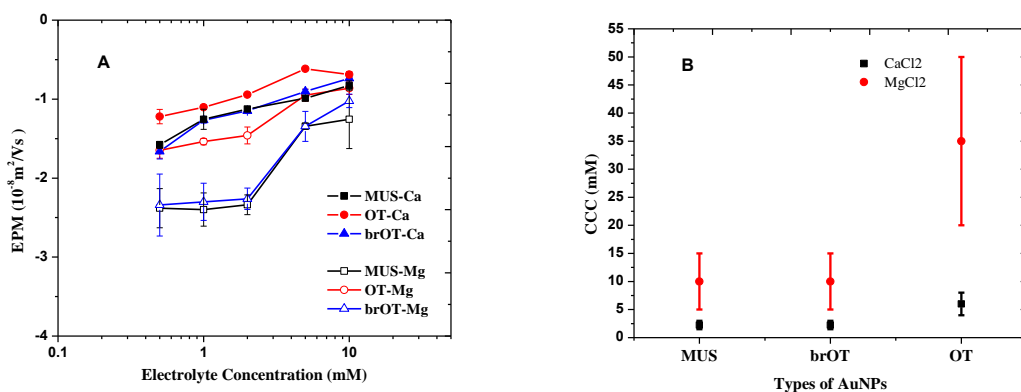


Figure 2-2 EPMs of the three types of AuNPs as functions of CaCl_2 and MgCl_2 concentrations at pH 7.0. Error bars represent standard deviations (A); The CCCs of the three types of AuNPs measured in CaCl_2 and MgCl_2 , error bars represent the uncertainty range of CCC (B).

Adsorption kinetics of AuNPs onto *E. coli* cells

Adsorption kinetics of the three types of AuNPs onto *E. coli* cells was shown in Figure 2-3 with OT particles as the fastest to adsorb onto *E. coli* cells, followed by brOT and MUS. The adsorption rate of a particle onto a surface is mainly determined by its diffusion coefficient (related to its size and density) and the interaction energy between the particle and the surface. Since the sizes of these AuNPs are similar, the different adsorption rates are most likely due to the different interaction energy that contributed from various interfacial forces. The results showed that MUS particles are the most stable and brOT the second, while OT particles are the least stable in terms of particle-surface interaction (*E. coli* cells are ~ 200 times larger than these AuNPs, thus it is being considered as a bulk surface for this interaction). The overall surface charge of *E. coli* cells is negative (ζ -potentials = -31.0 ± 0.4 mV), and the surface charge of the AuNPs is also negative (-30 to -50 mV). For particles with larger charge density, the interparticle electrostatic repulsion and the repulsion between particles and a surface of the same charge will be stronger when compared to particles with smaller charge density, making them more stable. The results are generally consistent with the qualitative prediction by the DLVO theory. The

deviation of OT particles as seen in the particle's self-aggregation was not observed in its adsorption onto bacterial cell surface, which may due to the difference in interfacial forces involved and their relative contribution. Further discussion of the possible interaction mechanism in the context of DLVO theory can be seen in Section 3.6.

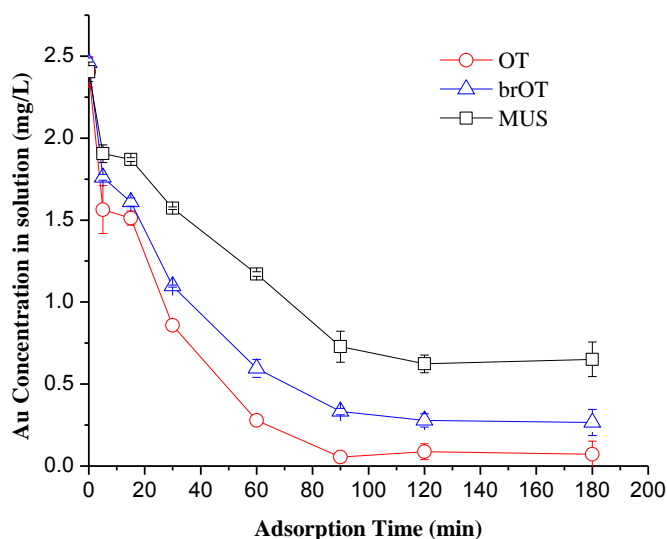


Figure 2-3 Adsorption kinetics of the AuNPs onto *E. coli* in 10 mM phosphate buffer (pH 7.4).

Electrical double layer structure and electrokinetics

The electrokinetic behavior of the three types of AuNPs is closely related with the behavior of water and ion at the interface, which is influenced by the physicochemical properties of the surface. Molecular dynamic simulation of the water distribution around AuNPs with similar alternating stripe-like structure to OT (the polar and nonpolar ligands are 6-mercaptohexan-1-ol and 1-octanethiol instead) has been performed (Kuna et al. 2009). Result showed that there was a cavity that deplete of water molecules formed over the nonpolar stripe and a hydrogen-bond network surrounding the cavity. Although there was no simulation result for particles with all polar ligand and particles with homogeneously-distributed mixing ligands,

no particular water structure would be expected to form besides a thin hydration layer in close contact with the surface. Based on this analysis, possible water distribution around the three types of AuNP was proposed in a qualitative manner (Figure 2-4).

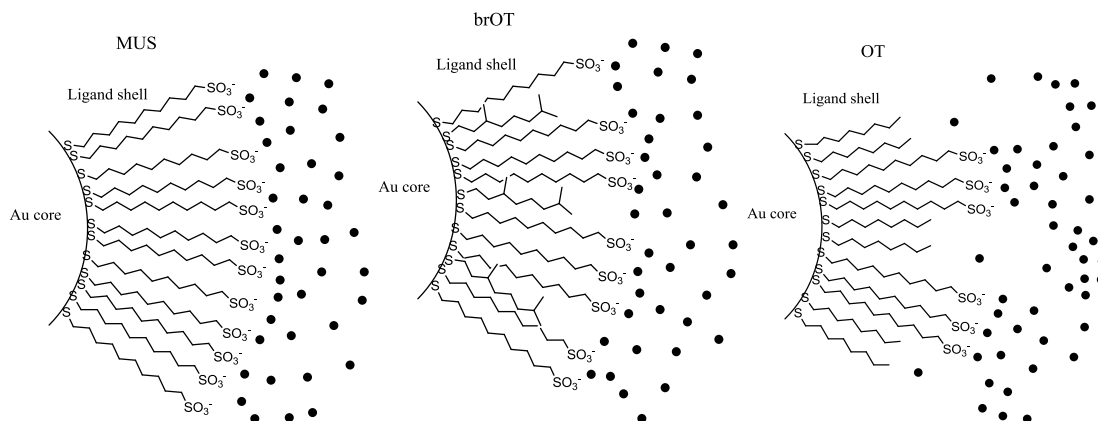


Figure 2-4 Schematic of possible water distribution around the three types of AuNPs.

Several models have been proposed to describe electrical double layer at the solid-liquid interface, including the Gouy-Chapman and the Stern-Gouy-Chapman model. The later considered the adsorption of ions and their finite sizes in the vicinity of a surface (Figure 2-5). Outside the Stern layer is the slipping plane with an operationally defined location. It extends from the solid surface to a location, within which the adhered thin layer of fluid is hydrodynamically stagnant during electrophoresis (Delgado et al. 2007). The diffusion layer extends from the Stern layer. Three potentials pertaining to the three characteristic positions are the potential at the particle surface (ψ_0 , can be calculated based on surface charge density), potential at the boundary between the stern layer and diffusion layer (ψ_s) and the slipping plane (ζ -potential, derived from EPM measurement), respectively. According to the chemical composition of the three types of AuNPs, the corresponding absolute value of ψ_0 should have an order of $MUS > brOT = OT$. If potential distribution throughout the interface and the location of

the slipping plane for the three types of AuNPs behaves consistently, the direct comparison of ζ -potential between the three types of AuNPs can accurately reflect the relative strength of their electrical field.

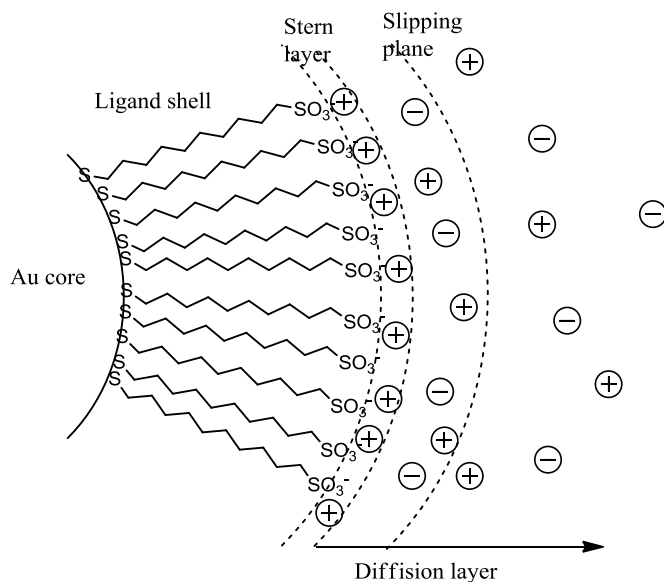


Figure 2-5 Schematic of electrical double layer structure surrounding the MUS particle.

For OT particles, although its charge density is similar to that of brOT, its EPM is relatively smaller than that of brOT. It is likely that the potential distribution of OT is different from the other two types of particles because: 1) the relative adsorption of counter- and co-ions, the hydration of these ions within the Stern layer may differ between them; 2) the position of slipping planes is different from that of the other two due to the presence of cavities and hydrogen bonding shells. As studies have shown that ion distribution at interface is the interplay between surface polarity, hydration and ion sizes (Calero et al. 2011; Horinek and Netz 2007; Parsons et al. 2011), different ion distributions for OT from MUS and brOT can be expected due to its heterogeneous surface at the nanoscale.

Analysis of the particle-particle and particle-surface interactions using DLVO theory

The interaction between two surfaces depends on the types of interactions and their relative contributions involved in the interaction process. Although the DLVO theory oversimplified the complexity of interactions in real systems by involving only electrostatic repulsion and VDW attraction, it has been successfully in predicting colloidal stability in a wide range of systems (Hermansson 1999; Petosa et al. 2010), when these two types of interfacial forces are the predominant interaction forces.

The electrostatic repulsion was commonly calculated based on the three potentials mentioned above (ψ_0 , ψ_s , ζ) with the modulation by solution chemistry (pH and ionic strength), the magnitude of the potentials thus indicate the magnitude of repulsion. DLVO theory can accurately predict the relative colloidal stability when there are changes in the potentials of each type of AuNPs at different ionic strengths. However, when comparing across different particles, the surface-dependent EDL structure complicates the application of the DLVO theory (which assumes uniform potential distribution around the surface and the dominance of the electrostatic interaction). As analyzed above, the insignificance of molecular-scale nonpolar moieties will likely cause brOT to behave like the homogeneously charged MUS. It is inappropriate to directly compare ζ -potential values of the different types of AuNPs because the nanoscale nonpolar stripes on the OT surface can significantly influence the EDL structure. In Chapter 4, the BSA adsorption behavior was to be similar for MUS and brOT, while that of OT particles behaved differently. In addition, the possible presence of non-DLVO forces will also complicate the application of DLVO theory in comparing the stability across particles. They are responsible for the failure of DLVO theory in environmental (Grasso et al. 2002) and biological system (Bostrom et al. 2001). As MD simulation show, a hydrogen-bond network can be developed over

the nanoscale nonpolar stripes (Kuna et al. 2009), this hydration shell would increase the interaction energy barrier that may help enhance the stability of OT particles. Results from our study suggest that, in order to accurately predict the stability of colloids, electrical double layer structure and interfacial forces involved should be carefully evaluated.

Bacterial cell surface is heterogeneous, consisting of a wide range of compounds, including lipids, polysaccharides and proteins (Eboigbodin and Biggs 2008). After the harvest of bacteria from culture medium, the cells were washed by phosphate buffer for three times and then diluted with phosphate buffer to the final concentration (as described in experimental section). The AuNPs were prepared in MilliQ water. The signal intensities of Mg^{2+} and Ca^{2+} (based on ICPMS measurements) between the samples (with cells) and the control/blank (without cells) were not significantly different from each other. Besides, the size of AuNPs in cell-free buffer (suspension of *E. coli* cells for 2 hours followed by removal using centrifugation) was stable for more than 2 hours. All these evidences suggest that, under the tested conditions, divalent cations (either present in the media or release by the cells) are not present in a quantity that is enough to cause detectable/substantial changes to the charge of AuNPs. While the long range electrostatic repulsion determines the accessibility of NPs to bacterial cell surfaces, as AuNPs get closer to the cell surface, some short range interactions like hydrophobic interactions will come into play in determining the final attachment. The short range hydration repulsion formed between the interacting OT particles probably will not exist between OT particle and the cell surface, due to the lack of extended hydration shell on the cell surface and the presence of short range attractions.

Conclusions

Natural surfaces are usually heterogeneous in terms of chemical composition and structure, making it a challenge to quantitatively evaluate and predict surfaces properties and interfacial processes. AuNPs with controllable surfaces serve as a good candidate for studying the effects of surface heterogeneity on certain interfacial processes. In this study, the electrokinetics and colloidal stability of three types of AuNPs of same size and shape but different chemical composition and structure were quantified. AuNPs with randomly distributed polar and nonpolar groups have less negative EPM values, smaller CCC and faster adsorption on *E.coli* than that of AuNPs with homogeneously charged groups, which agree with the DLVO prediction. However, when the ligand composition on the surface of AuNPs are the same, particles with nano-scale striations have less negative EPM values and faster adsorption, but much larger CCC compared to particles with disordered surface. The inconsistency of particles with nano-scale striations in their EPM and CCC reflects the complex EDL structure developed in the vicinity of a surface. Results from the present study suggest that direct comparison of the ζ -potentials of different particles should be made with caution. It is evident that in addition to ligand composition, ligand organization on the surface of AuNPs also plays an important role in controlling the electrokinetic properties and colloidal stability.

CHAPTER THREE

Protein–nanoparticle interactions: the effects of surface compositional and structural heterogeneity are scale dependent

This chapter has been published as Huang, R.; Carney, R. P.; Stellacci, F.; Lau, B. L. T., *Protein-nanoparticle interactions: the effects of surface compositional and structural heterogeneity are scale dependent*. *Nanoscale* 2013, 5(15), 6928-6935.

<http://pubs.rsc.org/en/content/articlelanding/2013/nr/c3nr02117c#!divAbstract>

Reproduced with permission from The Royal Society of Chemistry

Abstract

Nanoparticles (NPs) in the biological environment are exposed to a large variety and concentration of proteins. Proteins are known to adsorb in a ‘corona’ like structure on the surface of NPs. In this study, we focus on the effects of surface compositional and structural heterogeneity on protein adsorption by examining the interaction of self-assembled monolayer coated gold NPs (AuNPs) with two types of proteins: ubiquitin and fibrinogen. This work was designed to systematically investigate the role of surface heterogeneity in nanoparticle-protein interaction. We have chosen the particles as well as the proteins to provide different types (in distribution and length-scale) of heterogeneity. The goal was to unveil the role of heterogeneity and of its length-scale in the particle-protein interaction. Dynamic light scattering and circular dichroism spectroscopy were used to reveal different interactions at pH above and below the isoelectric points of the proteins, which is related to the charge heterogeneity on the protein surface. At pH 7.4, there was only a monolayer of proteins adsorbed onto the NPs and the secondary structure of proteins remained intact. At pH 4.0, large aggregates of nanoparticle-protein complexes were formed and the secondary structures of the proteins were significantly disrupted. In terms of interaction thermodynamics, results from isothermal titration calorimetry

showed that ubiquitin adsorbed differently onto (1) AuNPs with charged and nonpolar terminals organized into nano-scale structure (66-34 OT), (2) AuNPs with randomly distributed terminals (66-34 brOT), and (3) AuNPs with homogeneously charged terminals (MUS). This difference in adsorption behavior was not observed when AuNPs interacted with fibrinogen. The results suggested that the interaction between the proteins and AuNPs was influenced by the surface heterogeneity on the AuNPs, and this influence depends on the scale of surface heterogeneity and the size of the proteins.

Introduction

The interaction between nanoparticles (NPs) and proteins is of great relevance in nanotoxicology and biomedical applications of nanomaterials. Understanding the physicochemical interaction (e.g., interaction forces, binding sites and affinity) and the subsequent effects (e.g., conformation and activity of the interacting proteins, stability and functionality of the NPs) is crucial for understanding the mechanism of toxicity and better design and application of nanomaterials (Nel et al. 2009). The interaction and its subsequent effects were found to be governed by the properties of both nanomaterials and proteins, including size, shape and surface properties (Lacerda et al. 2010; Lundqvist et al. 2008; Meder et al. 2012; Singh et al. 2011).

Surface heterogeneity, the coexistence of different chemistry and structures, is ubiquitous in both natural and engineered systems (Pereira et al. 2009; Tombacz and Szekeres 2006). Proteins themselves, for example, possess exposed patches of polar/nonpolar and negatively/positively-charged chemical groups at molecular scale or nanoscale. In general, it has been found that surfaces with heterogeneous composition exhibit properties that do not change linearly with molar composition as expected by classical arguments (e.g., electrokinetics

(Zembala 2004) interfacial forces (Walz 1998) and surface tension (Drelich et al. 1996)).

However, quantitative relationship between surface heterogeneity and measurable properties has not been established, and the correlation between surface heterogeneity and interfacial processes is not self-evident.

It has been recognized that surface heterogeneity is scale-dependent. For example, colloidal adhesion was found to have heterogeneity-dominated or mean-field behavior depending on the scale of surface heterogeneity (Duffadar et al. 2009). Influence of surface heterogeneity on protein adsorption has been studied at the microscale (Hodgkinson and Hlady 2005; Ta and McDermott 2000). Although the adsorption extent, adsorption kinetics, and surface distribution of proteins are different between homogeneous and heterogeneous surfaces, the mechanisms of protein adsorption are similar, because the scale of surface heterogeneity is much larger than the size of proteins. Little is known about the effects on protein adsorption when surface heterogeneity approaches the nanoscale, comparable to the size of a single protein.

In this study, we investigated the effects of surface compositional and structural heterogeneity on protein-NP interaction using self-assembled monolayer coated AuNPs and two proteins of different sizes and shapes. The AuNPs are nearly identical in size distribution, shape, surface charge and ligand density, with quantitative differences only in the composition and arrangement of ligands on the surface (Jackson et al. 2006; Uzun et al. 2008; Verma et al. 2008). For particles with such nanoscale surface features, interesting properties regarding wettability (Centrone et al. 2008), interfacial energy (Kuna et al. 2009) and cell penetration (Verma et al. 2008) were found to be dependent on surface composition and structure. Thus, it is important to study how these properties correlate with the adsorption behavior of proteins (ubiquitin and

fibrinogen). These proteins were selected for this study because of their abundance in animal plasma and differences in size, shape, and properties.

Complementary to previous studies that used particles with different sizes and shapes but usually homogeneous surface chemistry, this study unveils the unique importance of the size of surface functionality (both on the NPs and on the proteins) in NP-protein interactions. The results of this work develop the emerging concept of “scale dependency” systematically by demonstrating that the effects of surface heterogeneity are dependent on the relative scale between protein and the NP surface feature. The novel findings presented here are crucial in 1) predicting the subsequent biological activity of NP-protein complexes and 2) improving the design of novel nanomaterials for applications in various biological and environmental systems (e.g., drug delivery, protein purification, and treatment of water and wastewater).

Adsorption was performed in defined aqueous solution at pH above and below the isoelectric point (IEP) of ubiquitin and fibrinogen to study the effects of surface charge, structure and exposed functional groups from proteins. The different sizes and shapes of the selected proteins and their different properties under the two pHs create different types of heterogeneity.

Surface charge of the AuNPs and the proteins was characterized by electrophoretic mobility measurements. The adsorption process was manifested through size change of the AuNPs and was monitored by dynamic light scattering (DLS). Isothermal titration calorimetry (ITC) was used to explore the thermodynamics behind the interaction. The conformational change of the proteins was monitored by circular dichroism (CD) spectroscopy. Results from individual technique were integrated to understand the mechanism of interaction.

Materials and Methods

Preparation of AuNPs and Protein Suspensions

The three types of ligand-coated AuNPs used in this study have been thoroughly characterized with respect to their size, surface chemical composition and structure. (Uzun et al. 2008; Verma et al. 2008) AuNPs are coated with (1) all negatively charged, sulfonated alkanethiols (11-mercapto-1-undecanesulfonate, MUS), (2) a 2:1 molar mixture of MUS and 1-octanethiol (OT) (now referred to as 66-34 OT), and 3) a 2:1 molar mixture of MUS and a branched, apolar version of OT (3,7 dimethyl octane 1-thiol, brOT) (66-34 brOT). Previously we have shown that the 66-34 OT AuNPs exhibit unique properties due to the ordering of molecules in its ligand shell. To prepare the AuNP stock solutions, around 6 mg of AuNP powder was added into 20 ml of ultrapure water (Millipore Simplicity, >18 M Ω -cm), the solutions were sonicated in an ultrasonic bath (VWR, B2500A-MT) for 30 min. After ultrasonication, the AuNP suspensions were centrifuged at 9 000 g (Avanti A-J., Beckman-Coulter, Brea, CA) for 30 min in order to remove nondispersive aggregates in the suspensions. Mass concentration of AuNPs was quantified by a Perkin Elmer ELAN 9000 inductively-coupled plasma mass spectrometer (ICP-MS) (Waltham, MA), from which the molar concentration was derived.

Ubiquitin from bovine erythrocytes (lyophilized powder) and fibrinogen from human plasma (lyophilized powder) were purchased from Sigma and used without further purification. The stock solution of the proteins was prepared in 10 mM sodium phosphate buffer solution (PBS) of pH 7.4 and stored at 4 °C, and the stock solution was used within one week. Buffers at pH 4.0 and 7.4 were prepared using 10 mM sodium acetate-acetic acid and PBS, respectively.

Surface Charge Measurements

The electrophoretic mobility (EPM) of the AuNPs and proteins at various pHs were measured using a Malvern Zetasizer (Nano ZS, Malvern Instruments, UK), and converted to ζ -potentials using the Smoluchowski equation. Proteins and AuNPs solutions for EPM measurements were prepared by diluting the stock solution into their respective buffer solutions. The NP concentrations for EPM measurements were around 0.1~0.2 times of the concentrations of the corresponding AuNP stock suspensions. The concentration of ubiquitin and fibrinogen were around 1 $\mu\text{mol/L}$. Around 600 μL solution was pipetted into the DTS 1060C disposable capillary cell. Six measurements were conducted for duplicate samples at each condition.

Dynamic Light Scattering

The hydrodynamic diameter change of the AuNPs in the absence and presence of proteins was measured using the Zetasizer Nano ZS with a fixed detector angle of 173° . Specifically, at pH 7.4, protein solution was sequentially added into the AuNP suspension (around 0.05 $\mu\text{mol/L}$) to reach certain final protein/AuNP molar ratios (ubiquitin: 0 to 100; fibrinogen: 0 to 10). The mixture was incubated for 30 min before DLS measurement and 15 measurements were taken. The maximum size change was chosen for comparison. At pH 4.0, a protein to AuNPs molar ratio of 10:1 was chosen. DLS measurements started immediately after the addition of proteins and 15 measurements were taken. The results were the average of at least two separate experiments.

Circular Dichroism Spectroscopy

CD measurements were undertaken by a Jasco J-810 spectropolarimeter (Easton, MD) with a 2 mm path length rectangular quartz cell at room temperature (22°C). The CD spectra were recorded from 190 to 260 nm and each spectrum was an average of 5 scans.

The test solutions for CD were prepared by mixing the proteins and AuNPs in their respective buffer and then incubated at 4 °C for at least 30 min before the spectra were collected. The concentration of ubiquitin and fibrinogen was fixed at 1 $\mu\text{mol/L}$ and 0.5 $\mu\text{mol/L}$, respectively, and the AuNPs concentration ranged from 0 to 0.05 $\mu\text{mol/L}$.

Isothermal Titration Calorimetry

ITC measurements were performed on a MicroCal ITC200 system (GE Healthcare). Both ubiquitin and fibrinogen was dialyzed overnight against 10 mmol/L sodium phosphate buffer (renewed two times) at pH 7.4, and the AuNPs were dissolved in the last dialysate (sonicated, then centrifuged at 9000 rpm for 15 min). The titration experiment involved 40 injections (1 μL per injection) of proteins (ubiquitin concentration = 1 m mol/L and fibrinogen concentration = 80 $\mu\text{mol/L}$) at 150 sec intervals into the sample cell (volume = 200 μL) containing the AuNPs solution (MUS con. = 7.03 $\mu\text{mol/L}$, 66-34 brOT con. = 8.43 $\mu\text{mol/L}$ and 66-34 OT con. = 7.73 $\mu\text{mol/L}$). The reference cell was filled with 10 mmol/L sodium phosphate buffer. During the experiment, the sample cell was stirred continuously at 1000 rpm. At least two separate experiments were conducted for each protein-AuNP pair.

The heat of protein dilution in the buffer alone was subtracted from the titration data (both normalized to 0) for each experiment. The data were analyzed to determine the binding stoichiometry (n), association constant (K_s), and other thermodynamic parameters of the reaction using the coupled Origin software. The reported thermodynamic parameters were an average of duplicate experiments.

Results and Discussion

Characterization of the AuNPs and Proteins

Detailed information regarding the synthesis and characterization can be found in our previous studies (Uzun et al. 2008; Verma et al. 2008). These three types of AuNPs were confirmed to be similar in size and shape, to the ones previously synthesized (Uzun et al. 2008; Verma et al. 2008). The core diameter of the three AuNPs was 4.4 ± 0.4 nm based on the size distribution determined by TEM (Appendix D). The ligand shell has a thickness of 1.5 nm, making the diameter of the whole particle around 7.4 nm. The ligand shell composition was based on ^1H NMR analysis of the ligands after decomposition of the gold core by KCN (Liu et al. 2012) and the ligand distribution was based on scanning tunneling microscopy (STM) studies performed in previous studies (Uzun et al. 2008; Verma et al. 2008). These characterizations showed that MUS particles were homogeneously coated with MUS only, 66-34brOT were coated with randomly distributed MUS and brOT, while MUS and OT ligands were separated into stripe-like domains (~ 1 nm) on the surface of the 66-34OT particles. The hydrodynamic diameter (d_h) of the AuNPs and proteins were measured by dynamic light scattering (DLS) and the results shown in Figure 3-1A. Ubiquitin, a compact protein that consists of only 76 amino acids (1.57 nm in diameter) (Uversky 1993; Vijaykumar et al. 1987), was too small to be reliably quantified by DLS. Fibrinogen is a high molecular weight, elongated protein (47.5 nm long), with three polypeptide domains that are around 5~6 nm in diameter (Fuss et al. 2001). Its d_h was 24.7 ± 0.4 nm. The d_h of fibrinogen was consistent with previous studies (Vijaykumar et al. 1987; Wasilewska et al. 2009). All proteins and AuNPs were stable in the buffer for more than 24 hours.

The electrophoretic mobility (EPM) of each of the particles and proteins was measured and converted to ζ -potential values (Figure 3-1B). For the AuNPs, the terminal sulfonate groups determine the surface charge of their protecting SAMs, the particles remain negatively-charged at the two pHs. Since the IEP of ubiquitin and fibrinogen are around 6.8 and 5.8 (Rossi et al. 2010; Wasilewska et al. 2009), respectively, the overall surface charge of ubiquitin and fibrinogen would be positive at pH 4.0 and negative at pH 7.4.

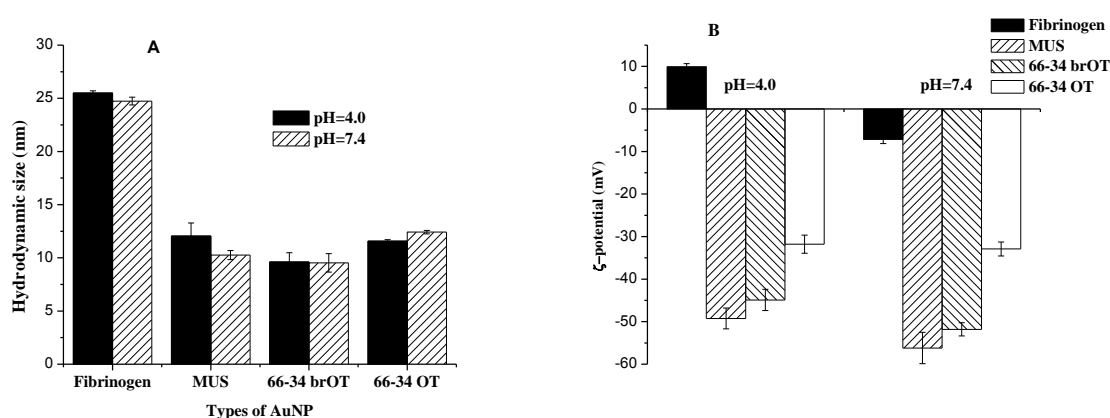


Figure 3-1 (A) Hydrodynamic diameter of unbound fibrinogen and AuNPs at pH 4.0 and pH 7.4. (B) ζ -potentials of proteins at pH 4.0 and pH 7.4.

Stability of AuNP-protein Complexes

DLS has been frequently used to characterize protein-nanoparticle interaction and to reveal their interaction mechanism (Hackley et al. 2011; Jans et al. 2009). The size change of AuNPs due to the addition of proteins was presented in Figure 3-2. It was found that the system behaved differently at the two pHs. At pH 4.0, size change of more than 100 nm was observed in all types of AuNPs in the presence of both types of protein (Figure 3-2A). Considering the relatively small size of the AuNPs and proteins, it is evident that large aggregates were formed at pH 4.0. It is likely that they were aggregates of AuNP-protein complexes connected by the denatured proteins initially coated on the particle surface (disruption of the secondary structure

of proteins due to adsorption at pH 4.0 as shown in the following section). It is noteworthy that the different size changes between different types of AuNPs may not simply be the result of AuNP surface difference, because the subsequent protein-protein interactions may have little relevance with the AuNPs. Thus, the result of these size changes should not be over-interpreted. At pH 7.4, the size changes following the addition of ubiquitin and fibrinogen were around 2 nm and 20 nm, respectively, which is comparable to the size of the proteins (Figure 3-2B). These size changes suggested that the AuNPs were probably coated with a monolayer of proteins at pH 7.4. These monolayer protein-coated AuNPs were found to be stable by DLS even after 24 hours (± 0.5 nm).

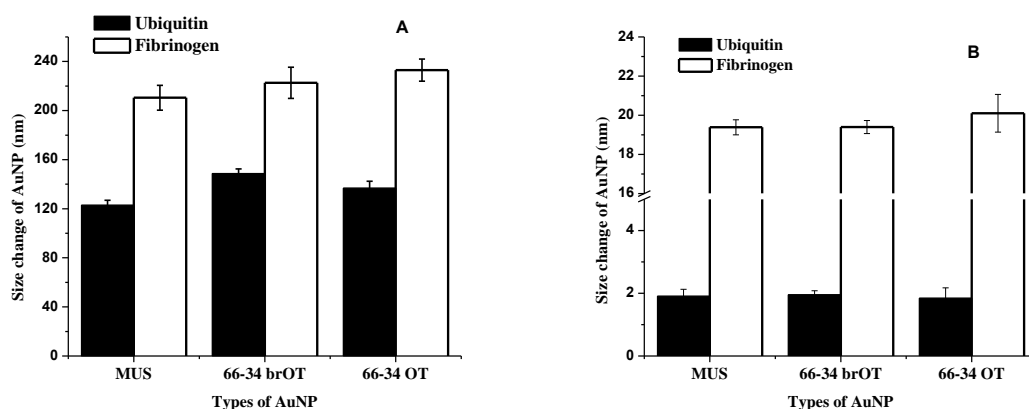


Figure 3-2 Hydrodynamic diameter change of AuNPs following the addition of proteins at pH 4.0 (A) and pH 7.4 (B), error bars represent the variations between duplicate experiments.

The different behaviors at pH above and below proteins' IEP reflect the different interaction modes between the proteins and AuNPs under different conditions. Several factors should be considered in order to identify the interaction modes. First, the overall surface charge of the proteins changed from negative to positive as pH changed from 7.4 to 4.0; second, proteins are big molecules with complex structure and heterogeneous surface, they consist of a long chain of amino acids with different side chains organized into three dimensions of structure

and their surface consists of a mixture or patches of polar/nonpolar functional groups; third, the structure of protein may change as a function of pH (Carter 1994). Therefore, the AuNP-protein interface is rather dynamic, with the interaction mode depending on the surface composition and structure of the proteins and the AuNPs, which is modulated by factors like pH and ionic strength.

All these considerations motivated the following application of spectroscopic and thermodynamic techniques to further understand protein-AuNP interactions.

Conformational Change of Proteins

CD spectroscopy is a powerful analytical tool to monitor the conformational change of proteins as a result of changes in solution chemistry (e.g., pH, temperature or ionic strength) or interactions with molecules or adsorption onto particle surface. It has been frequently used to measure the structural changes induced in proteins due to interaction with nanomaterials (Cukalevski et al. 2011; Dong et al. 2007; Singh et al. 2011).

In this study, the α -helix structure of both proteins, which is manifested by the negative peaks at around 208 nm and 222 nm in CD spectra, was monitored. At pH 7.4, there was no significant change of the ellipticity values of the proteins in the presence of all three types of AuNPs, which indicated that the proteins maintained its conformation after adsorption onto the surface of AuNPs (Figures 3-3 (right) and 3-4 (right)). Since the protein conformation remained intact, they were stable against further interactions with each other. At pH 4.0, in the presence of MUS and 66-34 brOT, the ellipticity significantly decreased and the peaks at 208 nm and 222 nm disappeared, which is a sign of disruption of the secondary structure (Figures 3-3 and 3-4 (left)). While at pH 4.0, the structural change for all types of proteins in the presence of 66-34 OT was less significant than that of MUS and 66-34 brOT.

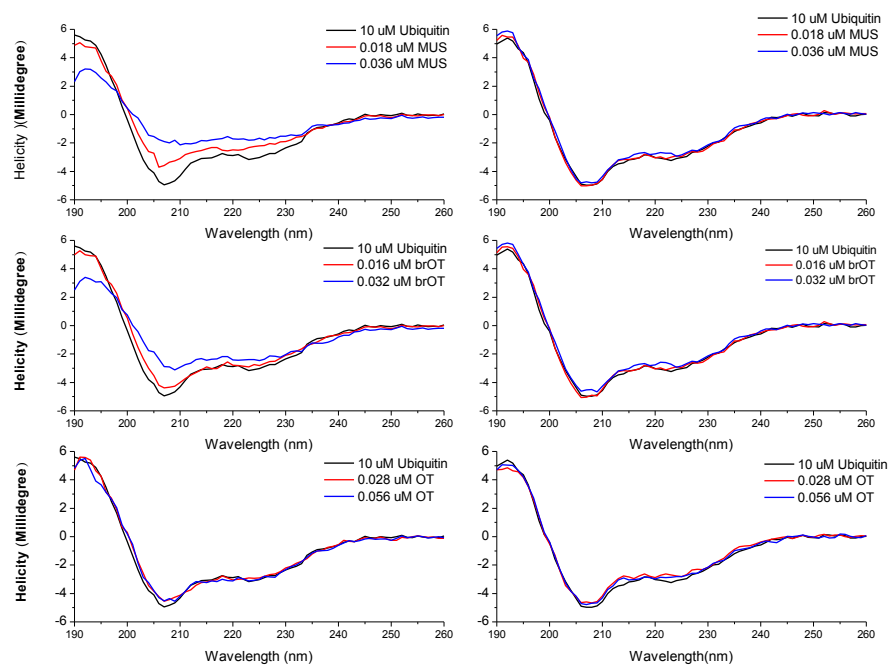


Figure 3-3 CD spectra of ubiquitin at pH 4.0 (left) and 7.4 (right) in the presence of varying AuNP concentrations.

In this study, AuNPs were coated by thiols with long carbon chains and the surface properties are only determined by the ligand shell. The negative charge of these SAM-coated AuNPs under the tested pHs was determined by the terminal $-\text{SO}_3^-$ groups. The interaction between proteins with these AuNPs was most likely directed by the positively-charged regions of the proteins toward the negatively-charged AuNP surface. As pH decreased from 7.4 and 4.0, more residues on the protein surface were protonated, thus there were more positively-charged regions available for interaction. This may have resulted in a tighter interaction between the proteins and AuNPs, and the protein structure was more vulnerable to disruption.

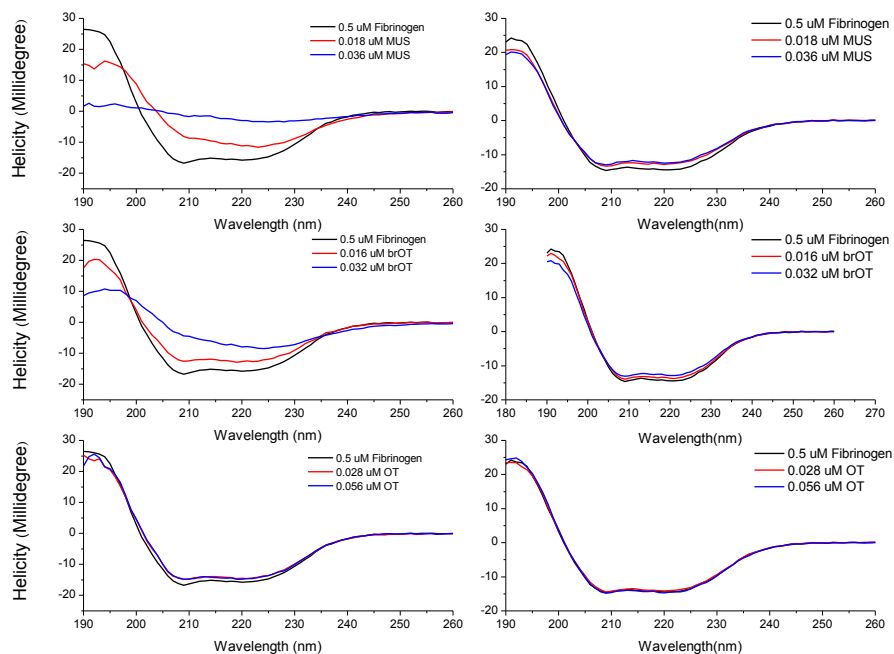


Figure 3-4 CD spectra of fibrinogen at pH 4.0 (left) and 7.4 (right) in the presence of varying AuNP concentrations.

With information on conformational change, it can be anticipated that large aggregates formed under opposite charge condition was because AuNPs disrupted the structure of the first adsorbed layer of proteins. The disrupted proteins could interact with other unbound proteins or protein-coated AuNPs, thus initiate aggregation.

Isothermal Titration Calorimetry and Binding Thermodynamics of NP-Protein Interactions

ITC directly measures the enthalpy changes and binding stoichiometry between NPs and proteins in solution, from these other thermodynamic quantities can be derived. These parameters reveal the mechanism of interaction in a quantitative manner, which makes ITC an excellent complement to other techniques. Therefore, it has been widely used to characterize protein-NP interaction (Cedervall et al. 2007; De et al. 2007; Lindman et al. 2007; Singh et al.

2011). Protein interactions with particles and surface is a complex process that not only involves the synergetic work of noncovalent forces including Van der Waals force, hydrogen bonding, electrostatic and hydrophobic interaction, but also involves the desolvation of both NPs and proteins and solvation of newly formed complexes (De et al. 2007). Depending on the structure of the proteins and the properties of the interacting surface, the relative importance of each noncovalent force is altered, and they contribute differently to the heat profile measured by ITC. Noncovalent interactions are exothermic ($\Delta H < 0$), while the disruption of structurally well-defined solvent shells is endothermic ($\Delta H > 0$).

The heat profiles of the titration of the two proteins into the three types of AuNPs are presented in Figure 3-5 and Appendix F. The heat change profiles were satisfactorily fit using isothermal functions to a model describing a single set of binding sites and best-fit parameters were calculated using nonlinear least-squares fitting (Tables 1 and 2). The thermodynamic quantities showed that the adsorption of ubiquitin onto all types of AuNPs featured a favorable enthalpy change ($\Delta H < 0$), which was offset partially by unfavorable entropy loss ($\Delta S < 0$), resulted in an overall negative free energy change ($\Delta G < 0$). Considering that $-\text{SO}_3^-$ terminal group covered the entire MUS surface and 67% of the surface of the other two types of AuNPs, the adsorption of ubiquitin onto AuNPs seems to be primarily driven by electrostatic interaction.

Although the interactions of the proteins with all three types of AuNPs were consistently exothermic, differences existed between different types of proteins and AuNPs as shown in the thermodynamic parameters derived from the heat profiles (Tables 3-1 and 3-2). For ubiquitin adsorbed onto MUS and OT particles, although the associated constant, free energy change, and enthalpy change were not significantly different from each other, there were roughly 6 ubiquitins

associated with MUS and only 3 ubiquitins attached per 66-34OT particle. The thermodynamic parameters (ΔG , ΔH and $T\Delta S$) were all normalized per titrant (e.g., the proteins). The

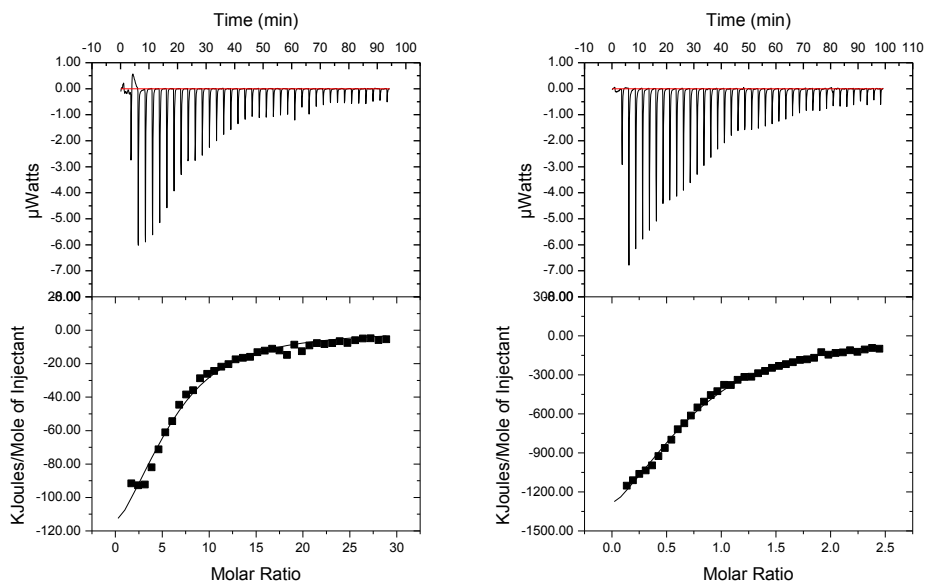


Figure 3-5 ITC data from the titration of 1 mmol/L ubiquitin (left) and 80 $\mu\text{mol/L}$ fibrinogen (right) into 7.03 $\mu\text{mol/L}$ MUS AuNP. Heat flow versus time during injection of proteins at 25 $^{\circ}\text{C}$ and heat evolved per mole of added proteins (corrected for the heat of protein dilution) against the molar ratio (protein/AuNP) for each injection are shown at the top and bottom, respectively. The line is the model fitting (The data corresponding to the heat of dilution of protein were shown in Appendix F).

similarity in these parameters suggests that the ubiquitins were adsorbed equivalently onto MUS and 66-34 OT. The similarity and difference between MUS and 66-34 OT in their interactions with ubiquitin is most likely originated from the difference in their surfaces. MUS particles were homogeneously coated with only 11-mercapto undecanesulfonate (MUS) ligands that ends with $-\text{SO}_3^-$, ubiquitin “recognized” no difference on the surface of the particles and all the ubiquitins attached equivalently. In contrast, the 66-34 OT particles coated with a mixture of MUS and octanethiol (OT) were found to form stripe-like domains in the particles’ ligand shell (Uzun et al. 2008). It is likely that ubiquitin selectively adsorbed close to the $-\text{SO}_3^-$ domains consequently

finding fewer available sites as compared to that of MUS. For ubiquitin adsorbed onto 66-34 brOT particles, the enthalpy and entropy change is smaller than that of the other two systems, while there were more ubiquitin (~9) attached to each 66-34 brOT particle (Table 3-1). Compared to MUS particles with only one type of ligand and 66-34 OT particles with stripes at nanoscale on the surface, 66-34 brOT particles have a mixture of MUS and 3,7-dimethyloctanethiol (brOT) that randomly distribute on its surface, forming molecular scale heterogeneity. Although ubiquitin also “recognized” no difference on the surface of 66-34 brOT (with a mixing of -CH₃ and -SO₃⁻) since the contact area is possibly much larger than the molecular scale heterogeneity, it may use a different site to adsorb onto 66-34 brOT compared to its adsorption onto MUS and 66-34 OT particles, which with only -SO₃⁻ available for adsorption. This is possibly responsible for the lower enthalpy and entropy in 66-34 brOT compared to the other two.

Table 3-1 Thermodynamic quantities of ubiquitin-AuNPs interaction derived from ITC (Error bar represents the variation between duplicate experiments).

NPs	K_s ($\times 10^5 \text{ M}^{-1}$)	$-\Delta G$ ($\text{kJ}\cdot\text{mol}^{-1}$)	$-\Delta H$ ($\text{kJ}\cdot\text{mol}^{-1}$)	$-T\Delta S$ ($\text{kJ}\cdot\text{mol}^{-1}$)	n
MUS	0.57 \pm 0.06	27.3 \pm 0.3	149.5 \pm 27.1	122.2 \pm 27.4	6.18 \pm 0.82
66-34 brOT	1.14 \pm 0.35	28.8 \pm 0.8	90.8 \pm 5.4	62.1 \pm 4.9	9.68 \pm 1.37
66-34 OT	0.66 \pm 0.09	27.5 \pm 0.2	195.0 \pm 5.7	167.0 \pm 5.5	3.31 \pm 0.57

For fibrinogen adsorbed onto the three types of AuNPs, the association constant, enthalpy and entropy change are about an order of magnitude larger than that of ubiquitin, and about two AuNPs attached to one fibrinogen. This is consistent with the results from a recent study, which also reported a AuNP/Fibrinogen molar ratio of 2:1 for 7 nm AuNPs (Deng et al. 2012). Interestingly, there is no significant difference between the adsorption onto the three types of AuNPs (Table 3-2). It is probably due to the relatively larger size of fibrinogen (340 kD)

compared to ubiquitin (8.5 kD). For each fibrinogen molecule, there were more electrostatic interactions involved compared to each ubiquitin molecule, as it wrapped two AuNPs, so the enthalpy and entropy change is much larger than that of ubiquitin. Since the contact area between fibrinogen and the AuNPs is much larger than the surface features of the AuNPs, fibrinogen “recognized” no difference on the surfaces of both 66-34 brOT and 66-34 OT. As a result, they interacted in the same way as that between fibrinogen and the homogeneously charged MUS.

Table 3-2 Thermodynamic quantities of fibrinogen-AuNPs interaction derived from ITC (Error bar represents the variation between duplicate experiments).

NPs	K_s ($\times 10^5 \text{ M}^{-1}$)	$-\Delta G$ ($\text{kJ}\cdot\text{mol}^{-1}$)	$-\Delta H$ ($\text{kJ}\cdot\text{mol}^{-1}$)	$-T\Delta S$ ($\text{kJ}\cdot\text{mol}^{-1}$)	n
MUS	6.46 \pm 3.29	31.64 \pm 0.89	1786.0 \pm 182.4	1753.7 \pm 183.3	0.78 \pm 0.10
66-34 brOT	8.05 \pm 0.73	57.0 \pm 27.7	1702.0 \pm 364.8	1645.0 \pm 337.1	0.83 \pm 0.11
66-34 OT	8.49 \pm 0.89	33.7 \pm 0.5	1704.0 \pm 31.1	1670.3 \pm 31.6	0.54 \pm 0.01

Scale-dependency of Surface Heterogeneity

Results from the present study demonstrated that the structural and compositional heterogeneity on the surface of both proteins and NPs have great influence on their interaction. For proteins, their stability in electrolytes can be largely attributed to the heterogeneity, as the surface heterogeneity may provide them forces other than Van der Waals force and electrostatic interaction (Bostrom et al. 2001; Rowe 2001).

At neutral pH, although there are positively-charged residues exposed and available for interacting with negatively-charged surface, the negatively-charged residues can help to maintain the repulsion between the protein and the negatively-charged particle. As pH decreased and most carboxyl groups became protonated (e.g., side chain of aspartic acid and glutamic acid), the surface charge heterogeneity was reduced, resulted in a tighter interaction between the proteins and AuNPs and the disruption of protein structure.

The protein adsorption results from the present study demonstrated the scale dependency of protein adsorption, and the scale is determined by both protein and the interaction surface. The size and shape of protein, and the size of surface features determine the potential contact area between them. The size of ubiquitin is around 1.5 nm and the contact area is possibly at the sub-nano scale, which is comparable to the surface feature on the particle surface. The stripe-like domain of the 66-34 OT particle is around 0.5 nm and the surface feature of 66-34 brOT is at molecular scale. The protein “recognizes” the difference between these surfaces and shows different adsorption behaviors, as the ITC results suggested. However, when the size of protein or the contact area is much larger than the surface feature, like fibrinogen in this case may wrap around the particles, the protein “recognizes” no difference between these surfaces, and the adsorption behavior will be very likely the same.

Similar scale-dependent protein adsorption phenomenon has recently been explored theoretically through molecular dynamic simulation (Hung et al. 2013; Hung et al. 2011). For particles similar to those used in this study, the amphiphilic side chains of lysine and arginine were found to respectively direct the interaction of cytochrome C and lysozyme with the particles, and the interaction modes (residues in contact with the particle surface and the geometry of the adsorbed protein) depend on the size of the surface structure.

Conclusions and Implications

The interactions between two common serum proteins (ubiquitin and fibrinogen) and three types of AuNPs were investigated. Both ubiquitin and fibrinogen can adsorb onto the three types of AuNPs at pH above and below the IEPs of the proteins, and the interaction may be predominantly electrostatic and through some positive patches of the proteins (e.g., sites with side chains of lysine or arginine). However, surface charge heterogeneity strongly affected the

interaction and the structure of the proteins. The protonation or deprotonation as a result of pH change modulates the surface charge of proteins, which determines the structural stability of the adsorbed proteins.

The adsorption of ubiquitin and fibrinogen on the AuNPs were found to be influenced by the surface chemistry and structure of the AuNPs, especially the scale of surface heterogeneity. Ubiquitin, a small protein that has comparable size to the surface features of the AuNPs, adsorbed differently (in terms of binding stoichiometry and thermodynamics) onto 1) AuNPs with charged and nonpolar terminals organized into nano-scale structure (66-34 OT), 2) AuNPs with randomly distributed terminals (66-34 brOT), and 3) AuNPs with homogeneously charged terminals (MUS). Fibrinogen, which is much larger than the surface features of the AuNPs, possessed similar adsorption behaviors onto the three types of AuNPs. Results from this study demonstrated the importance of surface structure in addition to surface chemical composition in determining NP-protein interactions.

CHAPTER FOUR

Effects of Surface Compositional and Structural Heterogeneity on Albumin-Nanoparticle Interactions: Protein Coronas or Protein Clouds?

Abstract

As nanoparticles (NPs) enter into biological systems, they are immediately exposed to a variety and concentration of proteins. The physicochemical interactions between proteins and NPs can be controlled by the surface properties of the NPs. In this study, the interactions between bovine serum albumin (BSA) and gold nanoparticles (AuNPs) with similar chemical composition but different surface structures were investigated to identify the effects of surface heterogeneity. Depending on the surface structure of AuNPs, different interaction modes and BSA conformations were found by dynamic light scattering, circular dichroism spectroscopy, fluorescence quenching and isothermal titration calorimetry (ITC). BSA adopted a “side-on” conformation on AuNPs with charged groups or randomly distributed polar and nonpolar groups and an “end-on” conformation on AuNPs with alternating stripe-like domains of polar and nonpolar groups. ITC demonstrated that the adsorption of BSA onto AuNPs with randomly distributed polar and nonpolar groups was primarily driven by electrostatic interaction and all BSA were adsorbed in the same process. The adsorption of BSA onto AuNPs covered with alternating domains of polar and nonpolar groups was a combination of different interactions. The loose protein coating as a result of the “end-on” conformation was termed “protein clouds”, to distinguish from the tight “protein corona” that is commonly identified with nonspecific protein adsorption on NPs. Results suggested that surface structural heterogeneity, as well as

chemical heterogeneity, is important in determining the protein-NP surface interaction and subsequent protein conformation.

Introduction

The interaction between nanoparticles (NPs) and proteins is a topic of high relevance for the medical application of NPs (Koegler et al. 2012; Nel et al. 2009). As NPs enter into biological system, they are exposed to a wide range of proteins of different amounts, and it is the NP-protein complexes rather than the NPs alone that would determine the biological responses (Lynch et al. 2007). Understanding the nature of interaction (e.g., interaction forces, binding sites, and affinity) and the subsequent effects (e.g., conformation and activity of the interacting proteins, stability and functionality of the NPs) are crucial for better design and handling of nanomaterials in a biological environment.

It has been shown that proteins can bind specifically or non-specifically to NPs suspended in a biological fluid (Rana et al. 2010), to form a tightly bound, yet dynamic surface coating known as the “protein corona”. The initial adsorption and subsequent exchange of proteins in the corona change over time as a function of the affinity of the proteins for the NP. The composition of protein corona is dependent on the NP size (Lundqvist et al. 2008), shape (Singh et al. 2011) and surface properties, including chemical composition (Meder et al. 2012), surface charge (Chen et al. 2011) and surface hydrophobicity (Cedervall et al. 2007). Typically, the mono- or bi-layer of proteins formed on NPs is described as the “hard corona” due to the slow timescale of protein exchange and strong binding energies associated with the complex (Walczyk et al. 2010). Following protein adsorption, this corona is “read” by the cellular surface machinery to direct subsequent NP-cell interactions (Lynch et al. 2007). Ultimately, the long-lived hard protein corona has been found to determine the fate of the NP upon transfer between

biological fluids (e.g., plasma, cytoplasm) (Lundqvist et al. 2011). Therefore, surface properties of NPs can be manipulated to bind proteins selectively (Gagner et al. 2012; Rana et al. 2010).

Surface heterogeneity, the coexistence of different chemistry and structures, is common in both natural and engineered systems. Although numerous studies have investigated the effects of surface properties on protein adsorption, few have targeted the influence of surface heterogeneity (Hodgkinson and Hlady 2005; Ta and McDermott 2000). Little is known about how surface heterogeneity at the nanoscale (which is comparable to the size of proteins) affects the adsorption of proteins and the resulting protein coating.

AuNPs, coated with binary mixture of hydrophobic and hydrophilic thiolated ligand molecules have been recently synthesized, and have been shown to have a ligand shell formed of stripe-like domains of alternating hydrophobic/hydrophilic composition (Jackson et al. 2006; Uzun et al. 2008; Verma et al. 2008). Interestingly, these stripe-like domains have a characteristic thickness on the order of a single nanometer, leading to surface heterogeneities commensurate with the ones found on proteins. This unique structure has been shown to possess interesting properties regarding wettability (Centrone et al. 2008), interfacial energy (Kuna et al. 2009) and cell membrane penetration (Verma et al. 2008). In the latter case, the role of the structure has been established by comparing particles that are nearly identical in size, size distribution, shape, surface charge, ligand density, and ligand composition, with differences only in arrangement of ligands on the surface. Only particles with striped ligand shells were shown to penetrate cell membranes in an energy-independent way, while particles with a random arrangement of ligand in their ligand shell show penetration in energy-dependent pathways.

A similar comparison between particles with nearly identical shape, size, and composition but differing only in the ligand shell morphology is ideal for studying the effects of

surface heterogeneity on protein adsorption. Two types of AuNPs were used in this study. The MUS-type AuNPs are coated with either 1) all negatively charged, sulfonated alkanethiols (11-mercapto-1-undecanesulfonate, MUS); 2) a 2:1 molar mixture of MUS and a branched, apolar version of OT (3,7 dimethyl octane 1-thiol, brOT) (MUS/brOT); and 3) a 2:1 molar mixture of MUS and 1-octanethiol (OT) (now referred to as MUS/OT). The MPA-type AuNPs are: MPA/brOT and MPA/OT, resembling MUS/brOT and MUS/OT in their surface organizations of the coating ligands, with the negatively-charged MUS substituted for mercaptopropionic acid (MPA). By using AuNPs with similar surface structure but different charged functional groups (i.e., with -COO^- terminals instead of -SO_3^-), we attempted to confirm that the protein adsorption behavior is dependent on structural heterogeneity and independent of particular polar groups.

A combination of dynamic light scattering (DLS), circular dichroism (CD) spectroscopy, fluorescence quenching and isothermal titration calorimetry (ITC) was applied to characterize the interaction between BSA and AuNPs with similar surface chemical composition but different surface organization. DLS was used to monitor the increases in AuNP size due to self-aggregation or BSA adsorption. CD spectroscopy characterized the secondary structure of adsorbed BSA. Fluorescence quenching revealed the possible binding sites by quantifying the quenching of fluorescence from certain chromophores by AuNPs. ITC characterized the underlying thermodynamics of the interaction. Results from individual techniques were integrated to understand the mechanism of interaction.

Materials and Methods

Preparation of AuNPs and Protein Suspension

The synthesis of SAM-coated AuNPs with diverse surface composition and structures can be found in previous studies (Jackson et al. 2006; Jackson et al. 2004; Uzun et al. 2008) and

in the Appendix G. To prepare the stock suspensions of AuNPs, the AuNP powder was added into either ultrapure water (Millipore Simplicity, $>18\text{ M}\Omega\text{-cm}$) or dialyzed sodium phosphate solution. The suspensions were sonicated in an ultrasonic bath (VWR, B2500A-MT) for 30 min. After ultrasonication, the AuNP suspensions were centrifuged at 9 000 rpm for 15 min (Eppendorf 5417c centrifuge) to remove non-dispersive aggregates from the suspensions. Molar concentration of AuNPs was derived after determining the mass concentration using a Perkin Elmer ELAN 9000 inductively-coupled plasma mass spectrometer (ICP-MS) (Waltham, MA).

Bovine serum albumin (BSA, lyophilized powder, $\geq 98\%$) was purchased from Sigma and used without further purification. The stock solution of the proteins was prepared in 10 mM sodium phosphate buffer solution (PBS) of pH 7.4 and stored at 4 °C, and the stock solution was used within one week. Buffers at pH 7.4 were prepared using 10 mM sodium phosphate buffer solution.

Dynamic Light Scattering

The size of the AuNPs was measured using the Malvern Zetasizer Nano ZS (Worcestershire, U.K.) with a fixed detector angle of 173°. Specifically, at pH 7.4, the AuNP stock suspension ($\sim 0.05\text{ }\mu\text{M}$) was sequentially added with protein stock solution to reach a series of final protein/AuNP molar ratio ranged from 1 to 20. The mixture was incubated for 30 min before DLS measurement and a total of 15 measurements were taken. The average maximum size changes from duplicate experiment were used for comparison.

Circular Dichroism Spectroscopy

CD measurements were undertaken by a Jasco J-810 spectropolarimeter (Easton, MD) with a 2 mm path length rectangular quartz cell at room temperature (22 °C). The CD spectra were recorded from 190 to 260 nm and each spectrum was an average of 5 scans. The

concentration of BSA was fixed (0.75 μM for MUS type AuNP, 1.5 μM for MPA type AuNP), and the AuNPs concentration ranged from 0 to 0.05 μM .

Fluorescence Quenching Measurements

Fluorescence measurements were performed on a HITACHI F-7000 fluorescence spectrophotometer (Tokyo, Japan) with the use of a 1.00 cm path length rectangular quartz cell. The spectra were recorded in the wavelength range of 310-500 nm upon excitation at 295 nm, using 10 nm/10 nm slit widths, and each spectrum was an average of two scans. The concentrations of BSA were set to be at 0.15 μM , and the concentration of AuNPs ranged from 0 to 0.004 μM for MUS-type AuNP, 0 to 0.0014 μM for MPA-type AuNP. Blanks corresponding to the buffer were subtracted from the sample spectra to correct the fluorescence background before performing the analysis. Duplicate experiments were conducted for each AuNP concentration.

Since the AuNP concentrations were relatively low, where fluorescence quenching was dominated by diffusive transport, a nonequilibrium model for the fluorescence quenching is considered to be more appropriate (Dong et al. 2007; Lacerda et al. 2010). The Stern-Volmer model (equation (1)), which predicts the ratio F_0/F at low concentrations of quenching agents to be linear, is the standard model for this regime. Thus, it was being used to analyze the fluorescence intensity data.

$$\frac{F_0}{F} = 1 + k_q \tau_0 [AuNP] = 1 + K_{sv} [AuNP] \quad (1)$$

where F_0 and F are the maximum fluorescence intensities in the absence and presence of AuNP, respectively, k_q is the quenching constant, τ_0 is the lifetime of the fluorophore in the

absence of quencher, K_{SV} is the Stern-Volmer fluorescence quenching constant, which is a measure of the quenching efficiency, and $[AuNP]$ is the quencher concentration.

Isothermal Titration Calorimetry

ITC measurements were performed on a MicroCal ITC200 system (GE Healthcare). BSA was dialyzed overnight against 10 mM sodium phosphate buffer (renewed three times), and the AuNPs were dissolved in the last dialysate (sonicated, then centrifuged at 9000 rpm for 15 min). A typical titration experiment involved 38 injections of BSA (titrant, 1 μ L per injection from a 500 μ M stock) at 150 sec intervals into the sample cell (volume = 200 μ l) containing the AuNPs solution (MUS - 7.03 μ M, MUS/brOT - 8.43 μ M, MUS/OT - 7.73 μ M, MPA/brOT - 8.95 μ M, MPA/OT - 9.3 μ M). The reference cell was filled with 10 mM sodium phosphate buffer. During the experiment, the sample cell was stirred continuously at 1000 rpm.

The heat of BSA dilution in the buffer alone was subtracted from the titration data (both normalized to 0) for each experiment. The data were analyzed to determine the binding stoichiometry (N), affinity constant (K_a), and other thermodynamic parameters of the reaction using the coupled Origin software. The reported thermodynamic parameters were an average of duplicate experiments.

Results and Discussion


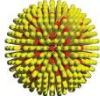
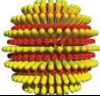
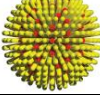
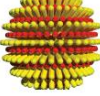
Characteristics of the AuNPs

The synthesis and characterization of these AuNPs have been performed in previous studies (Jackson et al. 2006; Uzun et al. 2008; Verma et al. 2008) (details are also available in Appendix G). To ensure the uniformity of particle size and shape, the AuNPs were characterized by TEM and DLS before use. TEM showed that the AuNPs are mostly spherical and slightly

angular. Size distribution of the two types of AuNPs based on TEM image analysis can be found in Appendix D and G. The physical and chemical characteristics of the two types of AuNPs were presented in Table 4-1. TEM revealed that the three MUS-type AuNPs are similar in size. The sizes of the two MPA-type AuNPs are similar to each other but slightly larger (~1 nm) in core diameter than the MUS-type AuNPs.

As shown in previous studies using scanning tunneling microscopy, depending on the types of self-assembled monolayer (SAM), the polar and nonpolar ligands can randomly distribute or form alternating stripes on the surface of AuNPs (Jackson et al. 2006; Uzun et al. 2008). The combination of 11-mercapto undecanesulfonate (MUS) and 3,7 dimethyloctane 1-thiol (brOT) forms a surface with randomly distributed ligands, the combination of MUS (or MPA) and octanethiol (OT) leads to alternating polar and nonpolar stripes, and the dimension of the stripes is dependent on the ratio of the MUS (or MPA) to OT. The head group spacing ranges from 0.7 to 1.0 nm, depending on the core diameter and mixed ligand types and ratio. More detailed information on the surface structure can be found in previous studies (Jackson et al. 2006; Uzun et al. 2008; Verma et al. 2008). The combination of mercaptopropionic acid (MPA) and brOT has not been investigated with scanning probe microscopy yet, but there is no reason to believe that it would have an ordered arrangement of ligands (Ghorai and Glotzer 2010; Singh et al. 2007).

Table 4-1 Physical and chemical properties of the two types of AuNPs used in this study.

Nanoparticles	Ligand Shell composition *	Ligand shell morphology and chemical structures	Core size, d_{TEM} (nm) [#]	Hydrodynamic diameter, d_{h} (nm) [§]
MUS	100% MUS	 <chem>CCCCCCCCCS(=O)(=O)[O-].[Na+]</chem> MUS	4.5±1.1	10.8±0.2
MUS/brOT	66% MUS 34% brOT	 <chem>CCCCCCCCCS(=O)(=O)[O-].[Na+]</chem> MUS <chem>CCCC(C)CS(=O)(=O)[O-].[Na+]</chem> branched-OT	4.7±0.9	12.5±2.4
MUS/OT	66% MUS 34% OT	 <chem>CCCCCCCCCS(=O)(=O)[O-].[Na+]</chem> MUS <chem>CCCCCCCCS(=O)(=O)[O-].[Na+]</chem> OT	3.9±0.8	9.4±1.0
MPA/brOT	66% MPA 34% brOT	 <chem>CCCC(C)C(=O)O</chem> HS <chem>CCCC(C)CS(=O)(=O)[O-].[Na+]</chem> brOT	5.8±0.3	10.6 ±0.4
MPA/OT	66% MPA 34% OT	 <chem>CCCC(C)C(=O)O</chem> HS <chem>CCCCCCCCS(=O)(=O)[O-].[Na+]</chem> OT	5.7±0.3	9.9±0.5

* based on ¹H NMR analysis of ligands after gold core decomposition by KCN (except for MPA/brOT) (Liu et al. 2012).
[#] Determined from TEM images and expressed as average diameter ± standard deviation.
[§] Determined by dynamic light scattering with a fixed detector angle of 173° based on volume-based size distribution.

Stability of the AuNP-protein Complexes

The hydrodynamic size change of the AuNPs following the addition of BSA was monitored by dynamic light scattering and the results are presented in Figure 4-1A and Appendix H. The size change due to BSA adsorption ranged from 5 to 8 nm, depending on the type of AuNPs. Previous studies also reported a thickness change of 3 nm due to the coating of human serum albumin (Rocker et al. 2009). These size changes suggested that the AuNPs were probably coated with a monolayer of proteins at pH 7.4.

Regarding the difference between different types of AuNPs, the first noticeable difference was the larger size change for the AuNPs with stripe domain (MUS/OT) compared to AuNPs with all sulfonated alkanethiols (MUS) and AuNPs with randomly distributed MUS and

brOT (MUS/brOT). Similarly, for the MPA-type AuNPs, MPA/OT has larger size increase than MPA/brOT. The different size changes may possibly due to different protein geometries on the AuNP surfaces or to different BSA affinities. Also there is a difference between the MUS-type and the MPA-type AuNPs, in which the MUS-type has relatively larger size changes than the MPA-type (see the isothermal titration calorimetry section below for further discussion of the different scenarios).

Following the adsorption onto surfaces, proteins may experience different degrees of conformational change, depending on proteins types and surface physicochemical properties (e.g., surface curvature, functionality) (Lundqvist et al. 2004; Roach et al. 2005). The degree of conformational change of the adsorbed proteins would influence the properties the AuNP-protein complex. Therefore, to see whether there is a change in the secondary structure of BSA after adsorption onto different AuNP surfaces, bound and unbound BSA were characterized by circular dichroism spectroscopy and the results are shown in Figure 4-1B and Appendix I. There was no significant change in the helicity of BSA in the presence of all types of AuNP, which indicated that BSA maintained its secondary structure after adsorption onto all types of AuNPs.

Fluorescence Quenching

Fluorescence quenching is a highly sensitive, reproducible, and convenient tool for identifying the binding sites and conformation changes of proteins upon association with small molecules, NPs and membranes. The efficiency of fluorescence quenching of chromophores (e.g., tryptophan, tyrosine, and phenylalanine residues) in proteins depends on the shielding degree of the chromophores by the quencher, thus this technique is useful in revealing the relative accessibility of AuNPs to the chromophore groups of protein (Lacerda et al. 2010; Sandros et al. 2005).

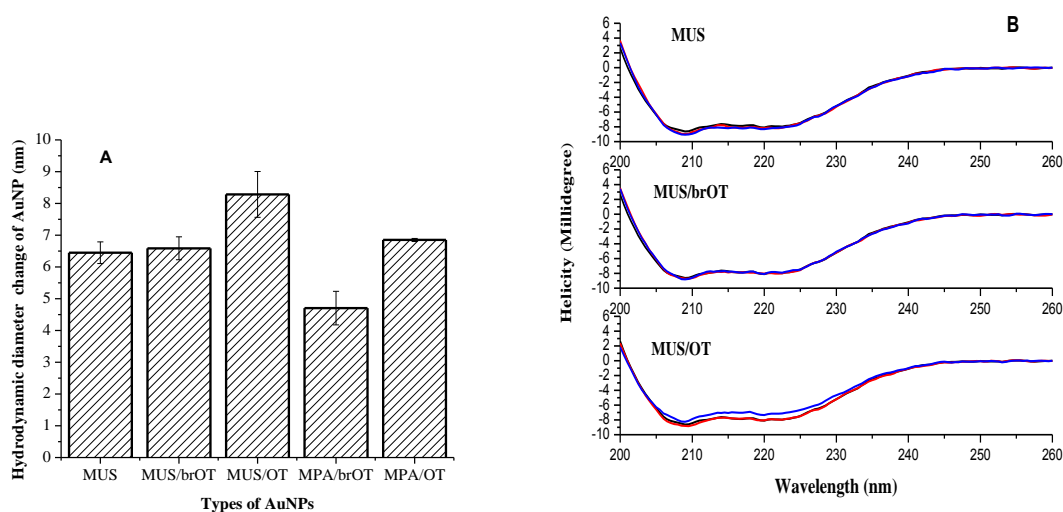


Figure 4-1 Hydrodynamic diameter change of AuNPs due to the adsorption of BSA (A) and the secondary structure of BSA following the addition of MUS-type AuNPs at pH 7.4.

In this study, the tryptophan (Trp) residues in BSA were selectively excited with an excitation wavelength of 295 nm, at which competing fluorescence from tyrosine and phenylalanine residues is much weaker. BSA has two Trp residues located in its lower hydrophobic pocket in domain II (Trp-213) and on the surface of the molecule in domain I (Trp-134), respectively (Dong et al. 2007). Fluorescence emission spectra showed that all types of AuNPs quenched the fluorescence of BSA, and the fluorescence intensity decreased gradually with increasing concentration of AuNPs. More quantitative information can be extracted by fitting the fluorescence quenching data with the Stern-Volmer model. The fitting by the Stern-Volmer model to the fluorescence spectra is presented in Figure 4-2A and Figure 4-3A, Table 4-2. The raw fluorescence emission spectra can be found in Appendix J.

All the k_q values (bimolecular quenching constant) obtained here for the three types of AuNPs were at least six orders of magnitude higher than the maximum value ($10^{10} \text{ M}^{-1} \text{ s}^{-1}$) for a diffusion-controlled quenching process. This suggested that the Trp fluorescence was quenched

by specific interaction between BSA and the AuNPs (i.e., static quenching was the dominant mechanism, with the formation of bioconjugates). The Stern-Volmer quenching constant (K_{SV}) showed the different quenching ability of the three types of AuNPs. For BSA, the K_{SV} for MUS and MUS/brOT were $2.13 \times 10^9 \text{ M}^{-1}$ and $1.33 \times 10^9 \text{ M}^{-1}$, respectively, while it was about an order of magnitude lower ($8.95 \times 10^7 \text{ M}^{-1}$) for MUS/OT. Similarly, between the two MPA-types of AuNPs, MPA/brOT showed higher quenching capability than the striped MPA/OT.

The shifting of emission spectra due to adsorption of BSA on AuNPs was also evaluated by a double wavelength method, in which the ratio of fluorescence intensity at 320 nm and 360 nm (F_{320}/F_{360}) was registered and plotted against the concentration of AuNPs added (Figure 4-2B and Figure 4-3B). As the slope of the ratio shown, F_{320}/F_{360} increased gradually with increasing concentration of MUS, MUS/brOT and MPA/brOT, while decreased slightly, if at all, with increasing concentration of MUS/OT and MPA/OT. An increasing F_{320}/F_{360} suggests a blue shift of the position of emission maximum, and blue shift was considered to be caused by the burying of Trp in a more hydrophobic environment (Cukalevski et al. 2011; Dong et al. 2007). The slight change of F_{320}/F_{360} in BSA-MUS/OT or MPA/OT indicates less alteration in the Trp environment following adsorption compared to that of MUS, MUS/brOT and MPA/brOT (further discussion of the cause and relevance to the interaction mode can be seen below).

The different fluorescence quenching efficiency of AuNPs with stripe-like domains (MUS/OT or MPA/OT) from that of MUS and MUS/brOT or MPA/brOT reflects less shielding of the Trp residues, confirming the DLS results that BSA may adsorb onto MUS/OT with a different orientation. Figure 4-4 is a schematic portraying a possible geometrical arrangement of BSA with respect to the MUS/brOT and MUS/OT particles based on the characterizations

presented thus far. These conformations, or ones very similar, would explain the size differences obtained with DLS, the persistence of BSA's secondary structure as measured by CD

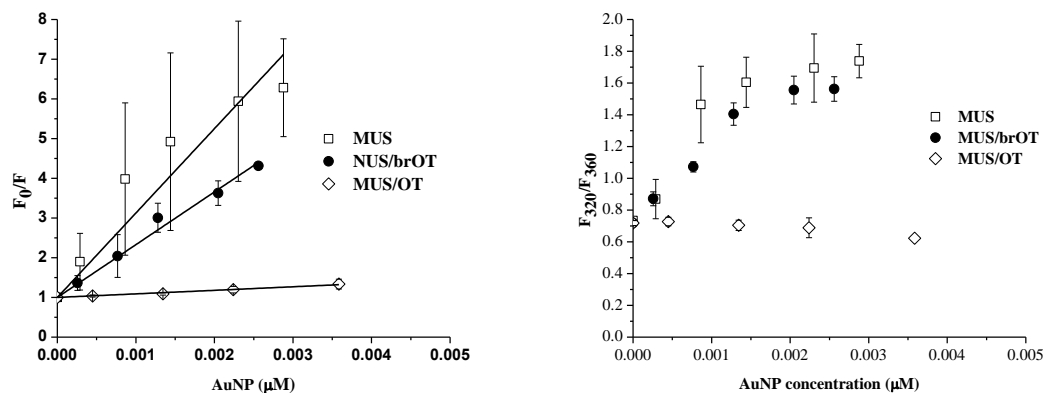


Figure 4-2 Stern-Volmer plot (left) and the shift of Trp emission (right) for BSA in the presence of increasing concentrations of MUS-type AuNPs.

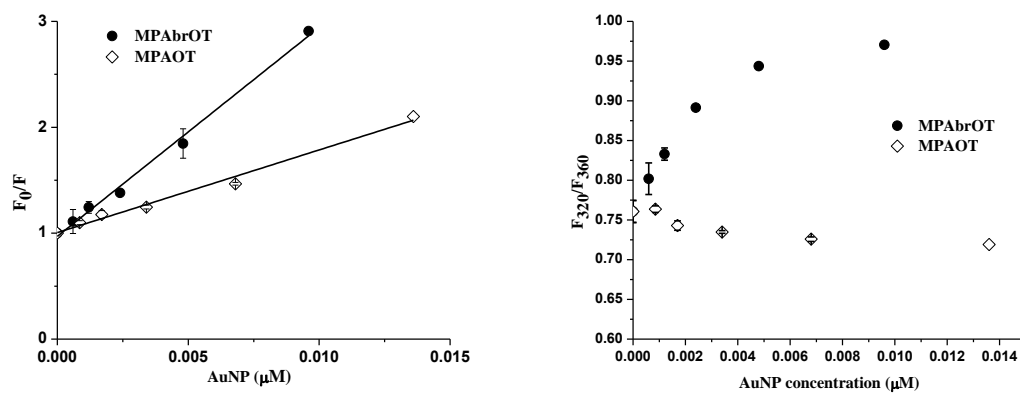


Figure 4-3 Stern-Volmer plot (left) and the shift of Trp emission (right) for BSA in the presence of increasing concentrations of MPA-type AuNPs.

Table 4-2 Fitting parameters of the Stern-Volmer model for BSA with different particles.

Types of NPs	MUS	MUS/brOT	MUS/OT	MPA/brOT	MPA/OT
$K_{SV} (\text{M}^{-1})$	2.13×10^9	1.33×10^9	8.95×10^7	1.97×10^8	7.8×10^7
$k_q (\text{M}^{-1} \text{s}^{-1})$	4.26×10^{17}	2.66×10^{17}	1.79×10^{16}	3.94×10^{16}	1.56×10^{16}

spectroscopy, and the proximity of the fluorescent Trp residues to the particles found in the fluorescent quenching experiments. BSA could attach its longest dimension onto the surface of the MUS/brOT particles to attain maximum contact, which results in the shielding of Trp from exposure to solution and tight interaction with the surface. This was the same as BSA adsorbed onto MUS, as it has a homogeneously distributed sulfonated alkanethiols shell. At this point, we shift from describing the geometrical conformation of the proteins to the binding affinity and thermodynamics of this new orientation.

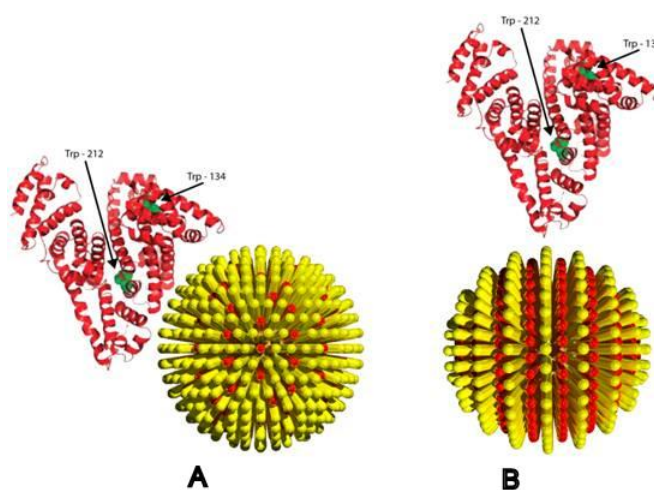


Figure 4-4 The proposed binding geometries for BSA and (A) MUS/brOT or MPA/brOT and (B) MUS/OT or MPA/OT AuNPs based on DLS and fluorescent quenching measurements. NP and protein size were not drawn to scale. The schematic illustration was to indicate the aspect ratio but not exact binding residues (cartoons of AuNP and BSA were adopted and modified from Verma et al. (Verma et al. 2008) and Dubeau et al. (Dubeau et al. 2010), respectively).

Isothermal Titration Calorimetry and Binding Thermodynamics of NP-Protein Interactions

Protein interaction with particle or surface is a complex process that involves various non-covalent forces like including Van der Waal force, hydrogen bonding, electrostatic and hydrophobic interaction, the desolvation of both NPs and proteins and solvation of newly formed complexes (De et al. 2007). Depending on the structure of the proteins and the properties of the interacting surface, the relative importance of various forces is different. ITC is a useful

technique in the characterization of protein-NP interaction, as it can directly measure the enthalpy changes and binding stoichiometry between NPs and proteins in solution, from these other thermodynamic quantities like binding constant, entropy and free energy change can be derived (De et al. 2009; Lindman et al. 2007). This quantitative information, in combination with other techniques, can reveal the mechanism of the interaction.

As can be seen from DLS and fluorescence quenching results, BSA may adopt different orientations when adsorbed onto AuNPs with different surface properties. Accordingly, different ITC heat profiles would result. As seen from the titration curves (Figure 4-5 and Appendix K), the adsorption of BSA onto MUS/OT exhibited significantly different heat change profile from the other two types (MUS and MUS/brOT), which have similar heat change profiles. The complexation of BSA with MUS/brOT was consistently exothermic throughout the titration process, while the complexation of BSA with AuNPs with stripe-like domains (MUS/OT) was exothermic only at the beginning (when molar ratio of protein/AuNP is < 4). Similarly, the complexation of BSA with MPA/brOT was also consistently exothermic throughout the titration process, and the complexation of BSA with MPA/OT was exothermic at the beginning (when molar ratio of protein/AuNP is < 2) and gradually changed to endothermic (Figure 4-6).

Interestingly, there is a small difference between the MUS-type AuNPs and MPA-type AuNPs. Although the heat profiles were all consistently exothermic, MUS and MUS/brOT showed an abrupt change at a molar ratio of 3, while MPA/brOT demonstrated no abrupt change. Despite the similar trends between MUS/OT and MPA/OT, MPA/OT showed endothermic peaks after the disappearance of exothermic peaks, while no endothermic process was observed for MUS/OT. This difference may possibly due to the difference in the curvature and chemistry between the MUS-type and MPA-type AuNPs (the MPA-type particles are 1 nm larger and the

charged ligands are carboxyl-terminated instead of sulphonate-terminated. Besides, the negatively-charged MPA is shorter than the nonpolar ligands for the MPA-type, while MUS is longer than OT for MUS-type). Adjustment of the initially adsorbed BSA to accommodate subsequent BSA adsorption or different interaction sites for later adsorbed BSA due to the smaller size of MUS-type NPs compared to MPA-type NPs may be responsible for the abrupt change observed.

Of all the heat profiles, only the complexation of BSA with MPA/brOT can be satisfactorily fit by available models. It was fit to a model describing a single set of binding sites and best-fit parameters were calculated using nonlinear least-squares fitting (Table 4-3). The thermodynamic quantities showed that the adsorption of BSA onto MPA/brOT featured a favorable enthalpy change ($\Delta H < 0$), which was offset partially by an unfavorable entropy loss ($\Delta S < 0$), resulted in an overall negative free energy change ($\Delta G < 0$). Considering that 67% of the ligands are the carboxyl-terminated MPA, the adsorption of BSA onto MPA/brOT was primarily driven by electrostatic interaction, and the binding sites were equivalent for all BSA adsorbed on one NP surface (since the heat profiles was satisfactorily fitted to a model for the single set of identical binding sites). Besides, a 5:1 binding ratio of BSA to MPA/brOT and a binding constant of $7.86 \times 10^5 \text{ M}^{-1}$ were derived. Despite the small difference between the MUS-type and the MPA-type, the overall similarity in heat profile and surface structure seems to suggest that similar electrostatic-driven adsorption was likely to occur with MUS and MUS/brOT.

The few exothermic peaks observed at the beginning of the BSA titration into MUS/OT and MPA/OT are likely due to the BSA initially titrated, which may adsorb onto the charged stripes mainly through electrostatic interaction. Due to the surface heterogeneity and inter-

protein repulsion, affinity for electrostatic adsorption is smaller compared to that of MPA/brOT, which would explain why the exothermic peaks decayed rapidly as a 2:1 molar ratio of BSA was titrated. After that, the insignificant endothermic peak in MUS/OT or small endothermic peak in MPA/OT would indicate the adsorption of BSA onto the surface with minimum contact, as the fluorescence quenching result suggested.

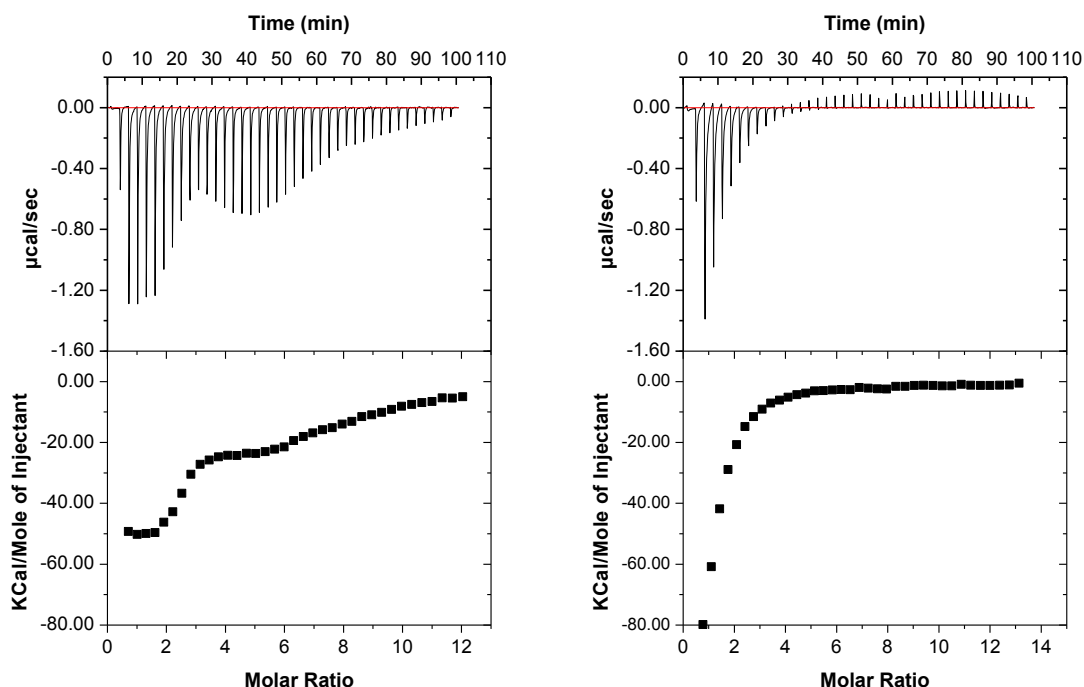


Figure 4-5 ITC data from the titration of 500 μM BSA into 8.4 μM MUS/brOT (left) and 7.7 μM MUS/OT AuNP (right). Heat flow versus time during injection of proteins at 25 $^{\circ}\text{C}$ and heat evolved per mole of added proteins (corrected for the heat of protein dilution) against the molar ratio (protein/AuNP) for each injection are shown at the top and bottom, respectively (The data corresponding to the heat of dilution of protein were shown in Appendix K).

The endothermic adsorption may involve an unfavorable enthalpy contribution ($\Delta H > 0$) and a large favorable entropy change ($\Delta S > 0$) to have a negative free energy of association ($\Delta G < 0$). The positive enthalpy change and favorable entropy change ($\Delta S > 0$) suggested the disruption and release of water from the interaction process (De et al. 2007), which was

associated with the adsorption of BSA onto the nonpolar stripes of the AuNPs. Previous studies on these types of AuNP using molecular dynamic simulation demonstrated that hydrophobic environment developed over the non-polar stripes (Kuna et al. 2009) and amphiphilic side chains of lysine and arginine can direct the adsorption of proteins onto the polar and non-polar ligands (Hung et al. 2013; Hung et al. 2011).

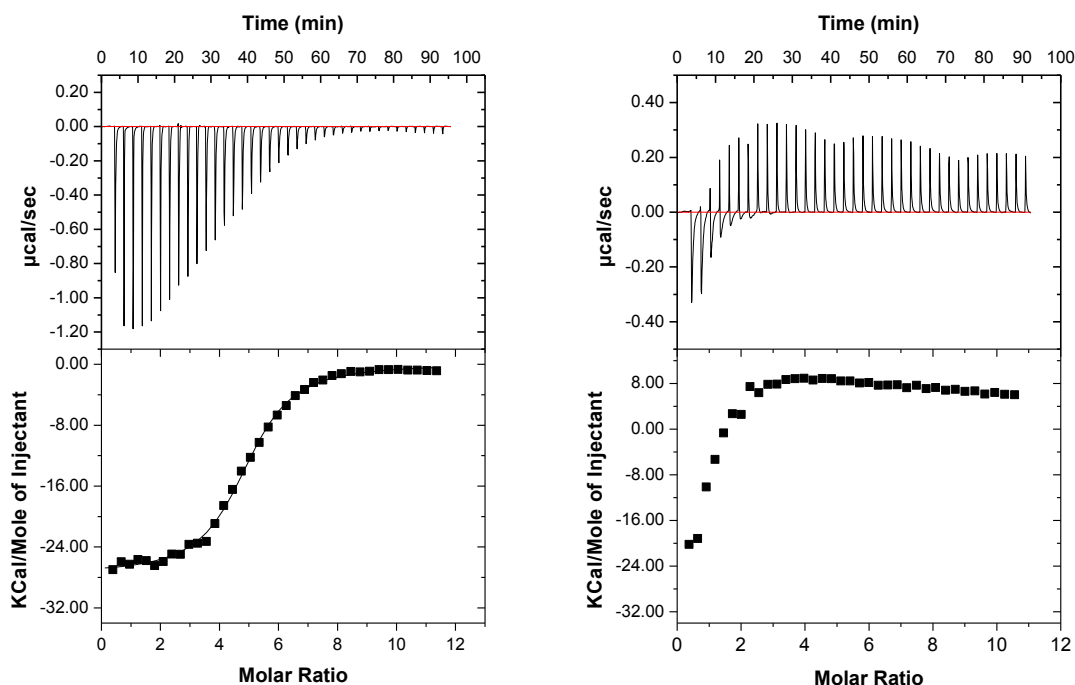


Figure 4-6 ITC data from the titration of 500 μM BSA into 9.0 μM MPA/brOT (left) and 9.3 μM MPA/OT (right). Heat flow versus time during injection of BSA at 25 $^{\circ}\text{C}$ and heat evolved per mole of added BSA (corrected for the heat of BSA dilution) against the molar ratio (BSA/AuNP) for each injection are shown at the top and bottom, respectively (The data corresponding to the heat of dilution of BSA are shown in Appendix K).

Table 4-3 Thermodynamic quantities of BSA and MPA-type NPs interaction derived from ITC.

NPs	K_s ($\times 10^5 \text{ M}^{-1}$)	ΔG ($\text{kcal} \cdot \text{mol}^{-1}$)	ΔH ($\text{kcal} \cdot \text{mol}^{-1}$)	$T\Delta S$ ($\text{kcal} \cdot \text{mol}^{-1}$)	n
MPA-brOT	7.86 ± 0.34	-8.03 ± 0.02	-28.10 ± 0.80	-20.07 ± 0.86	4.99 ± 0.15
MPA-OT	Heat profile could not be satisfactorily fitted by available models.				

Mode of Interaction

In line with the experimental evidence provided in this study, we propose that the interaction between BSA and the striped AuNPs (MUS/OT and MPA/OT) represents a special case where the protein adopts a unique conformation at the surface of the AuNPs. Instead of the typical hard protein corona observed in the literature for AuNPs mixed with proteins, this system is composed of a weakly bounded protein cloud, indicated by the small contact and small heat change observed. The likely cause of this new type of MUS/OT- or MPA/OT-BSA AuNP-protein complex is the structured surface of the AuNPs, in comparison to the MUS/brOT AuNPs (which only differs in surface composition) that did not exhibit the cloud type of adsorption. This finding is different from results on the adsorption of transferrin onto sulfonated (PSO₃H) and carboxylated (PSCOOH) polystyrene NPs, in which two layers of transferrin were found to coat on the NPs and the second layer of transferrin is “soft” while the first layer is still “hard” (Milani et al. 2012). For the same particles in this study, different conformations have been previously proposed for the globular protein cytochrome C and lysozyme in a simulation study (Hung et al. 2013; Hung et al. 2011). In these two studies, they found that the amphiphilic lysine and arginine side chains of Cyt C and lysosome, respectively, were able to interact simultaneously with polar and nonpolar surface ligands, and particles that exhibited close domains of each type of ligand adsorbed the protein with a varied geometrical conformation.

For the BSA in this study, the mode of interaction with MUS/OT and MPA/OT may be explained by the same phenomena, so that the nonpolar domains in MUS/OT and MPA/OT can help to maintain the unhydrated regions of the protein. On BSA, there are arginine- and lysine-rich positively-charged surface patches that are the possible sites of electrostatic interaction with the MUS sulfonate ligand head group. Since the -SO₃⁻ and -CH₃ terminals on MUS/brOT and

MPA/brOT surface are randomly distributed, MUS/brOT and MPA/brOT may behave like particles with a homogeneously charged surface. Since the contact area between the protein and the surface may be large enough to involve several charged and non-charged groups, the BSA “sees” no difference on the surface of MUS/brOT or MPA/brOT. However, due to the nanoscale striations of -SO_3^- and -CH_3 terminals on the surface of MUS/OT and MPA/OT, the cumulative effects of the nonpolar groups cannot be neglected, as demonstrated in the study of structurally heterogeneous surfaces by Kuna et al (Kuna et al. 2009). Thus, the adsorption of BSA onto MUS/OT and MPA/OT surface will be a combination of both electrostatic and hydrophobic interaction, rather than simply electrostatic interactions in the case of MUS or MUS/brOT or MPA/brOT. As a result, the final configuration of the bounded BSA may also depend on spatial restriction and inter-protein repulsion. It is likely that some BSA approached the charged stripes of the AuNPs through electrostatic interaction with a smaller contact area than that with MUS/brOT, and may lead to longer extension of BSA into solution and loose interaction with MUS/OT and MPA/OT surface.

In spite of their overall similarity in chemical composition, difference between the MUS/OT (MPA/OT) and MUS/brOT (MPA/brOT) indicated that structural organization of surface functional groups is no less important than the surface chemistry in protein adsorption. Despite some small difference, the overall similar phenomena observed in both MUS-type and MPA-type AuNPs suggested that surface structure-dependent protein conformation could be generalized regardless of the type of polar ligand used.

It would also be worthy to note that characteristics of the adsorbed proteins are also important, as the heterogeneity on the particle surface is scale-dependent. Size and shape of the protein would influence the scale of interaction. For example, the size and shape of proteins were

found to determine the binding stoichiometry for the same types of NPs (De et al. 2009). In the Hung et al. study, they also stressed the importance of the structural characteristics of the particular protein under examination for the prevalence of the conformational change of the protein upon adsorption to structured surfaces (Hung et al. 2011) .

These surface structure-determining protein coatings have important implications: 1) surface of NP can be manipulated to selectively adsorbed proteins as the protein binding affinity is determined by physicochemical interaction between them; 2) organization of the adsorbed proteins would affect their activity, as the esterase activity results showed that BSA retained higher esterase activity in the presence of MPA/OT than that of MPA/brOT (Appendix L). Therefore, NP can be specifically designed to modulate the activity of adsorbed molecules.

Conclusion and Implications

The adsorption of BSA onto three MUS-type and two MPA-type AuNPs was studied with a combination of DLS, CD spectroscopy, fluorescence quenching and ITC. The results showed different protein adsorption behaviors depending on the surface ligand composition and structure. BSA adsorption onto particles with nano-scale stripe-like polar and non-polar domains behaved differently from AuNPs with randomly distributed mixing terminals, which was similar to AuNPs with homogeneously charged terminals. The different binding modes affected protein configuration and interaction affinity. Two different protein coatings, “protein corona” and “protein cloud” were proposed for the tight and loose interaction scenarios. Results suggested that both surface chemical composition and structure are important in determining the physicochemical interaction between the proteins and AuNPs, and the resulting protein organization on the surface. The results have important implications regarding the functionality

of NP following their entrance into organism's body and surface manipulation for specific adsorption of biomolecules.

CHAPTER FIVE

Nanoparticle Adsorption onto Bacterial Cells: Effects of Surface Heterogeneity

Abstract

The interaction between nanoparticles (NPs) and bacterium is relevant for the application and toxicity of NPs. This study devoted to understand the effects of NP's surface heterogeneity and the roles of bacterial surface components on the interaction. Three types of gold NPs with quantitative difference on in surface chemistry and structure were used. They were coated with (1) one ligand with charged terminals (MUS), (2) two homogeneously distributed ligands with respectively charged and nonpolar terminals (brOT) and (3) two ligands with respectively charged and nonpolar terminals with stripe-like distribution (OT). Their adsorption on *Escherichia coli* and *Bacillus cereus* was studied by batch adsorption experiment. OT showed the fastest adsorption kinetics, followed by brOT, then MUS, which agrees with the DLVO theory. Proteins contribute to part of the surface active sites that were responsible for AuNP adsorption. Different adsorption capacity of the three types of AuNPs may due to the relative active site density and their different affinities to different types of AuNPs, reflecting the effects of surface heterogeneity.

Introduction

Nanoparticle-bacteria interaction is of great relevance to the application and toxicity of nanomaterials, disinfection (Panacek et al. 2006), biosensor (Phillips et al. 2008), and nanoparticle (NP) formation (Mandal et al. 2006). Therefore, it is important to understand the interaction mechanism between NPs and bacteria. Previous studies suggested that the interaction

is controlled by the properties of both the NPs and the bacterial surface. NP adsorption kinetics was shown to be controlled by the surface charge (Schwegmann et al. 2010) and size (Zhang et al. 2011b) of NPs, and the effects of these NP properties on adsorption kinetics generally agree with the DLVO theory. The interaction with smaller energy barrier will adsorb faster than interaction with larger energy barrier.

Bacterial surfaces are heterogeneous in terms of chemistry and organization. Chemically, it consists of a wide range of biopolymers (e.g., lipopolysaccharides and peptidoglycan), and usually have extracellular polymeric substances like proteins, polysaccharides and nucleic acids, coated on the surface. The content and composition of these compounds modulate the surface properties of the bacterial cells (e.g., charge and polarity) (Eboigbodin and Biggs 2008; Karunakaran and Biggs 2011). Spatially, they are distributed unevenly over the bacterial surface and anisotropically present in the three dimensional extracellular surface structure. This heterogeneity is considered to be responsible for the different adsorption behavior observed in bacteria, including contaminant adsorption and surface adhesion of bacteria (Camesano and Abu-Lail 2002; Dorobantu et al. 2008; Ma et al. 2008; Ngwenya et al. 2003). For example, the composition and content of acidic functional groups affect the adsorption of heavy metals (Fein et al. 2001; Ginn and Fein 2008). Studies on bacteria surface adhesion revealed the different functionality of various surface components, for example, lipopolysaccharides (Walker et al. 2004) and proteins (Tsuneda et al. 2003).

In the case of NP-bacterium interactions, the interaction is at the nanoscale. NPs are relatively very small when compared to the bacterial cells, and comparable to sizes of surface biopolymers (e.g., extracellular proteins have sizes around several to tens of nm). This means that the interaction with individual NPs may exclusively involve one biopolymer molecule. Most

of the previous studies on NP-bacterium interactions focused on the bulk behavior of interaction; only few provided a detailed picture of the specific interactions between NPs and surface components, and the physical and chemical states of NPs following attachment (Schwegmann et al. 2010; Zhang et al. 2011b). A study on positively-charged NP adsorption on bacterial surfaces observed patches of aggregated NP clusters and the strain-dependent clustering phenomenon is considered to be mainly due to the differences in surface protein composition (Hayden et al. 2012). Further research is needed to quantitatively measure the relative contribution of these surface components to and how bacterial surface features affect NP adsorption behavior.

In this study, we measured the adsorption behavior of three types of AuNPs onto two bacterial strains. The three types of AuNPs are self-assembled-monolayer-coated gold nanoparticles (AuNPs) with different surface compositional and structural heterogeneity. They were chosen to test how surface heterogeneity on NP surface affects their adsorption behavior. *Escherichia coli* and *Bacillus cereus*, were used as model gram negative and positive bacteria, respectively. Their different surface physicochemical properties were ideal for comparison and identification of bacterial surface effects. Adsorption on cells treated with trypsin was compared with adsorption without treatment to identify the relative contribution of proteins on NP adsorption.

Materials and Methods

Preparation of AuNPs Suspension

Three types of AuNPs used in this study are coated with (1) one ligand with charged headgroups (11-mercapto undecanesulfonate, MUS), (2) a random distribution of both charged and nonpolar headgroups (MUS and branched-octanethiol, brOT), and (3) an ordered pattern of charged and nonpolar headgroups (MUS and octanethiol, OT). Their synthesis, characteristics

and solution preparation can be found in previous studies (Huang et al. 2013a; Huang et al. 2013b; Uzun et al. 2008; Verma et al. 2008).

Bacterial Adsorption Experiment

E. coli K12 and *B. cereus* cells were grown in Luria-Bertani (LB) medium at 30°C with shaking until late exponential growth phase. The cells were washed three times with phosphate buffer (10 mM, pH 7.4) and resuspended in the buffer solution to reach a concentration of approximately 4×10^8 CFU/mL and 2×10^8 CFU/mL for *E. coli* and *B. cereus*, respectively.

For the adsorption kinetics experiments, AuNPs and bacterial cells were mixed in 15 mL polypropylene centrifuge tubes. Five mL of the cell suspension were transferred into the tubes and adsorption experiments were started by adding 100 μ L of the AuNP stock solutions to each tube. The final AuNP concentration was around 2.5 mg/L in $[\text{Au}^+]$. Adsorption kinetics was quantified by measuring the decrease in suspended AuNP concentration. 350 μ L solution was sampled at different time intervals and centrifuged at 6000 rpm for 5 min (Eppendorf 5417c centrifuge) to separate the suspended AuNPs from *E. coli* cells (with or without adsorbed NPs). 200 μ L of supernatant was pipetted into new clean 15 mL polypropylene centrifuge tubes and was digested by Aqua regia before ICP-MS analysis.

For the adsorption isotherm experiments, *E. coli* and *B. cereus* cell concentrations were maintained at around 4×10^8 CFU/mL and 2×10^8 CFU/mL, respectively. The AuNP concentrations were varied from 1.2 to 12.0 mg/L in $[\text{Au}^+]$. Based on the adsorption kinetics experiments, the adsorption was stopped after 2 hours when equilibrium has been reached. Similarly, 350 μ L of each solution was sampled and centrifuged, then a certain volume of suspension (depending on the initial Au concentration) was transferred into a new 15 mL polypropylene centrifuge tube for digestion and analysis as described above.

Trypsin Treatment

E. coli and *B. cereus* cells were treated with trypsin, a proteolytic enzyme, to remove some envelope proteins present on the cell surfaces. In brief, late exponential phase cells were harvested and washed in phosphate buffered saline (PBS, pH 7.4). Cells were resuspended in either sterile PBS (untreated control) or fresh 1 g/L trypsin in PBS (treated) and shaken for 2 hours at 37°C. After the incubation, the cells were washed in phosphate buffer and resuspended to a final concentration of 4×10^8 CFU/mL and 9×10^7 CFU/mL for *E. coli* and *B. cereus*, respectively. Two AuNP concentrations were used: 1.46 ± 0.03 and 3.01 ± 0.04 mg/L Au⁺. The sampling and analysis were the same as adsorption isotherm experiment.

Data Analysis

Mean comparison was tested by two-sample T-test for independent samples.

Modeling of NP adsorption kinetics and isotherm was based on Park *et al.* (Park et al. 2009). Specifically, adsorption kinetics of the AuNPs was modeled by a first order chemical reaction with rate constant K_{obs} :

$$\theta_t = \theta_{\infty} (1 - e^{-k_{obs}t})$$

Where θ_t is the number of adsorbed AuNPs (#/cell) at time t , θ_{∞} is the number of adsorbed AuNPs (#/cell) at infinite time, and k_{obs} is the rate constant.

Adsorption isotherm was modeled using the Langmuir adsorption isotherm

$$\theta_{eqm} = \frac{\theta_{\max} K_L C_e}{1 + K_L C_e},$$

Where θ_{eqm} is the number of adsorbed AuNPs at equilibrium (#/Cell) for different initial applied concentrations; θ_{\max} is the maximum adsorption capacity of the NPs at equilibrium, K_L is the Langmuir equilibrium constant (L/mg), which equals the ratio of adsorption and desorption

rate constants, and C_e is the equilibrium concentration of the NPs in solution (mg/L in $[\text{Au}^+]$).

Rearrangement of the Langmuir equation into a linear form gives

$$\frac{1}{\theta_{eqm}} = \frac{1}{\theta_{\max}} + \frac{1}{K_L \theta_{\max}} \times \frac{1}{C_e}.$$

Results and Discussion

Adsorption Kinetics

The unbound suspended AuNP concentrations over time are presented in Figure S5-1. The adsorbed AuNPs per cell over time was modeled and shown in Figure 5-1, with the fitting parameters shown in Table 5-1. The relative adsorption kinetics of the three types of AuNPs is similar for *E. coli* and *B. cereus*, with OT particles being the fastest to adsorb onto the bacterial cells, followed by brOT and MUS (Figure 5-1 and Appendix M). Adsorption kinetics of particles is mainly determined by its diffusion coefficient (related to its size and density) and the interaction energy between the particle and the surface. Due to their similar size, it is the difference in the interaction energy that caused the difference in the adsorption kinetics (please refer to Chapter two for more detailed discussion).

The most distinct difference between *E. coli* and *B. cereus* is that Gram-positive bacteria (*B. cereus*) have much thicker peptidoglycan cell wall layers and no outer membrane external to this structure (but with membrane proteins and teichoic acid) (Scott and Barnett 2006). If extracellular polymeric substances present, there also may be a difference in the types and relative abundance of polysaccharides or proteins (Bayer and Sloyer 1990). The ionized amine, phosphoryl and carboxyl groups on these compounds are responsible for the surface charge on bacterial surface, thus there is a difference in the surface charge of the two bacteria (Figure 5-4) (Lytle et al. 2002; Wilson et al. 2001). Since the surface charges of both bacteria are all negative

and similar to that of AuNPs, AuNP adsorption on both bacteria is similarly through unfavorable deposition and against the overall electrostatic repulsion. Therefore, the adsorption kinetics for the three types of AuNPs on *B. cereus* follows the same order as that on *E. coli*. Due to the different cell concentrations used, it is not appropriate to directly compare the parameters between the two types of bacteria.

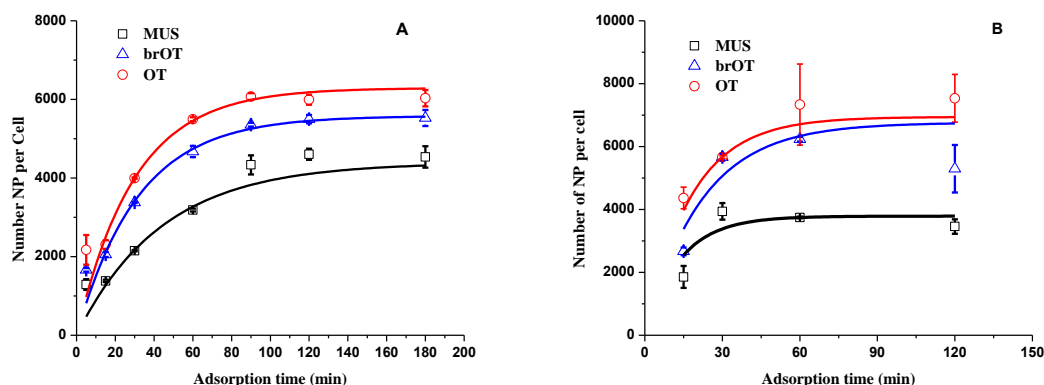


Figure 5-1 Adsorption kinetics of three types of AuNPs expressed as number of NPs per cell, onto *E. coli* (A) and *B. cereus* (B), error bar represent the variation of duplicate samples. Concentration of *E. coli* and *B. cereus* cell was 4.2×10^8 and 1.6×10^8 cell/mL, respectively. *E. coli* adsorption data was based on Huang et al. (Huang et al. 2013a).

Table 5-1 k_{obs} and θ_{∞} Values determined from three AuNPs adsorbed on *E. coli* and *B. cereus*.

Type of NPs	<i>E. coli</i>			<i>B. cereus</i>		
	θ_{∞} per cell	k_{obs} ($\times 10^{-2} \text{ s}^{-1}$)	R^2	θ_{∞} per cell	k_{obs} ($\times 10^{-2} \text{ s}^{-1}$)	R^2
MUS	4390 \pm 428	2.27 \pm 0.36	0.95	3787 \pm 120	7.70 \pm 4.14	0.50
brOT	5580 \pm 500	3.13 \pm 0.49	0.90	6760 \pm 821	4.54 \pm 1.65	0.83
OT	6290 \pm 137	3.33 \pm 0.11	0.99	6943 \pm 595	5.55 \pm 1.23	0.85

It is worthy to note that the adsorption equilibrium in the *B. cereus* experiment was achieved within the first 60 minutes but disrupted after 2 hours, with more particles being removed from the suspension (Appendix M). Possible causes for this phenomenon may be

enhanced adsorption due to a change of the surface properties of *B. cereus* (e.g., secretion of more extracellular polymeric substances), or even cellular uptake of the particles. Further experiments are needed to understand this phenomenon.

Adsorption Isotherm

The equilibrium adsorption capacity (number of NPs/cell) after 2 hours of adsorption as a function of equilibrium AuNP concentration was presented in Figure 5-2A, and these data were transformed and fit with the linear Langmuir adsorption isotherm (Figure 5-2B, Table 5-2). As the results shown, the data were satisfactorily fit by the Langmuir isotherm ($R^2 > 0.94$), and the maximum NP adsorption capacity was approximately 4000, 7000 and 8000 NPs/cell for MUS, brOT and OT, respectively. Considering the size of *E. coli* cells ($1\ \mu\text{m}$ in width $\times 3\ \mu\text{m}$ in length) (Velegol and Logan 2002) and AuNPs ($\text{Ø} = 7.5\ \text{nm}$), a monolayer coverage of the cell surface would need at least 10^5 NPs. Even for the AuNPs with the largest affinity (OT), its surface coverage is smaller than 10%. Therefore, instead of random adsorption and aggregation on the surface, the NPs are likely to adsorb specifically on certain sites of the bacterial surface (e.g., positively-charged patches on proteins), which resulted in the Langmuir-type isotherm.

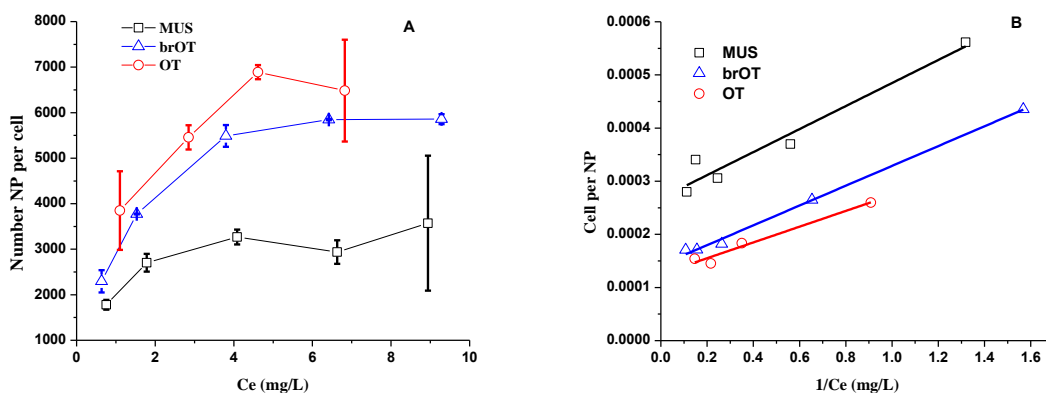


Figure 5-2 Adsorption isotherm (A) and with linear Langmuir isotherm fitting (B) of the three types of AuNP onto *E. coli* cells, error bar represent the variation of duplicate samples.

Table 5-2 Fitting parameters for Langmuir adsorption isotherm for *E. coli*.

Types of AuNP	MUS	brOT	OT
θ_{\max} (NP/Cell)	3730±256	7022±225	7974±584
K_L (L/mg)	1.24±0.16	0.76±0.02	0.85±0.10
R^2	0.94	0.99	0.96

The differences in adsorption capacity for the three types of AuNPs may be associated with their different affinities to the active sites. Our previous study showed that the interaction (e.g., binding stoichiometry) between these AuNPs and common serum proteins depends on their surface properties and the protein types (Huang et al. 2013b). As there is a variety of proteins of varying abundance on a bacterial surface (Eboigbodin and Biggs 2008; Karunakaran and Biggs 2011), it is likely that some of the proteins have higher affinities with OT than with the other two types of AuNPs. Some of the active sites for OT particle may not be active for brOT or MUS if their affinity is relatively smaller for brOT or MUS.

Effects of Trypsin Treatment

As hypothesized above, AuNP adsorption is likely to occur through specific interaction with certain active sites on cell surface. These active sites are possibly positively-charged patches of proteins. As our previous study shown, these AuNPs can interact with overall similarly-charged serum proteins through electrostatic interaction (Huang et al. 2013b). To test this hypothesis, AuNP adsorption on bacteria with and without trypsin treatment was performed. Trypsin is a protease that can hydrolyze proteins, and is commonly used to digest surface proteins of bacterial cells (Rosenbusch 1974). Therefore, it was used herein to reduce the protein content on the bacterial cell surface, which allows us to investigate the role of surface proteins in NP adsorption. As the result shown, trypsin treatment significantly reduced the adsorption of all

types of AuNPs (> 50%) (Figure 5-3). Trypsin treatment only hydrolyzed proteins and did not significantly change the physiological condition of the bacteria (Inouye and Yee 1972), surface proteins may significantly contribute to the adsorption of AuNPs (Figure 5-3). However, while previous studies have shown that approximately 40% of *E. coli* surface proteins may be removed by trypsin treatment (Inouye and Yee 1972), the absolute fraction and identities of surface-exposed proteins that were digested by trypsin treatment is unknown. Therefore, it may not be accurate to conclude that the reduced proportion of AuNP adsorption after trypsin treatment was solely due to the reduction of surface proteins.

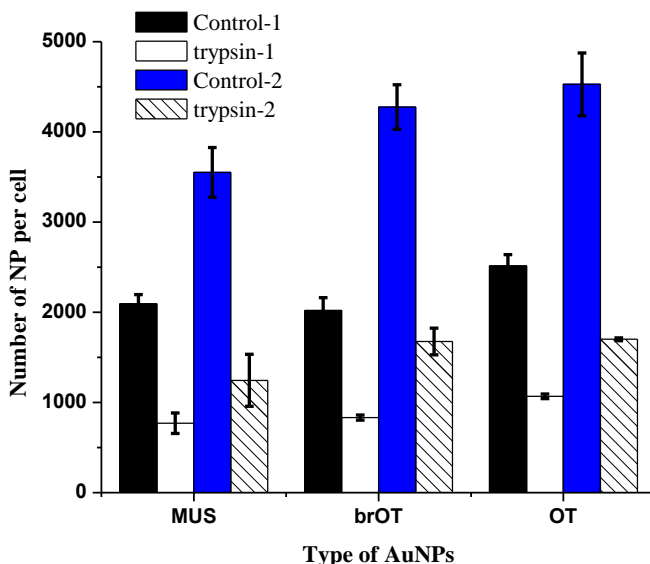


Figure 5-3 AuNP adsorption on *E. coli* with and without trypsin treatment, initial AuNPs concentration was 1.46 ± 0.03 and 3.01 ± 0.04 mg/L Au^+ for concentration 1 and 2, respectively. Error bar represent standard deviation ($n = 3$).

The electrophoretic mobilities of the bacterial cells with and without trypsin treatment are presented in Figure 5-4. After trypsin treatment, the electrophoretic mobility value decreased (statistically significant, $P < 0.05$, T-test), although the difference was small. Even though there was only a slight change in the bacterial surface charge, the adsorption capacity of AuNPs varied

by more than 50% (Figure 5-3). This suggests that the final attachment of the AuNPs depends on the available active sites and their affinities with the NPs, but not the overall interaction energy barrier between the AuNP and bacterial surface (which will not be significantly different before and after trypsin treatment considering the EPM values).

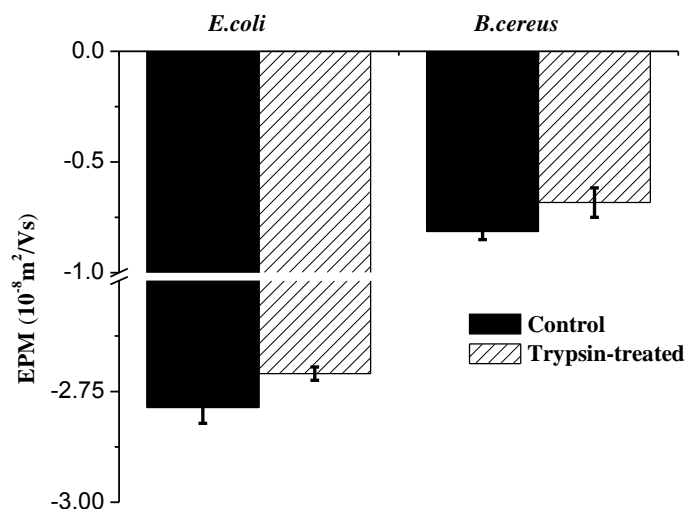


Figure 5-4 EPM of the bacteria with and without trypsin treatment, error bar represent standard deviation ($n = 3$).

Mechanism of Interaction

Based on the above results and analysis, AuNP deposition onto bacterial cell may follow the following processes (Schematic diagram depicting the interaction was present in Figure 5-5). First step, diffusion from bulk solution to the vicinity of cell surface, the diffusion rate and the possibility to overcome the interaction energy barrier to attach onto surface depends on the magnitude of the energy barrier, with OT the smallest, followed by brOT, then MUS (based on ζ -potential value). This explains why OT has the highest adsorption rate and MUS the smallest. Second step, there are adsorption and desorption simultaneously going on following the diffusion,

the rate of adsorption and desorption depends on the available active sites on the bacterial surface and the nature of interaction, equilibrium reached when irreversible adsorption rate equals desorption rate. There may be more active sites, or some sites have higher affinities for OT than brOT or MUS, which leads to its highest adsorption capacity among the three.

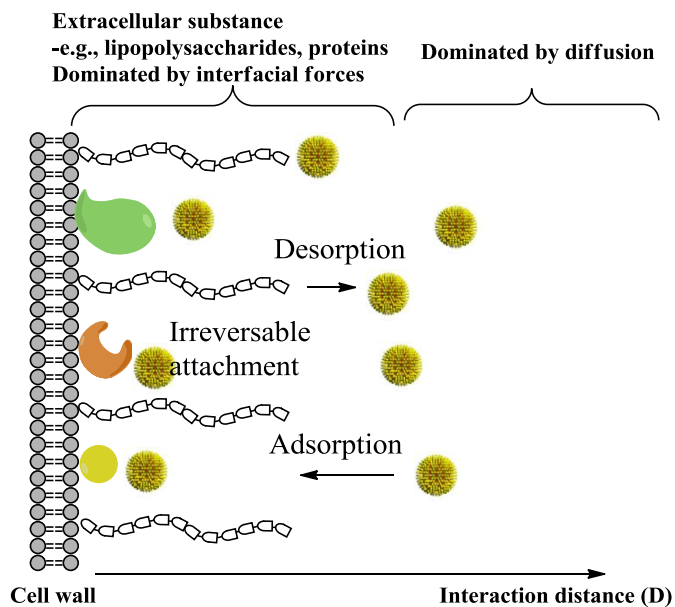


Figure 5-5 Schematic diagram of NP adsorption onto bacterial cell, the color symbols of different shapes represent different proteins and the long chains represent lipopolysaccharides.

Conclusions and Further Work

This study investigated the adsorption kinetics and adsorption isotherm of three types of AuNPs with different surface properties onto bacterial cells. Results suggested that the adsorption kinetics was controlled by the total interaction energy, which can be explained by the classical DLVO theory. The Langmuir-type adsorption isotherm indicated that AuNP may specifically interact with active sites on bacterial surface. These active sites may partly be positive patches on proteins, as supported by the trypsin experiment.

Further experiments are needed to visualize the NP-bacteria interaction, in order to see the physical states of the AuNP and confirm whether there is AuNPs penetration into the cells. More characterizations on bacterial surface with and without trypsin are also needed to quantitatively understand the relative contribution of proteins and other components to AuNP adsorption.

CHAPTER SIX

Conclusions, Implications and Future Research

Conclusions

This dissertation systematically investigated the effects of surface heterogeneity on the colloidal stability, proteins adsorption and bacterial interaction of self-assembled monolayer coated AuNPs.

In the case of self-aggregation, to test the applicability of the DLVO theory, the colloidal stability of these AuNPs was correlated with their electrokinetic properties and surface chemistry. brOT NPs have less negative EPM values, smaller CCC and faster adsorption on *E. coli* than that of MUS NPs, which agree with the DLVO prediction. However, OT NPs have less negative EPM values and faster adsorption, but much larger CCC compared to brOT, which can not be explained by the DLVO theory. The deviation of OT NPs from DLVO prediction is likely due to its nano-scale striped surface, which leads to complex EDL structure and interfacial forces when compared to that of NPs with homogeneous surface. The result suggests that, direct comparison of the ζ -potential of different NPs should be made with cautions, and the electrokinetic properties and colloidal stability of NPs are controlled not just by their surface chemistry, but also the organization of different functional groups.

The hetero-interaction between these AuNPs and two common serum proteins (ubiquitin and fibrinogen) with different sizes and shapes was investigated. Both ubiquitin and fibrinogen can adsorb onto the three types of AuNPs at pH above and below the IEPs of the proteins, and the interaction may be predominantly electrostatic and through some positive patches of the proteins. At pH above the IEPs, when the surface charge of the AuNPs and the proteins are

similar, the interactions were found to be influenced by the surface chemistry and structure of the AuNPs and the size of the proteins, in a scale-dependent manner. There was no significant difference between the three types of AuNPs with respect to their interaction with fibrinogen (binding ratio and interaction thermodynamics). However, there was a difference between these AuNPs in their interaction with ubiquitin, due to the comparable size of the contact area and the surface features.

The surface-dependent protein adsorption behavior was further manifested in the case of BSA. BSA adsorbed monotonously through electrostatic interaction onto the surface of MUS and brOT, while through more complex interaction onto OT surface due to its nano-scale heterogeneous surface. Fluorescence quenching experience indicated that the conformation of the BSA molecules surrounding OT particle was different from that of MUS and brOT. BSA possibly adapted an “end-on” conformation on OT surface, while a “side-on” conformation on MUS or brOT surface, which lead to two different types of protein coronas. This surface-dependent interaction behavior was also observed in AuNPs with similar surface structure while substituted with a different polar terminal.

Deposition kinetics of MUS, brOT and OT NPs on bacterial cells were in agreement with the DLVO prediction, in which the magnitude of electrostatic repulsion governs the diffusion rate of the AuNPs onto cell surface. Their adsorption isotherm on *E. coli* was satisfactorily fitted by the Langmuir isotherm, suggesting that they specifically interacted with some active sites on bacterial surface. These active sites were contributed partly by proteins as supported by trypsin treatment experiment. The different adsorption capacities of the three types of AuNPs reflect the effects of surface heterogeneity on the affinities between AuNPs and surface active sites.

Implications

Surface heterogeneity is ubiquitous in natural environment and engineering system. To understand the transport, fate and effects of NPs, it is important to understand how this surface property affects the interfacial processes that control the behavior of NPs. Despite its importance, surface heterogeneity has been relatively less studied. The results from this dissertation filled this gap and improved our understanding on the interplay between surface chemical and physical heterogeneity and its effects on representative interfacial processes.

Traditionally, ζ -potential is an important parameter in surface science that is commonly used for direct comparison of stability between different particles. Results from the colloidal stability study (Chapter 2) provided guidance for the appropriate use of ζ -potential. When surface property of different particles is significantly different, the direct comparison of ζ -potential between different particles and quantitative use of ζ -potential (e.g., for electrostatic interaction calculation) may not be accurate. Surface characterization may be needed to complement the use of ζ -potential.

Results from the protein adsorption study manifested the delicate control on interfacial processes by surface properties. Even subtle change on surface chemical and physical properties may result in different adsorption behavior. Therefore, results from this dissertation provided guidance for material scientists to design surface for specific purposes. For example, this dissertation identified factors that are crucial for the synthesis of nanomaterials with the capability to specifically adsorb biomolecules.

Future Research

One of the current challenges on this topic of research is to experimentally observe the distribution of water and ions at the solid-liquid interface. The advancement in instrumentation

together with theoretical and computational analyses may provide complementary information that is critical for a better understanding of surface-dependent EDL.

NPs with broader variation in surface heterogeneity (surface composition and organization) are needed to help establish quantitative relationship between observed phenomena and variables. NPs with more complex surfaces are also needed to better represent surfaces found in the natural environment.

APPENDICES

APPENDIX A

Derjaguin - Landau - Verwey - Overbeek (DLVO) Theory

Particle-particle interaction and particle-surface interaction in an electrolyte solution have been described by the classical DLVO theory. According to the DLVO theory, the overall force between particle-particle (or particle-surface) is determined by the sum of Van der Waals attraction (V_A) and electric double layer interaction (V_{EDL}) (Verwey 1947). Both V_A and V_{EDL} are critically affected by solution chemistry (e.g., pH and ionic strength) and nature of the materials. Solution chemistry, like pH, would determine the surface potential (or charge) while the ionic strength would control the extension of the electrical double layer which is quantified by the Debye length (the thickness of an electrical double layer). The material determines the Hamaker constant and surface charging used in the calculation of V_A and V_{EDL} .

VDW forces comprise of three major forces known as Keesom interaction (permanent dipole/ permanent dipole interactions), Debye interactions (permanent dipole/induced dipole interactions) and London interactions (induced dipole/induced dipole interactions). Explicit expressions have been derived for these forces at atomic interaction, and they have an inverse power dependence on the separation (x^{-n} , n depends on the type of force) (Hiemenz 1997). Due to their origins, they are always present and play an important role in interfacial interactions, and different approaches are available to calculate the VDW forces between macro objects as a function of separation distance (Gregory 1981). For example, for two spheres of equal radius, a , at a surface separation distance, x , the total interaction energy, V_A is given by

$$V_A(x) = -\frac{A_H}{6} \left[\frac{2a^2}{x^2 + 4ax} + \frac{2a^2}{(x + 2a)^2} + \ln \left(1 - \frac{4a^2}{(x + 2a)^2} \right) \right]$$

where A_H is the Hamaker constant, which depends on both the material of the spheres and medium. Thus, V_A decays rapidly with separation distance.

Particles (or plate surface) dispersed in water and other liquid of high dielectric constant usually acquire surface charge by mechanisms like ionization or dissociation of surface groups and preferential adsorption of ions from solution. In order to attain electrical neutrality, the excess of ions of one sign on the particle surface must be equilibrated by an excess of ions of the opposite sign in the surrounding solution. As a result, an electrical double layer (EDL) is formed. Two classical models describing the EDL are the Gouy-Chapman model and the Stern (triple layer) model (Figure A). The Gouy-Chapman model assumed that electrolyte is an ideal solution with uniform dielectric properties, the ions are point charges, and the diffusion layer begins from solid surface. While the Stern model considers the finite size of ions and the specific adsorption of ions at the interface, the diffusion layer begins from the boundary of the Stern layer.

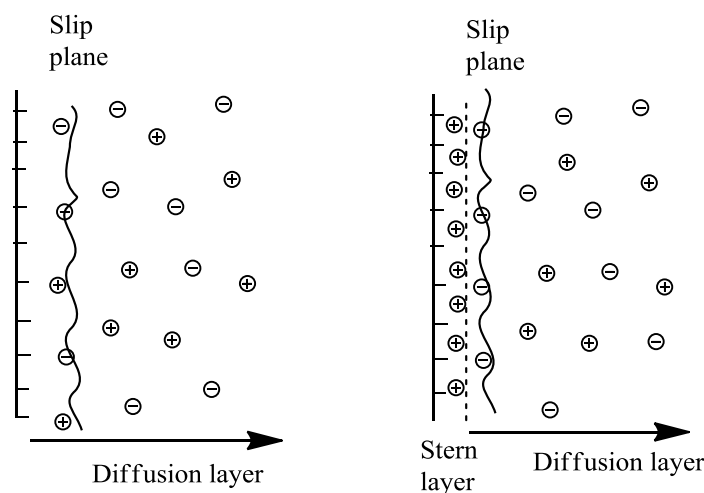


Figure A Gouy-Chapman model (left) and Stern model (right) for electrical double layer structure developed at a negatively-charged surface.

According to the Gouy-Chapman model, the average charge distribution within the EDL and the corresponding electrical potential function is related by the Poisson-Boltzman equation (PBE) (Hiemenz 1997):

$$\nabla^2 \psi = \frac{-e}{\epsilon_0 \epsilon_r} \sum_i n_i^0 z_i \exp\left(\frac{-z_i e \psi}{k_B T}\right)$$

where ψ is the electrical potential, n_i^0 is the number density of ions of valence z_i , k_B is the Boltzman constant, T is the absolute temperature, ϵ_0 is the permittivity of vacuum, and ϵ_r is the relative permittivity.

The solution of the PBE depends on the boundary conditions like geometry of the surface and the nature of surface (constant charge surface or constant potential surface).

The analytical expression for inter-particle electrostatic interaction energy (between unequal particles with radius of a_1 and a_2) at low surface potentials and symmetric electrolytes based on the linear superposition approximation (LSA) is

$$V_{EDL} = 64\pi\epsilon_0\epsilon_r \frac{a_1 a_2}{a_1 + a_2} \left(\frac{kT}{ze}\right)^2 \Gamma_1 \Gamma_2 e^{-\kappa d}$$

κ^{-1} is Debye length, d is inter-particle distance, Γ is the reduced surface potential expressed as $\Gamma = \tanh(ze\psi/4k_B T)$ (Gregory 1975).

Although the DLVO theory has been widely and successfully applied to explain colloid stability in a semi-quantitative manner, its applicability is limited in many occasions. First of all, the mathematical formulation of these interactions was based on simplified models that may not accurately represent the surface nature. For example, the Gouy-Chapman model for electrostatic interaction calculation does not consider the infinite size of ions, surface-dependent ion behavior in the vicinity of the surface, and the anisotropy of ion distribution at the interface when the surface is heterogeneous. There have been efforts to improve these models by including the role

of ion size and hydration, surface charge and polarity (Parsons et al. 2010; Schwierz et al. 2010). Besides, it oversimplifies the interaction by considering only the VDW and electrostatic interaction. In many cases, there are also non-DLVO forces, like steric force, oscillatory force, hydration force and hydrophobic interaction (Israelachvili 2011). Their relative contribution to the total interaction may increase when the complexity of surface increases. To better describe the stability of colloid and NPs, extended DLVO theories including non-DLVO forces have been developed (Grasso et al. 2002; Hoek and Agarwal 2006; Manciu and Ruckenstein 2001; Pashley 1981).

APPENDIX B

Dynamic Light Scattering

In essence, DLS determines the size of particles by correlating it with the fluctuation of scattered light intensity due to Brownian motion. The deduction of particle's hydrodynamic size was briefly described as follows (Berne 1976). A decay constant Γ (sec^{-1}) characterized particle movements is calculated from optical autocorrelation functions that derived from the scattered light measured and the particle movement. The diffusion coefficient D was then obtained based on the following equations:

$$D = \frac{\Gamma}{q^2}, \quad q = \frac{4\pi n}{\lambda} \sin\left(\frac{\theta}{2}\right)$$

Where n is refractive index of the material, λ is wavelength of the light source and θ the scattering angle. q^2 reflects the distance that the particle travels.

The diffusion coefficient is then translated into the hydrodynamic diameter of the particle through the Stokes-Einstein equation as follows:

$$R_H = \frac{k_B T}{6\pi\eta D}$$

where R_H is the hydrodynamic diameter, η is viscosity, k_B is Boltzmann constant, and T is temperature.

APPENDIX C

Isothermal Titration Calorimetry

An ITC instrument mainly consists of: a reference cell and a sample cell installed in an adiabatic jacket, a syringe controlling the titration of ligands (protein in this case) into a suspension of NPs, and a feedback system that controls the heat compensation and records the heat profile in real time (Figure C) (Pierce et al. 1999). During a typical titration experiment, each injection of the ligand solution (from the syringe) initiates the binding reaction, forming a certain amount of NP-protein complex depending on the binding affinity and the concentration of reactants (NPs and ligand) in the cell. The forming of a complex is usually accompanied with heat absorption (endothermic reaction) or heat release (exothermic reaction), depending on the types of interfacial interaction involved and their relative contribution. The heat exchange will cause a temperature difference between the reference cell and the sample cell, then the feedback system compensates the temperature imbalance by lowering or raising the thermal power applied to heat the cells. After each injection, the system will reach equilibrium and the temperature balance is restored within a certain time before the start of next injection. As a result, the recorded signal shows an interval-peak pattern.

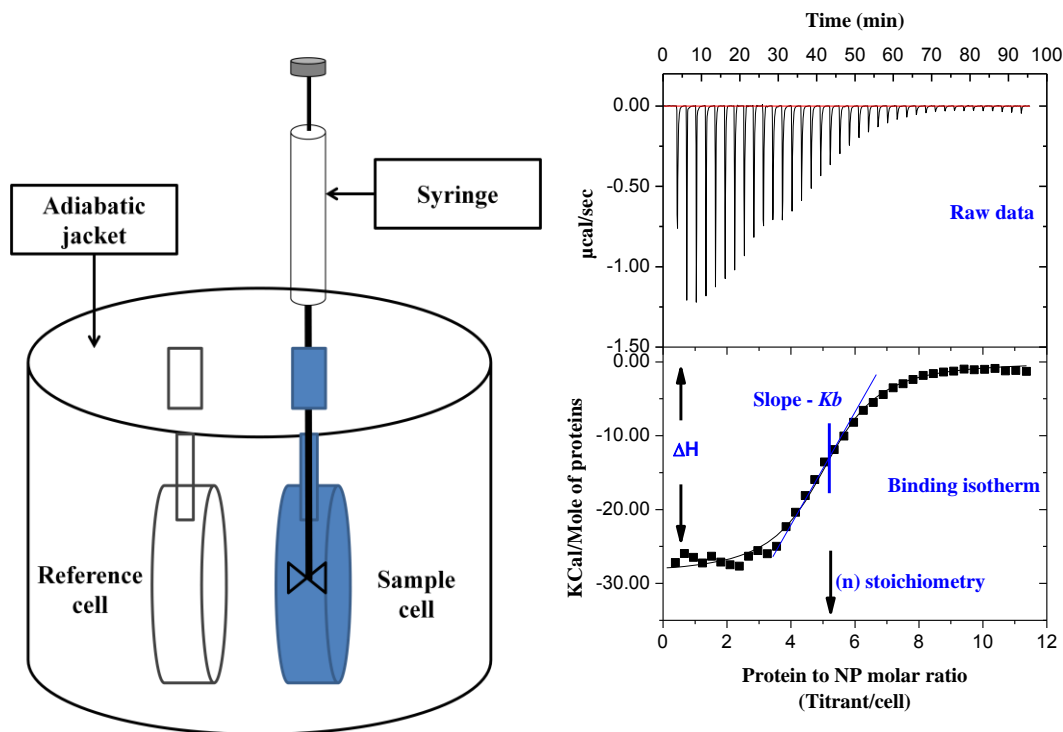


Figure C Schematic diagram of an ITC setup (left) and representative result and analysis (right).

Depending on the nature of interaction, the heat profile can be endothermic or exothermic, or even a combination of these two. There are several models available for fitting the heat profiles and provides quantitative thermodynamic parameters, such as one-site (n identical sites), two-site (two independent sites), and sequential sites models (Freyer and Lewis 2008). For ligands bind to a homogeneous particle surface, of which the nature of binding site and reaction are similar, the one-site model will be suitable in this case. If the surface is heterogeneous and with independent sites for ligand to bind, two-site or sequential sites model can be used.

APPENDIX D

Size Characterization of MUS, brOT and OT Particles

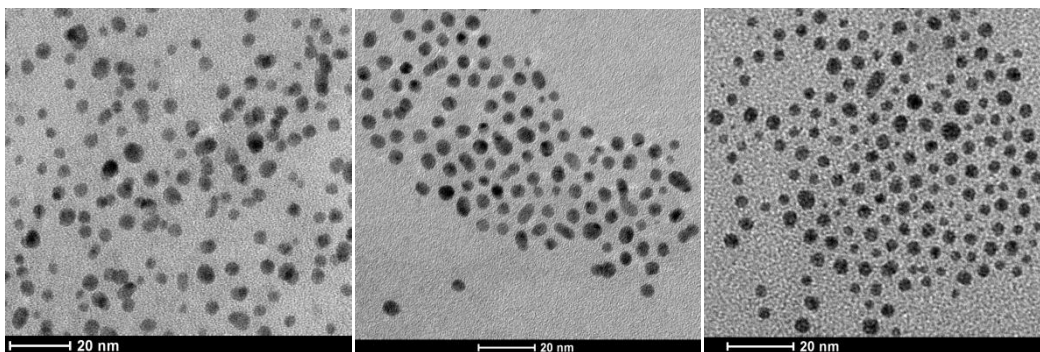


Figure D1 Representative TEM images of the MUS, brOT and OT AuNPs (from left to right).

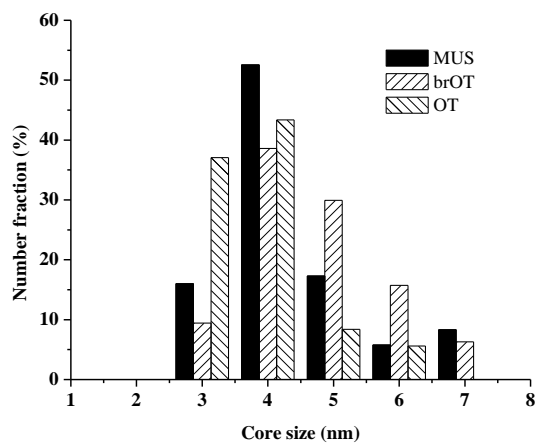


Figure D2 Size distribution of the three types AuNPs expressed in number fraction.

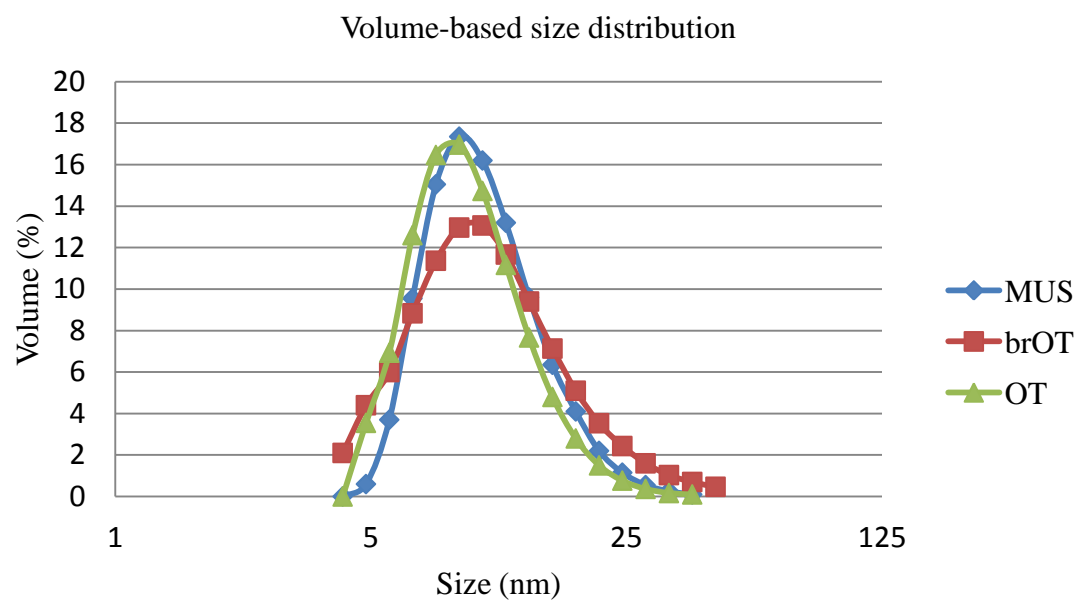


Figure D3 Volume-based size distribution of the three types of AuNPs from DLS measurement.

APPENDIX E

Representative Aggregation Profiles of AuNPs in a Range of NaCl Concentration

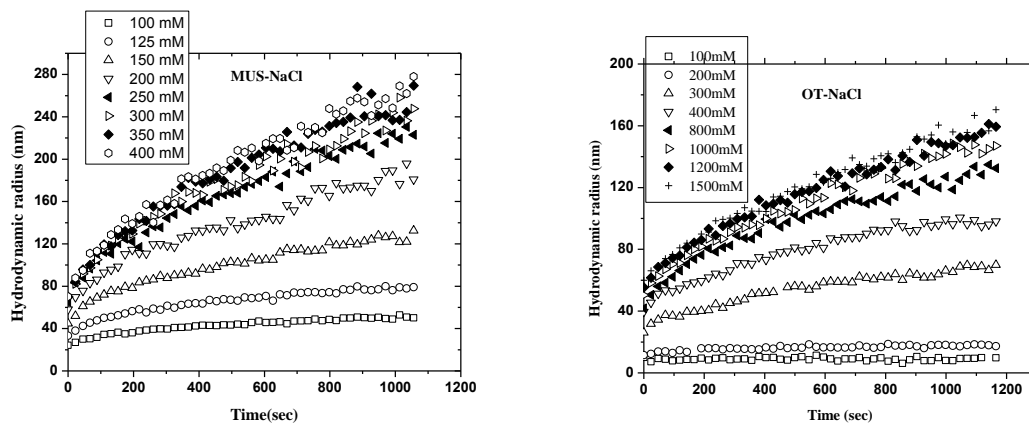


Figure E Representative aggregation profiles of MUS (left) and OT (right) obtained from time-resolved DLS measurements over a range of NaCl concentrations. The CCC uncertainty was found to range from 250 mM to 350 mM and 800 mM to 1200mM.

APPENDIX F

ITC Results on the Interaction between AuNPs and Ubiquitin or Fibrinogen.

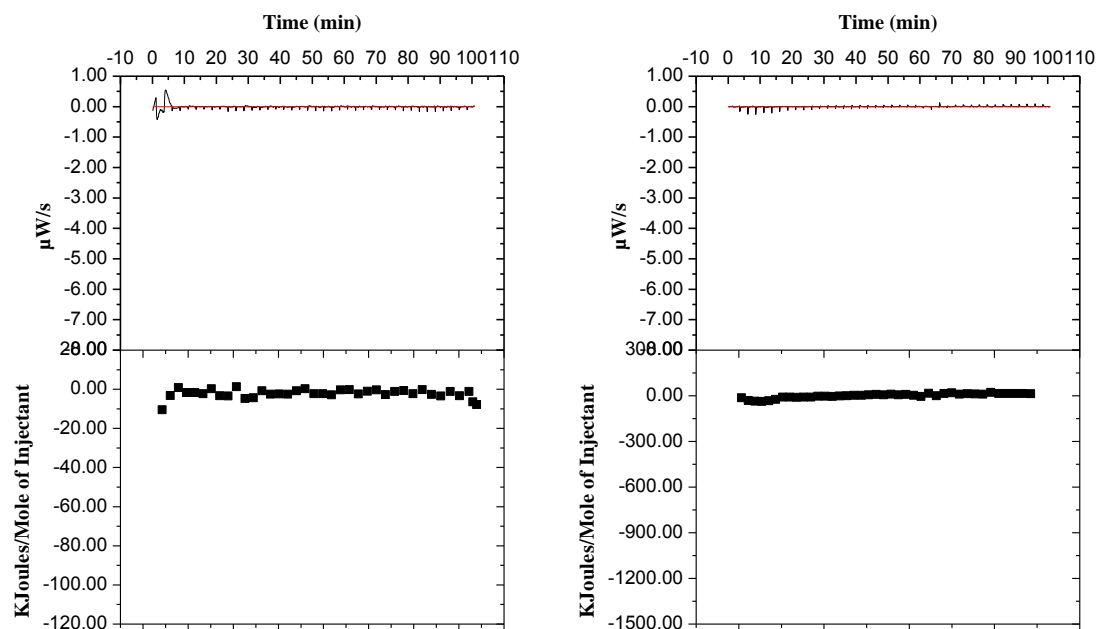


Figure F1 ITC data from the titration of 100 μM ubiquitin (left) and 80 μM fibrinogen (right) into 10 mM phosphate buffer (pH 7.4). Heat flow versus time during injection of proteins at 25 $^{\circ}\text{C}$ and heat evolved per injection of proteins was present above and below respectively.

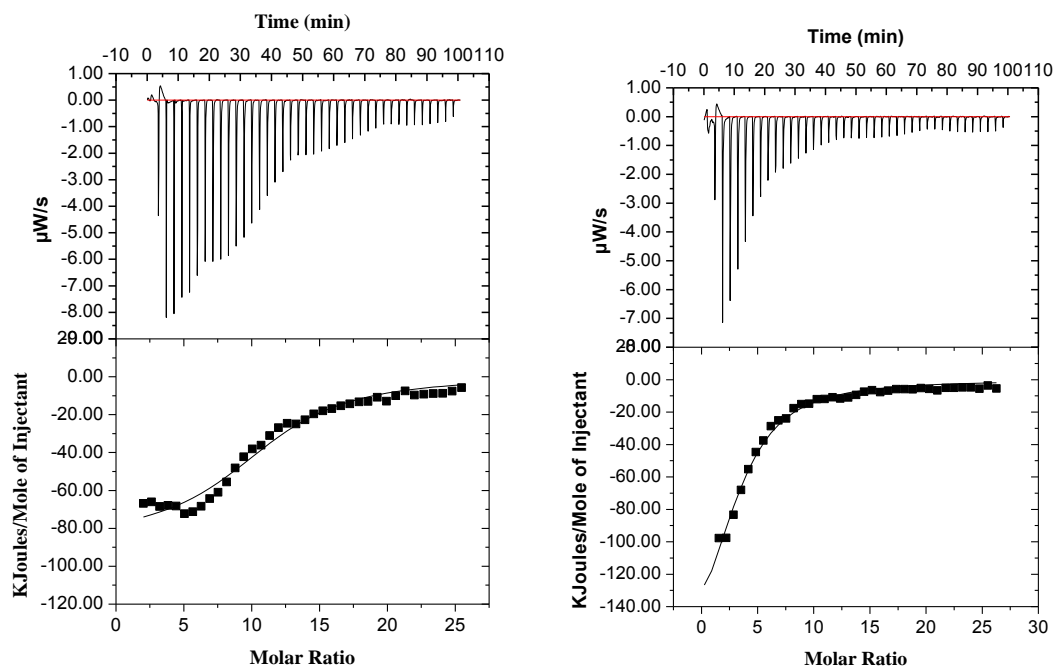


Figure F2 ITC data from the titration of 1 mM ubiquitin into 8.4 μM 66-34 brOT (left) and 7.7 μM 66-34 OT (right) AuNP. Heat flow versus time during injection of proteins at 25 °C and heat evolved per mole of added proteins (corrected for the heat of protein dilution) against the molar ratio (protein/AuNP) for each injection are shown at the top and bottom, respectively.

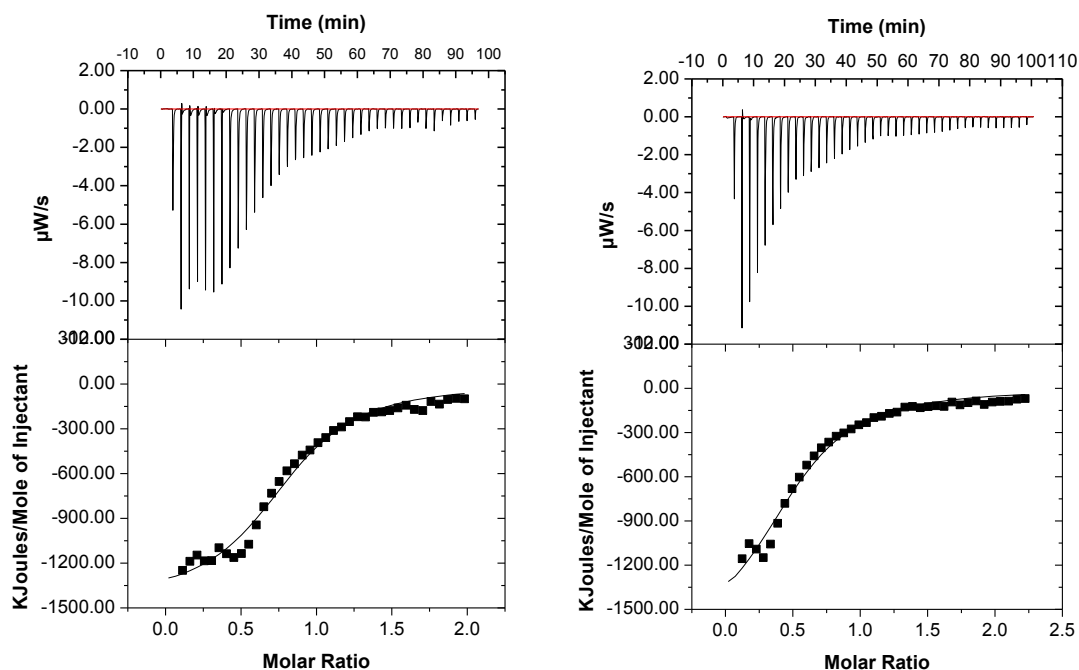


Figure F3 ITC data from the titration of 0.08 mM fibrinogen into 8.4 μM 66-34 brOT (left) and 7.7 μM 66-34 OT (right) AuNP. Heat flow versus time during injection of proteins at 25 $^{\circ}\text{C}$ and heat evolved per mole of added proteins (corrected for the heat of protein dilution) against the molar ratio (protein/AuNP) for each injection are shown at the top and bottom, respectively.

APPENDIX G

Synthesis and Size Characterization of MPA/brOT and MPA/OT Particles

Synthesis of MPA/brOT and MPA/OT Particles

0.9 mmol of gold salt (HAuCl_4) was dissolved in 150 mL ethanol and the reaction vessel was put in an ice bath. All solvents were purged with nitrogen gas for at least 30 minutes prior to use in this protocol. 0.75 mmol of the desired thiol ligand mixture (66MPA-34OT or 66MPA-34brOT) was added while stirring the solution. After 5 minutes, 1 g of sodium borohydride (NaBH_4) was dissolved in 150 mL ethanol and subsequently added drop wise to the gold-thiol mixture over a period of 1 h. The resulting solution was heavily stirred for 2 h and transferred to a refrigerator overnight for particle precipitation. The supernatant was removed and the pellet was washed via centrifugation with ethanol, methanol, and acetone, in order to remove unbound ligands. 30 mg aliquots of NPs were dissolved in ultrapure water (MilliQ) and then transferred to centrifugal filter units (Millipore Amicon Ultra, regenerated cellulose, 3,000 Da MWCO) and spun for 15 minutes at 4000 g. This washing procedure was repeated for each aliquot up to 5 times. The resulting NPs were crashed out with a non-solvent, acetone, under ultracentrifugation at 300,000 g for 30 minutes. The pellet was dried overnight under high vacuum.

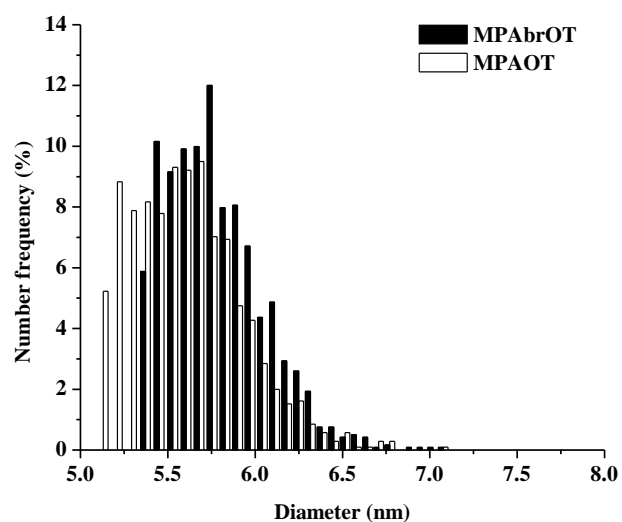


Figure G1 Size distribution of the MPA-type AuNPs based on TEM characterization (number frequency was based on random counting of more than 1000 particles).

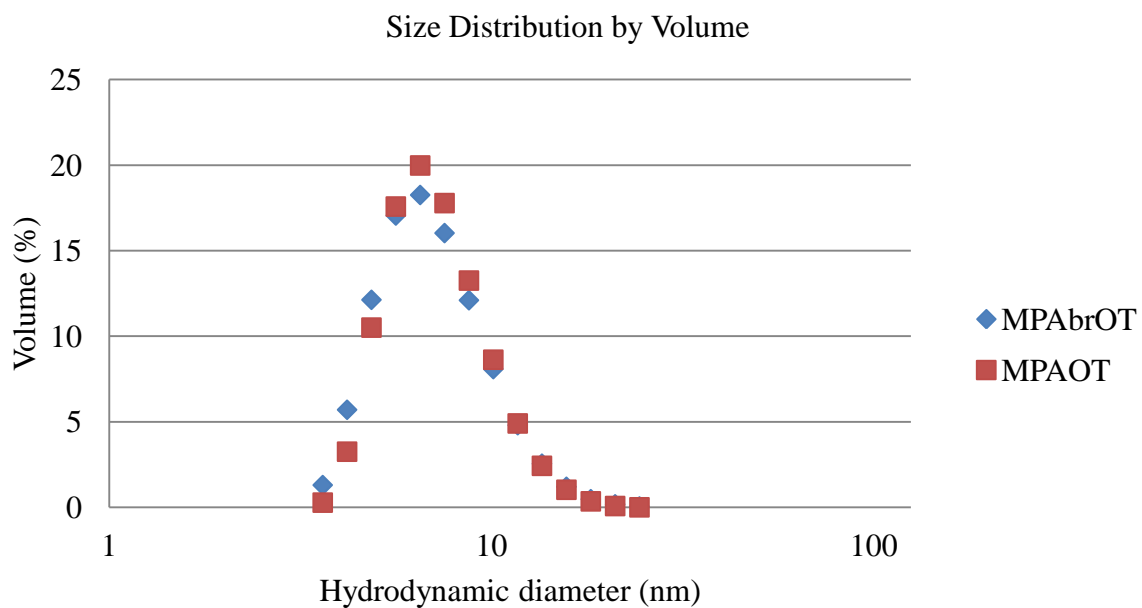


Figure G2 Hydrodynamic size distribution of the two types of AuNPs measured by DLS.

APPENDIX H

Size Change of MUS, brOT and OT Particles in the Presence of Different Concentrations of BSA

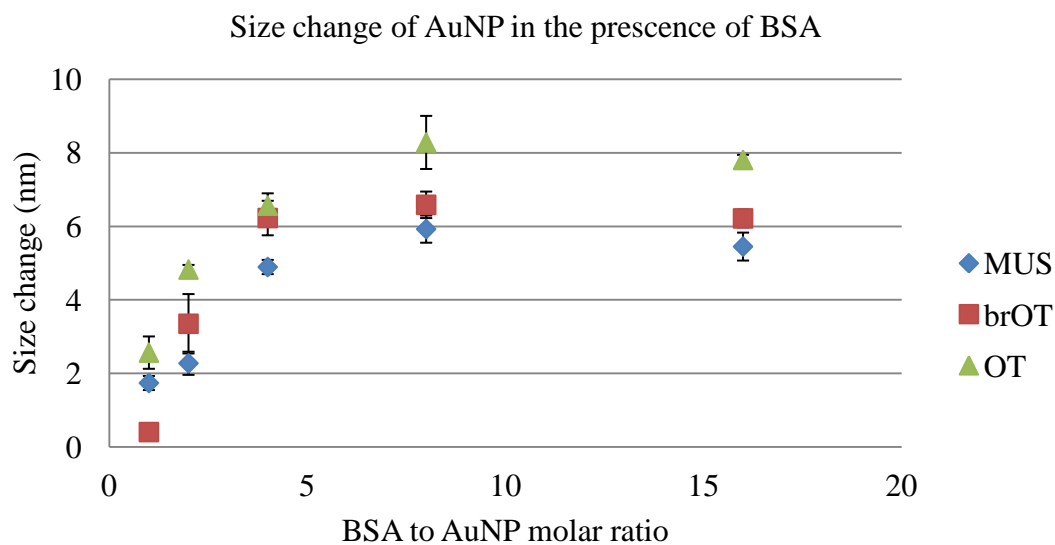


Figure H Hydrodynamic size change of three types of AuNPs in the presence of a series concentration of BSA.

APPENDIX I

The Secondary Structure of BSA in the Presence of MPA-type AuNPs

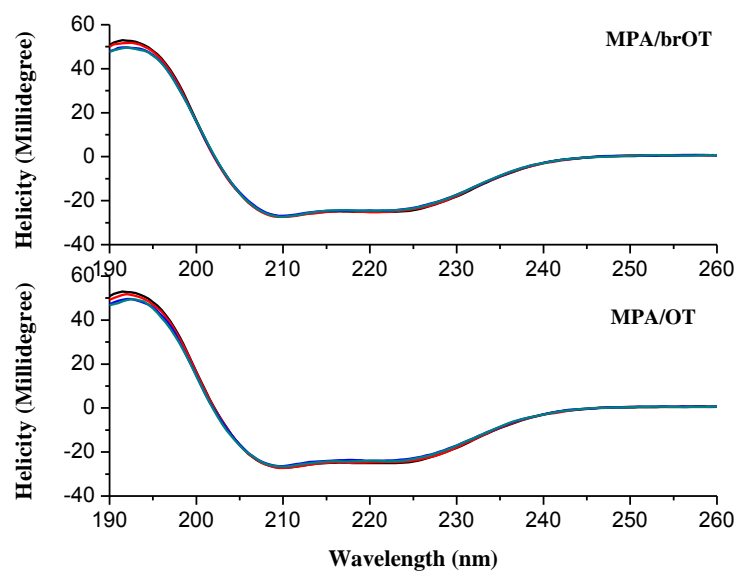


Figure I The secondary structure of BSA following the addition of MPA-type AuNP at pH 7.4.

APPENDIX J

Fluorescence Quenching of BSA by AuNPs

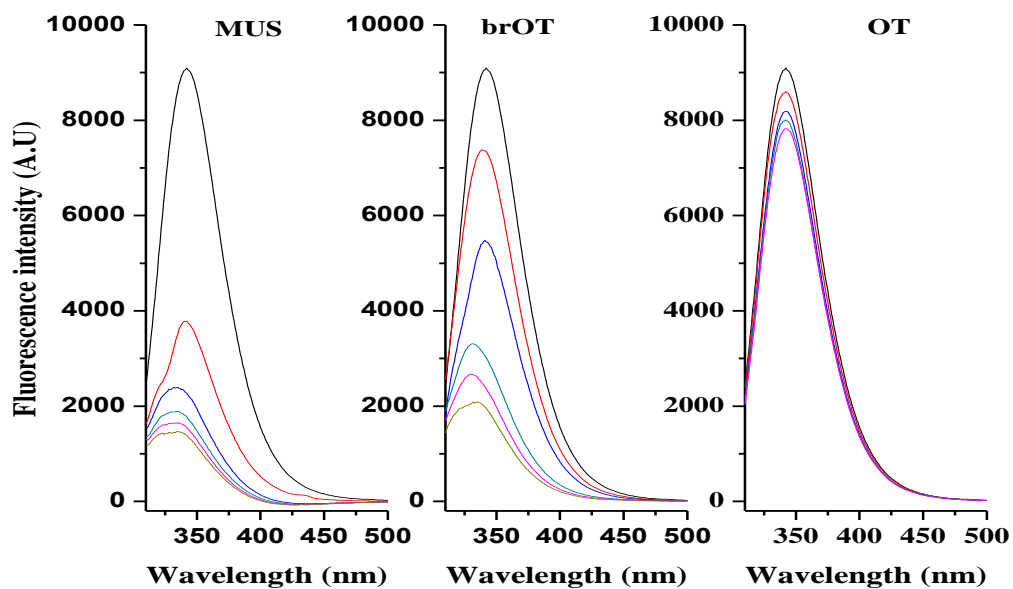


Figure J Tryptophan fluorescence emission of BSA in the presence of varying AuNP concentration (0~0.004 μM).

APPENDIX K

ITC Results for BSA-MUS AuNP interaction.

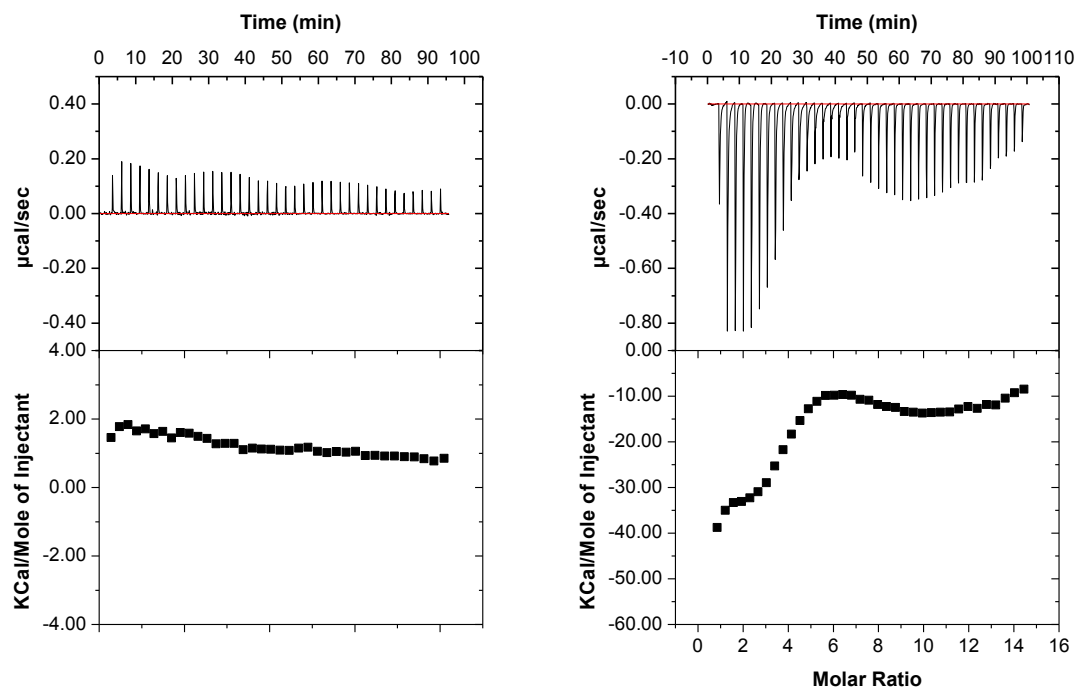


Figure K ITC data from the titration of 500 μM of BSA into 10 mM 7.4 phosphate buffer (left) and into 7.03 μM MUS AuNP. Heat flow versus time during injection of proteins at 25 $^{\circ}\text{C}$ and heat evolved per injection of proteins was present above and below respectively.

APPENDIX L

Measurement of the Esterase Activity of BSA

Esterase activity of BSA in the absence and presence of AuNPs was determined using 4-nitrophenyl acetate (Sigma Aldrich) as the substrate. The formation of 4-nitrophenol was monitored at 400 nm by using a UV–visible spectrophotometer (Agilent 8453, CA, USA). The 2 ml reaction mixture (10 mM phosphate buffer at pH 7.4) contained 100 μ M 4-nitrophenyl acetate, 2.5 μ M BSA and various concentrations of AuNPs, the reaction was initiated by the addition of 4-nitrophenyl acetate. Adsorption due to 4-nitrophenol formation was calculated from the adsorption of the mixture at 5 min subtracted the adsorption before substrate addition. Enzyme activity was defined as moles of 4-nitrophenol formed per min. A molar extinction coefficient for p-nitrophenol of $\epsilon = 17\,700\text{ M}^{-1}\cdot\text{cm}^{-1}$ was used for the p-nitrophenol calculation.

Evaluation of the effects of AuNPs complexation on BSA functionality was done using the well-established esterase activity assay. The catalytic function of Tyr-411 in BSA is considered to be responsible for the esterase activity of serum albumin, and factors that influence the local environment of this site will affect the catalytic activity (Sakurai et al. 2004).

It is showed that the esterase activity of BSA was inhibited by AuNP adsorption, and the degree of inhibition increased as AuNPs concentration increased (Figure L). Overall, MPA-brOT inhibited more than MPA-OT. Two possible factors may contribute to the difference in the inhibition between MPA-brOT and MPA-OT: 1) the different affinity of BSA to these AuNPs; 2) the different conformations of the complex BSA

between the two types of AuNPs. Considering the larger size increase in BSA-MPA-OT complexation, the number of BSA on MPA-OT should not be less than that in BSA-MPA-brOT. Therefore, the activity difference is more likely due to different conformations of BSA on the surface of AuNPs. First of all, side-on orientation adopted by BSA on MPA-brOT lead to tighter interaction and higher degree of alteration of protein structure (possibly tertiary, if not secondary at pH 7.4), compared to end-on orientation on MPA-OT. Secondly, side-on orientation is more likely to shield the active site (Tyr-411) from interaction with the substrates than the end-on orientation, due to large contact area (similar to fluorescence quenching).

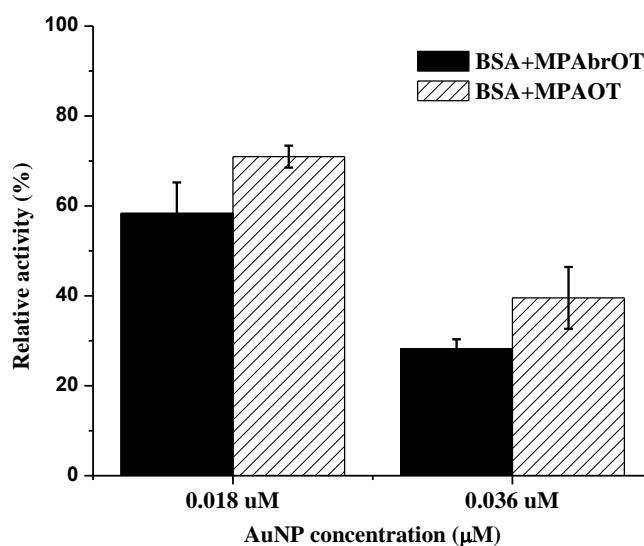


Figure L Effect of MPA/brOT and MPA/OT on the esterase activity of BSA, the activity was expressed as the activity relative to that of free BSA without the presence of AuNPs (error bar represent standard deviation, $n = 3$).

APPENDIX M

AuNP Adsorption Kinetics onto *E.coli* and *B.cereus* cell

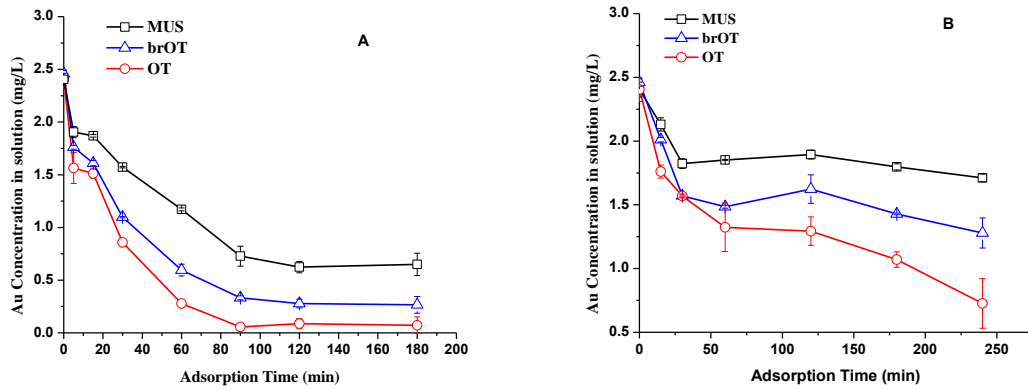


Figure M Unbounded AuNP concentration in suspension during the adsorption kinetics experiment of *E. coli* (A) and *B. cereus* (B). Concentration of *E. coli* and *B. cereus* cell was 4.2×10^8 and 1.6×10^8 cell/mL, respectively. *E. coli* adsorption data was based on Huang et al. (Huang et al. 2013a).

REFERENCES

- Avissar, R., 1990, A Statistical-Dynamical Approach to Parameterize Subgrid-Scale Land-Surface Heterogeneity in Climate Models, *in* Wood, E., ed., Land Surface — Atmosphere Interactions for Climate Modeling: Springer Netherlands, p. 155-178.
- Bayer, M.E., and Sloyer, J.L., 1990, THE ELECTROPHORETIC MOBILITY OF GRAM-NEGATIVE AND GRAM-POSITIVE BACTERIA - AN ELECTROKINETIC ANALYSIS: *Journal of General Microbiology*, v. 136, p. 867-874.
- Benn, T.M., and Westerhoff, P., 2008, Nanoparticle Silver Released into Water from Commercially Available Sock Fabrics: *Environmental Science & Technology*, v. 42, no. 11, p. 4133-4139.
- Berne, B.J., 1976, Dynamic light scattering: with applications to chemistry, biology and physics, DoverPublications. com.
- Bhattacharya, D., and Gupta, R.K., 2005, Nanotechnology and potential of microorganisms: *Critical Reviews in Biotechnology*, v. 25, no. 4, p. 199-204.
- Bolis, V., Cavenago, A., and Fubini, B., 1997, Surface Heterogeneity on Hydrophilic and Hydrophobic Silicas: Water and Alcohols as Probes for H-Bonding and Dispersion Forces†: *Langmuir*, v. 13, no. 5, p. 895-902.
- Bostrom, M., Williams, D.R.M., and Ninham, B.W., 2001, Specific ion effects: Why DLVO theory fails for biology and colloid systems: *Physical Review Letters*, v. 8716, no. 16, p. 168103.
- Calero, C., Faraudo, J., and Bastos-Gonzalez, D., 2011, Interaction of Monovalent Ions with Hydrophobic and Hydrophilic Colloids: Charge Inversion and Ionic Specificity: *Journal of the American Chemical Society*, v. 133, no. 38, p. 15025-15035.
- Camesano, T.A., and Abu-Lail, N.I., 2002, Heterogeneity in bacterial surface polysaccharides, probed on a single-molecule basis: *Biomacromolecules*, v. 3, no. 4, p. 661-667.
- Carter, D.C., Ho, J. X, 1994, Structure of Serum Albumin: *Adv. Protein Chem.*, v. 37, p. 153-203.

- Cedervall, T., Lynch, I., Lindman, S., Berggård, T., Thulin, E., Nilsson, H., Dawson, K.A., and Linse, S., 2007, Understanding the nanoparticle–protein corona using methods to quantify exchange rates and affinities of proteins for nanoparticles: *Proceedings of the National Academy of Sciences*, v. 104, no. 7, p. 2050-2055.
- Centrone, A., Penzo, E., Sharma, M., Myerson, J.W., Jackson, A.M., Marzari, N., and Stellacci, F., 2008, The role of nanostructure in the wetting behavior of mixed-monolayer-protected metal nanoparticles: *Proceedings of the National Academy of Sciences of the United States of America*, v. 105, no. 29, p. 9886-9891.
- Chen, K., Xu, Y., Rana, S., Miranda, O.R., Dubin, P.L., Rotello, V.M., Sun, L., and Guo, X., 2011, Electrostatic Selectivity in Protein–Nanoparticle Interactions: *Biomacromolecules*, v. 12, no. 7, p. 2552-2561.
- Chen, K.L., and Elimelech, M., 2006, Aggregation and deposition kinetics of fullerene (C-60) nanoparticles: *Langmuir*, v. 22, no. 26, p. 10994-11001.
- Cukalevski, R., Lundqvist, M., Oslakovic, C., Dahlback, B., Linse, S., and Cedervall, T., 2011, Structural Changes in Apolipoproteins Bound to Nanoparticles: *Langmuir*, v. 27, no. 23, p. 14360-14369.
- De, M., Miranda, O.R., Rana, S., and Rotello, V.M., 2009, Size and geometry dependent protein-nanoparticle self-assembly: *Chemical Communications*, no. 16, p. 2157-2159.
- De, M., You, C.-C., Srivastava, S., and Rotello, V.M., 2007, Biomimetic Interactions of Proteins with Functionalized Nanoparticles: A Thermodynamic Study: *Journal of the American Chemical Society*, v. 129, no. 35, p. 10747-10753.
- Delgado, A.V., González-Caballero, F., Hunter, R.J., Koopal, L.K., and Lyklema, J., 2007, Measurement and interpretation of electrokinetic phenomena: *Journal of Colloid and Interface Science*, v. 309, no. 2, p. 194-224.
- Deng, Z.J., Liang, M.T., Toth, I., Monteiro, M.J., and Minchin, R.F., 2012, Molecular Interaction of Poly(acrylic acid) Gold Nanoparticles with Human Fibrinogen: *Acs Nano*, v. 6, no. 10, p. 8962-8969.
- Dong, S.J., Shang, L., Wang, Y.Z., and Jiang, J.G., 2007, pH-dependent protein conformational changes in albumin : gold nanoparticle bioconjugates: A spectroscopic study: *Langmuir*, v. 23, no. 5, p. 2714-2721.
- Dorobantu, L.S., Bhattacharjee, S., Foght, J.M., and Gray, M.R., 2008, Atomic force microscopy measurement of heterogeneity in bacterial surface hydrophobicity: *Langmuir*, v. 24, no. 9, p. 4944-4951.

- Dorobantu, L.S., Bhattacharjee, S., Foght, J.M., and Gray, M.R., 2009, Analysis of Force Interactions between AFM Tips and Hydrophobic Bacteria Using DLVO Theory: *Langmuir*, v. 25, no. 12, p. 6968-6976.
- Drelich, J., and Miller, J.D., 1994, The Effect of Solid Surface Heterogeneity and Roughness on the Contact Angle/Drop (Bubble) Size Relationship: *Journal of Colloid and Interface Science*, v. 164, no. 1, p. 252-259.
- Drelich, J., and Wang, Y.U., 2011, Charge heterogeneity of surfaces: Mapping and effects on surface forces: *Advances in Colloid and Interface Science*, v. 165, no. 2, p. 91-101.
- Drelich, J., Wilbur, J.L., Miller, J.D., and Whitesides, G.M., 1996, Contact Angles for Liquid Drops at a Model Heterogeneous Surface Consisting of Alternating and Parallel Hydrophobic/Hydrophilic Strips: *Langmuir*, v. 12, no. 7, p. 1913-1922.
- Dubeau, S., Bourassa, P., Thomas, T.J., and Tajmir-Riahi, H.A., 2010, Biogenic and Synthetic Polyamines Bind Bovine Serum Albumin: *Biomacromolecules*, v. 11, no. 6, p. 1507-1515.
- Duffadar, R., Kalasin, S., Davis, J.M., and Santore, M.M., 2009, The impact of nanoscale chemical features on micron-scale adhesion: Crossover from heterogeneity-dominated to mean-field behavior: *Journal of Colloid and Interface Science*, v. 337, no. 2, p. 396-407.
- Dunphy Guzman, K.A., Finnegan, M.P., and Banfield, J.F., 2006, Influence of Surface Potential on Aggregation and Transport of Titania Nanoparticles: *Environmental Science & Technology*, v. 40, no. 24, p. 7688-7693.
- Duval, J.F.L., Leermakers, F.A.M., and van Leeuwen, H.P., 2004, Electrostatic interactions between double layers: Influence of surface roughness, regulation, and chemical heterogeneities: *Langmuir*, v. 20, no. 12, p. 5052-5065.
- Eboigbodin, K.E., and Biggs, C.A., 2008, Characterization of the extracellular polymeric substances produced by *Escherichia coli* using infrared spectroscopic, proteomic, and aggregation studies: *Biomacromolecules*, v. 9, no. 2, p. 686-695.
- Elimelech, M., Chen, J.Y., and Kuznar, Z.A., 2003, Particle deposition onto solid surfaces with micropatterned charge heterogeneity: The "hydrodynamic bump" effect: *Langmuir*, v. 19, no. 17, p. 6594-6597.
- Fabrega, J., Renshaw, J.C., and Lead, J.R., 2009, Interactions of Silver Nanoparticles with *Pseudomonas putida* Biofilms: *Environmental Science & Technology*, v. 43, no. 23, p. 9004-9009.

- Fein, J.B., Martin, A.M., and Wightman, P.G., 2001, Metal adsorption onto bacterial surfaces: Development of a predictive approach: *Geochimica Et Cosmochimica Acta*, v. 65, no. 23, p. 4267-4273.
- Franz, M., Arafat, H.A., and Pinto, N.G., 2000, Effect of chemical surface heterogeneity on the adsorption mechanism of dissolved aromatics on activated carbon: *Carbon*, v. 38, no. 13, p. 1807-1819.
- Freyer, M.W., and Lewis, E.A., 2008, Isothermal Titration Calorimetry: Experimental Design, Data Analysis, and Probing Macromolecule/Ligand Binding and Kinetic Interactions, *in* Dr. John, J.C., and Dr. H. William Detrich, III, eds., *Methods in Cell Biology*: Academic Press, p. 79-113.
- Fuss, C., Palmaz, J.C., and Sprague, E.A., 2001, Fibrinogen: Structure, Function, and Surface Interactions: *Journal of Vascular and Interventional Radiology*, v. 12, no. 6, p. 677-682.
- Gaboriaud, F., and Dufrene, Y.F., 2007, Atomic force microscopy of microbial cells: Application to nanomechanical properties, surface forces and molecular recognition forces: *Colloids and Surfaces B-Biointerfaces*, v. 54, no. 1, p. 10-19.
- Gagner, J.E., Shrivastava, S., Qian, X., Dordick, J.S., and Siegel, R.W., 2012, Engineering Nanomaterials for Biomedical Applications Requires Understanding the Nano-Bio Interface: A Perspective: *Journal of Physical Chemistry Letters*, v. 3, no. 21, p. 3149-3158.
- Ghorai, P.K., and Glotzer, S.C., 2010, Atomistic Simulation Study of Striped Phase Separation in Mixed-Ligand Self-Assembled Monolayer Coated Nanoparticles: *Journal of Physical Chemistry C*, v. 114, no. 45, p. 19182-19187.
- Ginn, B.R., and Fein, J.B., 2008, The effect of species diversity on metal adsorption onto bacteria: *Geochimica Et Cosmochimica Acta*, v. 72, no. 16, p. 3939-3948.
- Grasso, D., Subramaniam, K., Butkus, M., Strevett, K., and Bergendahl, J., 2002, A review of non-DLVO interactions in environmental colloidal systems: *Reviews in Environmental Science and Biotechnology*, v. 1, no. 1, p. 17-38.
- Gregory, J., 1975, Interaction of unequal double layers at constant charge: *Journal of Colloid and Interface Science*, v. 51, no. 1, p. 44-51.
- Gregory, J., 1981, Approximate expressions for retarded van der waals interaction: *Journal of Colloid and Interface Science*, v. 83, no. 1, p. 138-145.

- Hackley, V.A., Tsai, D.H., DelRio, F.W., Keene, A.M., Tyner, K.M., MacCuspie, R.I., Cho, T.J., and Zachariah, M.R., 2011, Adsorption and Conformation of Serum Albumin Protein on Gold Nanoparticles Investigated Using Dimensional Measurements and in Situ Spectroscopic Methods: *Langmuir*, v. 27, no. 6, p. 2464-2477.
- Han, G., Ghosh, P., and Rotello, V.M., 2007, Functionalized gold nanoparticles for drug delivery: *Nanomedicine*, v. 2, no. 1, p. 113-123.
- Hayden, S.C., Zhao, G.X., Saha, K., Phillips, R.L., Li, X.N., Miranda, O.R., Rotello, V.M., El-Sayed, M.A., Schmidt-Krey, I., and Bunz, U.H.F., 2012, Aggregation and Interaction of Cationic Nanoparticles on Bacterial Surfaces: *Journal of the American Chemical Society*, v. 134, no. 16, p. 6920-6923.
- Hermansson, M., 1999, The DLVO theory in microbial adhesion: *Colloids and Surfaces B-Biointerfaces*, v. 14, no. 1-4, p. 105-119.
- Hetrick, E.M., Shin, J.H., Paul, H.S., and Schoenfisch, M.H., 2009, Anti-biofilm efficacy of nitric oxide-releasing silica nanoparticles: *Biomaterials*, v. 30, no. 14, p. 2782-2789.
- Hiemenz, P.C., Rajagopalan, R., 1997, *Principles of Colloid and Surface Chemistry* (3th Edition) New York, USA, CRC press, p. 499-530.
- Hochella, M.F., Lower, S.K., Maurice, P.A., Penn, R.L., Sahai, N., Sparks, D.L., and Twining, B.S., 2008, Nanominerals, Mineral Nanoparticles, and Earth Systems: *Science*, v. 319, no. 5870, p. 1631-1635.
- Hodgkinson, G., and Hlady, V., 2005, Relating material surface heterogeneity to protein adsorption: the effect of annealing of micro-contact-printed OTS patterns: *Journal of Adhesion Science and Technology*, v. 19, no. 3-5, p. 235-255.
- Hoek, E.M.V., and Agarwal, G.K., 2006, Extended DLVO interactions between spherical particles and rough surfaces: *Journal of Colloid and Interface Science*, v. 298, no. 1, p. 50-58.
- Horinek, D., and Netz, R.R., 2007, Specific ion adsorption at hydrophobic solid surfaces: *Physical Review Letters*, v. 99, no. 22, p. 226104.
- Huang, R., Carney, R.P., Stellacci, F., and Lau, B.L.T., 2013a, Colloidal Stability of Self-Assembled Monolayer-Coated Gold Nanoparticles: The Effects of Surface Compositional and Structural Heterogeneity: *Langmuir*, v. 29, no. 37, p. 11560-11566.

- Huang, R., Carney, R.P., Stellacci, F., and Lau, B.L.T., 2013b, Protein-nanoparticle interactions: the effects of surface compositional and structural heterogeneity are scale dependent: *Nanoscale*, v. 5, no. 15, p. 6928-6935.
- Hung, A., Mager, M., Hembury, M., Stellacci, F., Stevens, M.M., and Yarovsky, I., 2013, Amphiphilic amino acids: a key to adsorbing proteins to nanopatterned surfaces?: *Chemical Science*, v. 4, no. 3, p. 928-937.
- Hung, A., Mwenifumbo, S., Mager, M., Kuna, J.J., Stellacci, F., Yarovsky, I., and Stevens, M.M., 2011, Ordering Surfaces on the Nanoscale: Implications for Protein Adsorption: *Journal of the American Chemical Society*, v. 133, no. 5, p. 1438-1450.
- Inouye, M., and Yee, M.-L., 1972, Specific Removal of Proteins from the Envelope of *Escherichia coli* by Protease Treatments: *Journal of Bacteriology*, v. 112, no. 1, p. 585-592.
- Israelachvili, J.N., 2011, *Intermolecular and surface forces: revised third edition*, Academic press.
- Jackson, A.M., Hu, Y., Silva, P.J., and Stellacci, F., 2006, From homoligand- to mixed-ligand-monolayer-protected metal nanoparticles: A scanning tunneling microscopy investigation: *Journal of the American Chemical Society*, v. 128, no. 34, p. 11135-11149.
- Jackson, A.M., Myerson, J.W., and Stellacci, F., 2004, Spontaneous assembly of subnanometre-ordered domains in the ligand shell of monolayer-protected nanoparticles: *Nature Materials*, v. 3, no. 5, p. 330-336.
- Jans, H., Liu, X., Austin, L., Maes, G., and Huo, Q., 2009, Dynamic Light Scattering as a Powerful Tool for Gold Nanoparticle Bioconjugation and Biomolecular Binding Studies: *Analytical Chemistry*, v. 81, no. 22, p. 9425-9432.
- Karunakaran, E., and Biggs, C.A., 2011, Mechanisms of *Bacillus cereus* biofilm formation: an investigation of the physicochemical characteristics of cell surfaces and extracellular proteins: *Applied Microbiology and Biotechnology*, v. 89, no. 4, p. 1161-1175.
- Kissa, E., 1999, *Dispersions: characterization, testing, and measurement*: New York, USA, CRC Press.
- Klaine, S.J., Alvarez, P.J.J., Batley, G.E., Fernandes, T.F., Handy, R.D., Lyon, D.Y., Mahendra, S., McLaughlin, M.J., and Lead, J.R., 2008, Nanomaterials in the environment: Behavior, fate, bioavailability, and effects: *Environmental Toxicology and Chemistry*, v. 27, no. 9, p. 1825-1851.

- Koegler, P., Clayton, A., Thissen, H., Santos, G.N.C., and Kingshott, P., 2012, The influence of nanostructured materials on biointerfacial interactions: *Advanced Drug Delivery Reviews*, v. 64, no. 15, p. 1820-1839.
- Koster, R.D., and Suarez, M.J., 1992, A Comparative Analysis of Two Land Surface Heterogeneity Representations: *Journal of Climate*, v. 5, no. 12, p. 1379-1390.
- Kuna, J.J., Voitchovsky, K., Singh, C., Jiang, H., Mwenifumbo, S., Ghorai, P.K., Stevens, M.M., Glotzer, S.C., and Stellacci, F., 2009, The effect of nanometre-scale structure on interfacial energy: *Nature Materials*, v. 8, no. 10, p. 837-842.
- Lacerda, S.H.D., Park, J.J., Meuse, C., Pristinski, D., Becker, M.L., Karim, A., and Douglas, J.F., 2010, Interaction of Gold Nanoparticles with Common Human Blood Proteins: *Acs Nano*, v. 4, no. 1, p. 365-379.
- Lee, D., Cohen, R.E., and Rubner, M.F., 2005, Antibacterial properties of Ag nanoparticle loaded multilayers and formation of magnetically directed antibacterial microparticles: *Langmuir*, v. 21, no. 21, p. 9651-9659.
- Levard, C., Hotze, E.M., Lowry, G.V., and Brown, G.E., 2012, Environmental Transformations of Silver Nanoparticles: Impact on Stability and Toxicity: *Environmental Science & Technology*, v. 46, no. 13, p. 6900-6914.
- Li, X.Q., Elliott, D.W., and Zhang, W.X., 2006, Zero-valent iron nanoparticles for abatement of environmental pollutants: Materials and engineering aspects: *Critical Reviews in Solid State and Materials Sciences*, v. 31, no. 4, p. 111-122.
- Lin, S., 2012, Deposition of Nano-scale Particles in Aqueous Environments--Influence of Particle Size, Surface Coating, and Aggregation State, Duke University.
- Lindman, S., Lynch, I., Thulin, E., Nilsson, H., Dawson, K.A., and Linse, S., 2007, Systematic investigation of the thermodynamics of HSA adsorption to N-isopropylacrylamide/N-tert-butylacrylamide copolymer nanoparticles. Effects of particle size and hydrophobicity: *Nano Letters*, v. 7, no. 4, p. 914-920.
- Liu, X., Yu, M., Kim, H., Mameli, M., and Stellacci, F., 2012, Determination of monolayer-protected gold nanoparticle ligand-shell morphology using NMR: *Nature communications*, v. 3, p. 1182.
- Love, J.C., Estroff, L.A., Kriebel, J.K., Nuzzo, R.G., and Whitesides, G.M., 2005, Self-Assembled Monolayers of Thiolates on Metals as a Form of Nanotechnology: *Chemical Reviews*, v. 105, no. 4, p. 1103-1170.
- Lundqvist, M., Sethson, I., and Jonsson, B.H., 2004, Protein adsorption onto silica nanoparticles: Conformational changes depend on the particles' curvature and the protein stability: *Langmuir*, v. 20, no. 24, p. 10639-10647.

- Lundqvist, M., Stigler, J., Cedervall, T., Berggard, T., Flanagan, M.B., Lynch, I., Elia, G., and Dawson, K., 2011, The Evolution of the Protein Corona around Nanoparticles: A Test Study: *Acs Nano*, v. 5, no. 9, p. 7503-7509.
- Lundqvist, M., Stigler, J., Elia, G., Lynch, I., Cedervall, T., and Dawson, K.A., 2008, Nanoparticle size and surface properties determine the protein corona with possible implications for biological impacts: *Proceedings of the National Academy of Sciences of the United States of America*, v. 105, no. 38, p. 14265-14270.
- Lynch, I., Cedervall, T., Lundqvist, M., Cabaleiro-Lago, C., Linse, S., and Dawson, K.A., 2007, The nanoparticle - protein complex as a biological entity; a complex fluids and surface science challenge for the 21st century: *Advances in Colloid and Interface Science*, v. 134-35, p. 167-174.
- Lytle, D.A., Johnson, C.H., and Rice, E.W., 2002, A systematic comparison of the electrokinetic properties of environmentally important microorganisms in water: *Colloids and Surfaces B-Biointerfaces*, v. 24, no. 2, p. 91-101.
- Ma, H., Winslow, C.J., and Logan, B.E., 2008, Spectral force analysis using atomic force microscopy reveals the importance of surface heterogeneity in bacterial and colloid adhesion to engineered surfaces: *Colloids and Surfaces B-Biointerfaces*, v. 62, no. 2, p. 232-237.
- Madden, A.S., and Hochella, M.F., 2005, Nanoscience meets geochemistry: Size-dependent reactivity of hematite: *Geochimica Et Cosmochimica Acta*, v. 69, no. 10, p. A514-A514.
- Madden, A.S., Hochella, M.F., and Luxton, T.P., 2006, Insights for size-dependent reactivity of hematite nanomineral surfaces through Cu²⁺ sorption: *Geochimica Et Cosmochimica Acta*, v. 70, no. 16, p. 4095-4104.
- Magrez, A., Kasas, S., Salicio, V., Pasquier, N., Seo, J.W., Celio, M., Catsicas, S., Schwaller, B., and Forró, L., 2006, Cellular Toxicity of Carbon-Based Nanomaterials: *Nano Letters*, v. 6, no. 6, p. 1121-1125.
- Manciu, M., and Ruckenstein, E., 2001, Role of the Hydration Force in the Stability of Colloids at High Ionic Strengths: *Langmuir*, v. 17, no. 22, p. 7061-7070.
- Mandal, D., Bolander, M.E., Mukhopadhyay, D., Sarkar, G., and Mukherjee, P., 2006, The use of microorganisms for the formation of metal nanoparticles and their application: *Applied Microbiology and Biotechnology*, v. 69, no. 5, p. 485-492.
- Mayer, L.M., 1982, Aggregation of colloidal iron during estuarine mixing: Kinetics, mechanism, and seasonality: *Geochimica Et Cosmochimica Acta*, v. 46, no. 12, p. 2527-2535.

- McEwen, G.D., Wu, Y., and Zhou, A., 2010, Probing nanostructures of bacterial extracellular polymeric substances versus culture time by Raman microspectroscopy and atomic force microscopy: *Biopolymers*, v. 93, no. 2, p. 171-177.
- Meder, F., Daberkow, T., Treccani, L., Wilhelm, M., Schowalter, M., Rosenauer, A., Madler, L., and Rezwan, K., 2012, Protein adsorption on colloidal alumina particles functionalized with amino, carboxyl, sulfonate and phosphate groups: *Acta Biomaterialia*, v. 8, no. 3, p. 1221-1229.
- Milani, S., Bombelli, F.B., Pitek, A.S., Dawson, K.A., and Radler, J., 2012, Reversible versus Irreversible Binding of Transferrin to Polystyrene Nanoparticles: Soft and Hard Corona: *Acs Nano*, v. 6, no. 3, p. 2532-2541.
- Monopoli, M.P., Aberg, C., Salvati, A., and Dawson, K.A., 2012, Biomolecular coronas provide the biological identity of nanosized materials: *Nature Nanotechnology*, v. 7, no. 12, p. 779-786.
- Mylon, S.E., Chen, K.L., and Elimelech, M., 2004, Influence of Natural Organic Matter and Ionic Composition on the Kinetics and Structure of Hematite Colloid Aggregation: Implications to Iron Depletion in Estuaries: *Langmuir*, v. 20, no. 21, p. 9000-9006.
- Namba, K., and Vonderviszt, F., 1997, Molecular architecture of bacterial flagellum: *Quarterly Reviews of Biophysics*, v. 30, no. 01, p. 1-65.
- Nel, A., Xia, T., Madler, L., and Li, N., 2006, Toxic Potential of Materials at the Nanolevel: *Science*, v. 311, no. 5761, p. 622-627.
- Nel, A.E., Madler, L., Velegol, D., Xia, T., Hoek, E.M.V., Somasundaran, P., Klaessig, F., Castranova, V., and Thompson, M., 2009, Understanding biophysicochemical interactions at the nano-bio interface: *Nature Materials*, v. 8, no. 7, p. 543-557.
- Ngwenya, B.T., Sutherland, I.W., and Kennedy, L., 2003, Comparison of the acid-base behaviour and metal adsorption characteristics of a gram-negative bacterium with other strains: *Applied Geochemistry*, v. 18, no. 4, p. 527-538.
- Nowack, B., and Bucheli, T.D., 2007, Occurrence, behavior and effects of nanoparticles in the environment: *Environmental Pollution*, v. 150, no. 1, p. 5-22.
- Ohshima, H., Healy, T.W., and White, L.R., 1982, Improvement on the Hogg—Healy—Fuerstenau formulas for the interaction of dissimilar double layers: I. Second and third approximations for moderate potentials: *Journal of Colloid and Interface Science*, v. 89, p. 484-493.

- Panacek, A., Kvitek, L., Pucek, R., Kolar, M., Vecerova, R., Pizurova, N., Sharma, V.K., Nevecna, T., and Zboril, R., 2006, Silver colloid nanoparticles: Synthesis, characterization, and their antibacterial activity: *Journal of Physical Chemistry B*, v. 110, no. 33, p. 16248-16253.
- Park, J.J., Lacerda, S.H.D.P., Stanley, S.K., Vogel, B.M., Kim, S., Douglas, J.F., Raghavan, D., and Karim, A., 2009, Langmuir Adsorption Study of the Interaction of CdSe/ZnS Quantum Dots with Model Substrates: Influence of Substrate Surface Chemistry and pH: *Langmuir*, v. 25, no. 1, p. 443-450.
- Park, J.M., Muhoberac, B.B., Dubin, P.L., and Xia, J., 1992, Effects of protein charge heterogeneity in protein-polyelectrolyte complexation: *Macromolecules*, v. 25, no. 1, p. 290-295.
- Parsons, D.F., Bostrom, M., Lo Nostro, P., and Ninham, B.W., 2011, Hofmeister effects: interplay of hydration, nonelectrostatic potentials, and ion size: *Physical Chemistry Chemical Physics*, v. 13, no. 27, p. 12352-12367.
- Parsons, D.F., Bostrom, M., Maceina, T.J., Salis, A., and Ninham, B.W., 2010, Why Direct or Reversed Hofmeister Series? Interplay of Hydration, Non-electrostatic Potentials, and Ion Size: *Langmuir*, v. 26, no. 5, p. 3323-3328.
- Pashley, R.M., 1981, DLVO and hydration forces between mica surfaces in Li⁺, Na⁺, K⁺, and Cs⁺ electrolyte solutions: A correlation of double-layer and hydration forces with surface cation exchange properties: *Journal of Colloid and Interface Science*, v. 83, no. 2, p. 531-546.
- Pereira, S., Zille, A., Micheletti, E., Moradas-Ferreira, P., De Philippis, R., and Tamagnini, P., 2009, Complexity of cyanobacterial exopolysaccharides: composition, structures, inducing factors and putative genes involved in their biosynthesis and assembly: *Fems Microbiology Reviews*, v. 33, no. 5, p. 917-941.
- Petosa, A.R., Jaisi, D.P., Quevedo, I.R., Elimelech, M., and Tufenkji, N., 2010, Aggregation and Deposition of Engineered Nanomaterials in Aquatic Environments: Role of Physicochemical Interactions: *Environmental Science & Technology*, v. 44, no. 17, p. 6532-6549.
- Phillips, R.L., Miranda, O.R., You, C.-C., Rotello, V.M., and Bunz, U.H.F., 2008, Rapid and Efficient Identification of Bacteria Using Gold-Nanoparticle-Poly(para-phenyleneethynylene) Constructs: *Angewandte Chemie International Edition*, v. 47, no. 14, p. 2590-2594.
- Pierce, M.M., Raman, C.S., and Nall, B.T., 1999, Isothermal titration calorimetry of protein-protein interactions: *Methods-a Companion to Methods in Enzymology*, v. 19, no. 2, p. 213-221.

- Quadros, M.E., Pierson, R., Tulve, N.S., Willis, R., Rogers, K., Thomas, T.A., and Marr, L.C., 2013, Release of Silver from Nanotechnology-Based Consumer Products for Children: *Environmental Science & Technology*, v. 47, no. 15, p. 8894-8901.
- Rana, S., Yeh, Y.C., and Rotello, V.M., 2010, Engineering the nanoparticle-protein interface: applications and possibilities: *Current Opinion in Chemical Biology*, v. 14, no. 6, p. 828-834.
- Roach, P., Farrar, D., and Perry, C.C., 2005, Interpretation of Protein Adsorption: Surface-Induced Conformational Changes: *Journal of the American Chemical Society*, v. 127, no. 22, p. 8168-8173.
- Rocker, C., Potzl, M., Zhang, F., Parak, W.J., and Nienhaus, G.U., 2009, A quantitative fluorescence study of protein monolayer formation on colloidal nanoparticles: *Nat Nano*, v. 4, no. 9, p. 577-580.
- Rosenbusch, J.P., 1974, Characterization of the Major Envelope Protein from *Escherichia coli* : Regular arrangement on the peptidoglycan and unusual dodecyl sulfate binding: *Journal of Biological Chemistry*, v. 249, no. 24, p. 8019-8029.
- Rossi, F., Calzolari, L., Franchini, F., and Gilliland, D., 2010, Protein-Nanoparticle Interaction: Identification of the Ubiquitin-Gold Nanoparticle Interaction Site: *Nano Letters*, v. 10, no. 8, p. 3101-3105.
- Rowe, A.J., 2001, Probing hydration and the stability of protein solutions — a colloid science approach: *Biophysical Chemistry*, v. 93, no. 2–3, p. 93-101.
- Sakurai, Y., Ma, S.F., Watanabe, H., Yamaotsu, N., Hirono, S., Kurono, Y., Kragh-Hansen, U., and Otagiri, M., 2004, Esterase-like activity of serum albumin: Characterization of its structural chemistry using p-nitrophenyl esters as substrates: *Pharmaceutical Research*, v. 21, no. 2, p. 285-292.
- Saleh, N.B., Pfefferle, L.D., and Elimelech, M., 2008, Aggregation Kinetics of Multiwalled Carbon Nanotubes in Aquatic Systems: Measurements and Environmental Implications: *Environmental Science & Technology*, v. 42, no. 21, p. 7963-7969.
- Sandros, M.G., Gao, D., Gokdemir, C., and Benson, D.E., 2005, General, high-affinity approach for the synthesis of fluorophore appended protein nanoparticle assemblies: *Chemical Communications*, no. 22, p. 2832-2834.
- Savage, N., and Diallo, M.S., 2005, Nanomaterials and water purification: Opportunities and challenges: *Journal of Nanoparticle Research*, v. 7, no. 4-5, p. 331-342.

- Schwegmann, H., Feitz, A.J., and Frimmel, F.H., 2010, Influence of the zeta potential on the sorption and toxicity of iron oxide nanoparticles on *S. cerevisiae* and *E. coli*: *Journal of Colloid and Interface Science*, v. 347, no. 1, p. 43-48.
- Schwierz, N., Horinek, D., and Netz, R.R., 2010, Reversed Anionic Hofmeister Series: The interplay of Surface Charge and Surface Polarity: *Langmuir*, v. 26, no. 10, p. 7370-7379.
- Scott, J.R., and Barnett, T.C., 2006, Surface proteins of gram-positive bacteria and how they get there: *Annual Review of Microbiology*, v. 60, p. 397-423.
- Shannon, M.A., Bohn, P.W., Elimelech, M., Georgiadis, J.G., Marinas, B.J., and Mayes, A.M., 2008, Science and technology for water purification in the coming decades: *Nature*, v. 452, no. 7185, p. 301-310.
- Sigleo, A.C., and Means, J.C., 1990, Organic and Inorganic Components in Estuarine Colloids: Implications for Sorption and Transport of Pollutants, *in* Ware, G., ed., *Reviews of Environmental Contamination and Toxicology*: Springer New York, p. 123-147.
- Singh, C., Ghorai, P.K., Horsch, M.A., Jackson, A.M., Larson, R.G., Stellacci, F., and Glotzer, S.C., 2007, Entropy-mediated patterning of surfactant-coated nanoparticles and surfaces: *Physical Review Letters*, v. 99, no. 22.
- Singh, S.P., Chakraborty, S., Joshi, P., Shanker, V., Ansari, Z.A., and Chakrabarti, P., 2011, Contrasting Effect of Gold Nanoparticles and Nanorods with Different Surface Modifications on the Structure and Activity of Bovine Serum Albumin: *Langmuir*, v. 27, no. 12, p. 7722-7731.
- Sokolov, I., Smith, D.S., Henderson, G.S., Gorby, Y.A., and Ferris, F.G., 2000, Cell Surface Electrochemical Heterogeneity of the Fe(III)-Reducing Bacteria *Shewanella putrefaciens*: *Environmental Science & Technology*, v. 35, no. 2, p. 341-347.
- Song, J.E., Phenrat, T., Marinakos, S., Xiao, Y., Liu, J., Wiesner, M.R., Tilton, R.D., and Lowry, G.V., 2011, Hydrophobic Interactions Increase Attachment of Gum Arabic- and PVP-Coated Ag Nanoparticles to Hydrophobic Surfaces: *Environmental Science & Technology*, v. 45, no. 14, p. 5988-5995.
- Sun, Y.-P., Fu, K., Lin, Y., and Huang, W., 2002, Functionalized Carbon Nanotubes: Properties and Applications: *Accounts of Chemical Research*, v. 35, no. 12, p. 1096-1104.
- Ta, T.C., and McDermott, M.T., 2000, Mapping Interfacial Chemistry Induced Variations in Protein Adsorption with Scanning Force Microscopy: *Analytical Chemistry*, v. 72, no. 11, p. 2627-2634.

- Taboada-Serrano, P., Vithayaveroj, V., Yiacoumi, S., and Tsouris, C., 2005, Surface charge heterogeneities measured by atomic force microscopy: *Environmental Science & Technology*, v. 39, no. 17, p. 6352-6360.
- Tenzer, S., Docter, D., Rosfa, S., Wlodarski, A., Kuharev, J., Rekik, A., Knauer, S.K., Bantz, C., Nawroth, T., Bier, C., Sirirattanapan, J., Mann, W., Treuel, L., Zellner, R., Maskos, M., Schild, H., and Stauber, R.H., 2011, Nanoparticle Size Is a Critical Physicochemical Determinant of the Human Blood Plasma Corona: A Comprehensive Quantitative Proteomic Analysis: *Acs Nano*, v. 5, no. 9, p. 7155-7167.
- Theron, J., Walker, J.A., and Cloete, T.E., 2008, Nanotechnology and water treatment: Applications and emerging opportunities: *Critical Reviews in Microbiology*, v. 34, no. 1, p. 43-69.
- Tombacz, E., and Szekeres, M., 2006, Surface charge heterogeneity of kaolinite in aqueous suspension in comparison with montmorillonite: *Applied Clay Science*, v. 34, no. 1-4, p. 105-124.
- Tsuneda, S., Aikawa, H., Hayashi, H., Yuasa, A., and Hirata, A., 2003, Extracellular polymeric substances responsible for bacterial adhesion onto solid surface: *FEMS Microbiology Letters*, v. 223, no. 2, p. 287-292.
- Tufenkji, N., and Elimelech, M., 2004, Deviation from the Classical Colloid Filtration Theory in the Presence of Repulsive DLVO Interactions: *Langmuir*, v. 20, no. 25, p. 10818-10828.
- Tufenkji, N., and Elimelech, M., 2005, Breakdown of Colloid Filtration Theory: Role of the Secondary Energy Minimum and Surface Charge Heterogeneities: *Langmuir*, v. 21, no. 3, p. 841-852.
- Uversky, V.N., 1993, Use of Fast Protein Size-Exclusion Liquid-Chromatography to Study the Unfolding of Proteins Which Denature through the Molten Globule: *Biochemistry*, v. 32, no. 48, p. 13288-13298.
- Uzun, O., Hu, Y., Verma, A., Chen, S., Centrone, A., and Stellacci, F., 2008, Water-soluble amphiphilic gold nanoparticles with structured ligand shells: *Chemical Communications*, no. 2, p. 196-198.
- Velegol, S.B., and Logan, B.E., 2002, Contributions of Bacterial Surface Polymers, Electrostatics, and Cell Elasticity to the Shape of AFM Force Curves: *Langmuir*, v. 18, no. 13, p. 5256-5262.
- Verma, A., Uzun, O., Hu, Y.H., Hu, Y., Han, H.S., Watson, N., Chen, S.L., Irvine, D.J., and Stellacci, F., 2008, Surface-structure-regulated cell-membrane penetration by monolayer-protected nanoparticles: *Nature Materials*, v. 7, no. 7, p. 588-595.

- Verwey, E.J.W., 1947, Theory of the Stability of Lyophobic Colloids: The Journal of Physical and Colloid Chemistry, v. 51, no. 3, p. 631-636.
- Vijaykumar, S., Bugg, C.E., and Cook, W.J., 1987, Structure of Ubiquitin Refined at 1.8 Å Resolution: Journal of Molecular Biology, v. 194, no. 3, p. 531-544.
- Walczyk, D., Bombelli, F.B., Monopoli, M.P., Lynch, I., and Dawson, K.A., 2010, What the Cell "Sees" in Bionanoscience: Journal of the American Chemical Society, v. 132, no. 16, p. 5761-5768.
- Walker, S.L., Redman, J.A., and Elimelech, M., 2004, Role of Cell Surface Lipopolysaccharides in Escherichia coli K12 Adhesion and Transport: Langmuir, v. 20, no. 18, p. 7736-7746.
- Walz, J.Y., 1998, The effect of surface heterogeneities on colloidal forces: Advances in Colloid and Interface Science, v. 74, no. 1-3, p. 119-168.
- Wasilewska, M., Adamczyk, Z., and Jachimska, B., 2009, Structure of Fibrinogen in Electrolyte Solutions Derived from Dynamic Light Scattering (DLS) and Viscosity Measurements: Langmuir, v. 25, no. 6, p. 3698-3704.
- Weir, E., Lawlor, A., Whelan, A., and Regan, F., 2008, The use of nanoparticles in antimicrobial materials and their characterization: Analyst, v. 133, no. 7, p. 835-845.
- Wigginton, N.S., Haus, K.L., and Hochella Jr, M.F., 2007, Aquatic environmental nanoparticles: Journal of Environmental Monitoring, v. 9, no. 12, p. 1306-1316.
- Wilson, W.W., Wade, M.M., Holman, S.C., and Champlin, F.R., 2001, Status of methods for assessing bacterial cell surface charge properties based on zeta potential measurements: Journal of Microbiological Methods, v. 43, no. 3, p. 153-164.
- Xiao, Y., and Wiesner, M.R., 2013, Transport and Retention of Selected Engineered Nanoparticles by Porous Media in the Presence of a Biofilm: Environmental Science & Technology, v. 47, no. 5, p. 2246-2253.
- Yi, P., and Chen, K.L., 2011, Influence of Surface Oxidation on the Aggregation and Deposition Kinetics of Multiwalled Carbon Nanotubes in Monovalent and Divalent Electrolytes: Langmuir, v. 27, no. 7, p. 3588-3599.
- Zembala, M., 2004, Electrokinetics of heterogeneous interfaces: Advances in Colloid and Interface Science, v. 112, no. 1-3, p. 59-92.

- Zhang, H.Z., Burnum, K.E., Luna, M.L., Petritis, B.O., Kim, J.S., Qian, W.J., Moore, R.J., Heredia-Langner, A., Webb-Robertson, B.J.M., Thrall, B.D., Camp, D.G., Smith, R.D., Pounds, J.G., and Liu, T., 2011a, Quantitative proteomics analysis of adsorbed plasma proteins classifies nanoparticles with different surface properties and size: *Proteomics*, v. 11, no. 23, p. 4569-4577.
- Zhang, W., Rittmann, B., and Chen, Y.S., 2011b, Size Effects on Adsorption of Hematite Nanoparticles on *E. coli* cells: *Environmental Science & Technology*, v. 45, no. 6, p. 2172-2178.